

Discovering molecular differences between pioneer and follower neurons in neural development

Benjamin Martin Woodruff

A DISSERTATION

Dissertation submitted to the Department of Cell, Development, and Cancer
Biology
Oregon Health & Science University
School of Medicine

In partial fulfillment of the requirements for the degree of

Doctor of Philosophy

March 2025

CERTIFICATE OF APPROVAL

This is to certify that the PhD dissertation of
Benjamin Woodruff
has been approved

Advisor, Alex V. Nechiporuk, Ph.D.

Member & Chair, Kevin Wright, Ph.D.

Member, John Brigande, Ph.D.

Member, Anthony Barnes, Ph.D.

Member, Kelly Monk, Ph.D.

Outside Reader, Philip Copenhaver, Ph.D.

I. Table of Contents

I. TABLE OF CONTENTS.....	I
II. COMMON ABBREVIATIONS	III
III. DEDICATION	IV
IV. ABSTRACT.....	V
CHAPTER 1: INTRODUCTION	1
1.1: PREFACE	1
1.2: HISTORY OF PIONEER NEURONS.....	2
1.3 PIONEER AND FOLLOWER NEURONS IN DIFFERENT SYSTEMS	3
Figure ¹⁻¹	4
1.4 NEUROGENIC CRANIAL PLACODES	5
Figure ¹⁻²	7
1.5 POSTERIOR LATERAL LINE DEVELOPMENT.....	7
Figure ¹⁻³	8
1.6 PIONEERS AND FOLLOWERS IN THE PLL	9
1.7 RELEVANT SIGNALING PATHWAYS IN PLL DEVELOPMENT	10
CHAPTER 2: AXON TARGETING OF TRANSCRIPTIONALLY DISTINCT PIONEER NEURONS IS REGULATED BY RETINOIC ACID SIGNALING	12
2.1: ABSTRACT.....	13
2.2: INTRODUCTION.....	13
2.3: RESULTS.....	16
2.3.1 Single cell RNA sequencing identifies two distinct populations of neurons within the pLL	16
Figure ²⁻¹	18
2.3.2 <i>ret</i> marks pioneer neurons.....	19
Figure ²⁻²	21
2.3.3 Posterior lateral line pioneer neurons are required for followers' axon extension.....	22
Figure ²⁻³	23
Table ²⁻¹	24
2.3.4 Follower-specific markers define posterior lateral line neuron ground state.....	24
Figure ²⁻⁴	25
Figure ²⁻⁵	28
2.3.5 Pioneer precursors exhibit distinct cellular behavior.....	29
Figure ²⁻⁶	31
2.3.6 Downregulation of retinoic acid is required for proper pioneer axon targeting.....	32
Figure ²⁻⁷	33
2.3.7 Retinoic acid negatively regulates <i>ret</i> and is critical for correct pioneer neuron axon targeting.....	34
Figure ²⁻⁸	35
2.4: DISCUSSION	37
2.4.1 Summary and significance of study.....	37
2.4.2 Do neurons retain molecular differences over time, once wiring is complete?.....	37
2.4.3 Is pioneer cell state molecularly distinct in other systems?.....	38
2.4.4 A model of pioneer versus follower lineage specification.....	38
2.4.5 Regulation of the pLL pioneer development by retinoic acid.....	39
2.4.6 Summary	40

2.5: MATERIALS & METHODS	41
2.6: ACKNOWLEDGEMENTS	45
2.7: SUPPLEMENTAL INFORMATION	46
2.7.1 Movie Legends	46
2.7.2 Supplemental Figures.....	48
Figure ^{S2-1}	48
Figure ^{S2-2}	49
Figure ^{S2-3}	50
Figure ^{S2-4}	51
Figure ^{S2-5}	52
Figure ^{S2-6}	53
Figure ^{S2-7}	54
Figure ^{S2-8}	55
Figure ^{S2-9}	56
Figure ^{S2-10}	57
2.7.3 Key Resources Table	58
CHAPTER 3: CONCLUSIONS AND FUTURE DIRECTIONS.....	61
SECTION 3.1: SUMMARY.....	61
SECTION 3.2: FUTURE DIRECTIONS	61
Subsection 3.2.1: An updated view of pLL delamination	62
Figure ³⁻¹	63
Subsection 3.2.2: Notch signaling in neuron specification	63
Subsection 3.2.3: Retinoic acid downregulation in pioneers	64
Subsection 3.2.4: Interactions between pioneers and followers.....	65
Subsection 3.2.5: Tool development for early stages of pioneer and follow development.....	66
Subsection 3.2.6: Pioneers in the context of regeneration	66
SECTION 3.3: ACKNOWLEDGEMENTS.....	68

II. Common Abbreviations

Abv	Abbreviation
aLL	anterior Lateral Line
caRAR	constitutively active Retinoic Acid Receptor
CNS	Central Nervous System
CRISPR	Clustered Regularly Interspaced Short Palindromic Repeats
DE	Differentially Expressed
DMSO	Dimethyl sulfoxide
dnRAR	dominant negative Retinoic Acid Receptor
ECM	Extracellular Matrix
EGFP	Enhanced Green Fluorescent Protein
EMT	Epithelial to Mesenchymal Transition
Fgf	Fibroblast growth factor
FISH	Fluorescent <i>in situ</i> Hybridization
Gdnf	Glial derived neurotrophic factor
GEARs	Genetically Encoded Affinity Reagents
hpf	hours post fertilization
NM	Neuromast
pLL	posterior Lateral Line
pLLg	posterior Lateral Line ganglion
pLLP	posterior Lateral Line Primordium
PNS	Peripheral Nervous System
RA	Retinoic Acid
RAR	Retinoic Acid Receptor
scRNA-seq	single cell RNA sequencing
UMAP	Uniform Manifold Projection

III. Dedication

To Michelle, my partner in life and in science. Your love and support pulled me through.

To my mother, who fostered in me a curiosity for the natural world.

To my family and friends, who keep me grounded, and remind me to live a life outside of science.

To my high school biology teacher, Louis Armin-Hoiland, who encouraged me to consider myself a biologist.

To Oregon.

IV. Abstract

The nervous system links organs and tissues to the brain and spinal cord, forming neural pathways that are essential for communication and coordination across the body. Establishing these connections begins with pioneer neurons (“pioneers”), which extend axons into distant tissues, creating a pathway for later-extending follower neurons (“followers”) to refine and expand. Pioneers garnered significant interest due to their unique capabilities in pathfinding and axon guidance and for being conserved across the animal kingdom. However, the lack of specific molecular markers for pioneers has precluded investigations into the factors driving their unique behavior. For example, it is not known whether pioneers are transcriptionally distinct from followers. Many other aspects of pioneer neuron development remain obscure, such as their specification, axon targeting, and communication with followers. Finally, it is debated whether pioneers should be considered a specialized class of neuron with unique abilities, or whether they simply have the same properties as their followers but employ them in different contexts. This dissertation provides evidence for the former and showcases a study that leverages the zebrafish model system to reveal some of these elusive features of pioneers. Chapter 2 serves as a first look into the molecular regulation of pioneers and followers by evaluating differentially expressed genes, validating their expression *in vivo*, and testing how signaling molecules drive differences between pioneers and followers. Collectively, this work contributes significantly to our understanding of pioneer neuron biology and provides a platform for studying pioneers in other systems. These findings advance the field of neurodevelopment while also promoting clinical applications by enabling comparative studies between pioneer neurons and regenerating nervous tissue.

Chapter 1: Introduction

1.1: Preface

The human nervous system is a vast network consisting of billions of neurons, so complex that early theories, like the “reticular theory,” proposed it as a seamless, continuous web^{1,2}. The idea that the nervous system was composed of individual, discrete units remained unproven until Ramón y Cajal’s work in the late 19th and early 20th centuries³. His work allowed the field to consider the contribution of individual neurons to the overall nervous system; a paradigm shift critical for the field of neuroscience. It also set the stage for a conceptual model in which early-born neurons are the first step in building the nervous system. Officially designated “pioneer neurones” in 1976, these cells establish initial pathways from their cell bodies to target tissues⁴. Pioneer neurons are now recognized as a conserved feature across the animal kingdom, essential for wiring the nervous system in both vertebrate and invertebrate embryos⁵. This strategy is evolutionarily advantageous, as early pathfinding occurs when embryos are small and distances are short, allowing subsequent neurons, called followers, to navigate quickly and accurately to their targets.

Our understanding of the ubiquity of pioneer neurons (hereafter, pioneers) across vertebrates and invertebrates has grown with advances in imaging and experimental methods. However, most studies of pioneers remain focused on morphology and behavior, leaving their definition largely reliant on these characteristics. Without reliable methods to label and distinguish pioneers from followers, the field still lacks insight into the molecular mechanisms that bestow upon pioneers their unique abilities.

There are few systems in which pioneers can be unambiguously visualized and manipulated. One such system is the lateral line (LL) of *Danio rerio*, or zebrafish, the focus of this study. The LL is a mechanosensory system in fish and amphibians that detects changes in water currents, transmitting sensory input to the brain for processing⁶. This function is essential for behaviors such as feeding, mating, and shoaling⁷. The sensory neurons that innervate the trunk lateral line are clustered in the posterior lateral line ganglion (pLLg).

During development, pioneers from the pLLg begin axon outgrowth around 22 hours post-fertilization (hpf), extending until approximately 48 hpf when they reach the tip of the tail. Follower neurons (hereafter, followers) begin extending axons during this period, growing along the scaffold laid down by pioneers. Both pioneers and followers project to and eventually innervate mechanosensory organs called neuromasts. The zebrafish pLL is an ideal system for studying pioneers, as it allows observation of differentiation between 14 and 18 hpf and axon extension/targeting between 22 and 48 hpf. Additionally, zebrafish embryos are optically transparent, facilitating visualization and manipulation *in vivo*, and the availability of genetic tools further enhances their utility for studying pioneer neurons.

This introduction will broadly cover the history of pioneer neurons, different model organisms in which pioneers have been studied, embryonic origin and development of pLL pioneers, as well as relevant signaling pathways.

1.2: History of pioneer neurons

Attaining an understanding of how the nervous system is formed has been a goal of neuroscientists for over 100 years. Ramón Y Cajal performed early experiments using the Golgi staining technique, and through meticulous illustrations he recorded observations of neuronal anatomy during development^{2,3}. He discovered a structure at the tip of axons and postulated that neurons are equipped with a “growth cone”, a specialized and dynamic structure that directs axon growth³. This suggested that this growth cone was responsible for early-born neurons’ ability to forge a pathway to their target, and that the axon would serve as a guide for later-growing axons. This relationship between the axon responsible for pathfinding and follower axons is fundamental to our modern view of how the nervous system develops.

It was not until many decades later, in 1976, that the term “pioneer neuron” was formally introduced to describe these pathfinding neurons⁴. By utilizing the *Locusta migratoria*, or migratory locust, model system and performing serial sections of the developing antenna bud, Dr. Michael Bate described the early outgrowth of a group of precisely two axons⁴. These “twin” axons grew outward from early differentiating neurons,

housed in the distal antenna bud, and toward the central nervous system (CNS)⁴. In this same study, he next turned his attention to the limb bud, at a slightly earlier developmental stage, and observed a similar paradigm: a lone pair of peripheral axons projecting axons toward the CNS. He then noted that the axons of subsequent neurons consistently adhered to the previously pioneered pathways. This led him to conclude that a subset of neurons will pioneer axonal pathways early, serving as a guide for later neurons as development progresses. This work both supports Cajal's hypothesis and expands on it by providing a framework for understanding neurodevelopment as a process involving stepwise scaffolding with pioneer neurons as the starting point. It also demonstrated that these pioneers extend along reproducible, stereotyped pathways, suggesting the existence of robust guidance mechanisms.

In summary, the concept of pioneer neurons can be traced back to Cajal's descriptions and illustrations, and this concept was later experimentally confirmed by Bate. While Bate's work in grasshopper provided foundational insights into how early axons navigate through the embryonic environment, it also raised questions whether similar pioneer mechanisms exist in other organisms and systems. Subsequent research has revealed that pioneer neurons are not unique to a single species but are a widespread and conserved feature of nervous system development.

1.3 Pioneer and follower neurons in different systems

The field understood pioneers as neurons that extend their axons first, and followers as neurons that extend later along the pathway laid down by the pioneer (**Fig. 1-1**). With this formalized definition, researchers began investigating pioneers' contributions in other systems. However, the grasshopper, as an established model system, had numerous advantages for studying pioneers; relative simplicity of the nervous system, externally developing, large embryos, and ease of manipulation^{4,8-10}. Due to these features, the experiments utilizing the grasshopper system continued to expand the field's understanding of pioneers. Ho and Goodman made important discoveries about an array of cells they described as "landmark cells" responsible for helping to guide pioneers to their destination¹⁰. This suggested that there are guidance cues in place to help direct pioneering

axons to their target within naive tissue. Klose and Bentley investigated whether pioneers are truly required for follower extension by preventing the differentiation of neuroblasts into pioneers, and found that in their absence followers failed to reach the CNS¹¹.

Figure 1-1



1-1 **Schematic of pioneer and follower neuron behaviors.** Pioneer axons extend outward toward a target, before later extending, follower neurons. Followers grow along the axon scaffold left by the pioneer. Schematic created with BioRender.com.

Concurrently, researchers began utilizing other invertebrate model systems to study pioneers such as *Drosophila melanogaster*, the fruit fly. Early studies using *Drosophila* also investigated the effect of pioneer ablation to study the dependency of followers on previously pioneered pathways^{12,13}. The roundworm, *C. elegans*, also emerged as a powerful system to study pioneers as the entire cell lineage was mapped out from zygote to larva¹⁴. Early axonal projections were described along the body wall and another study provided a detailed characterization of pioneers and how they guide followers^{15,16}. Together, these studies supported the notion that pioneers are evolutionarily conserved and established different invertebrate models as valuable tools to study pioneers.

Early studies of pioneers in vertebrates drew from discoveries made in invertebrate models. For example, research in zebrafish described the presence of pioneers in the spinal cord and showed that pioneer ablation disrupts axon targeting^{17,18}. Pioneers were also

described in *Xenopus* and found to exhibit elaborate and dynamic growth cones, suggesting a role in pathfinding¹⁹. Mammals became a focus of study as technological improvements, such as confocal microscopy, brain slicing, transgenesis, and retrograde tracers, allowed the study of more complex organisms. Researchers studying mammalian brain development determined that the subplate, a transient layer of the cortex, houses pioneers that send the first group of axons into the cortex^{20,21}. This landmark study suggested that the first axons to invade the cerebral cortex are none other than pioneer neurons. In addition, studies of eye development in mice investigated the optic chiasm as a choice point for retinal nerves. They found that the first axons to extend out of the eye, contralateral axons, crossed the midline and established a pathway, acting as pioneers²². Further, they identified that a second group, ipsilateral axons, acted first as followers as they extended to the midline, but then exhibited more pioneer-like behavior after avoiding the midline. These early studies using vertebrates confirmed that pioneer neurons are not unique to invertebrates but are present throughout taxa where they play fundamental roles in neurodevelopment.

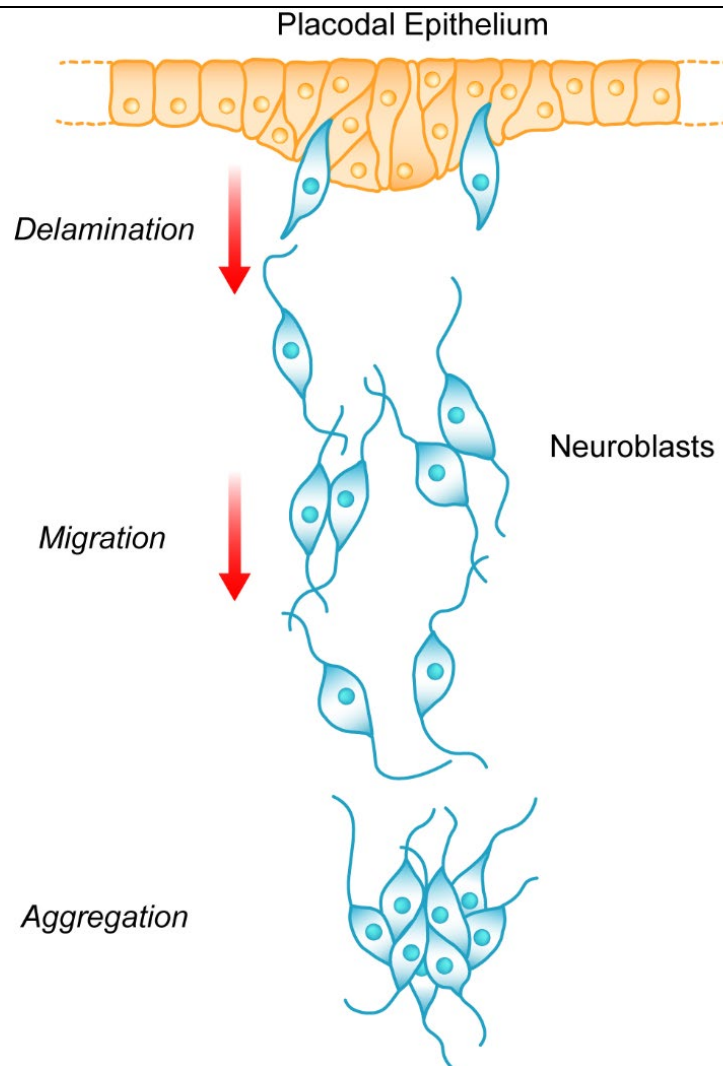
1.4 Neurogenic cranial placodes

Pioneer neurons play crucial roles in establishing pathways and scaffolding in both the central as well as the peripheral nervous system (PNS). Cranial placodes, transient embryonic structures, contribute sensory and neural cells that innervate the head and neck. Many cranial placodes have neurogenic capacity that give rise to pioneer neurons which build these sensory neural pathways. Among these are olfactory, trigeminal, epibranchial, otic, and lateral line placodes²³. Each placode originally develops from a common tissue origin, termed the pre-placodal ectoderm. This horseshoe-shaped region gives rise to each placode as distinct zones. Development of each placode involves dynamic morphogenetic processes such as delamination or invagination, which enable the generation of multiple cell types, including neurons.

In neurogenic placodes, such as the trigeminal, epibranchial, and lateral line placodes, generating neurons first requires that epithelial progenitors detach from the epithelium. This process, known as delamination, involves individual cells within the epithelial sheet detaching and migrating into the underlying mesenchyme. Here, they coalesce into ganglia

and differentiate into neurons (**Fig. 1-2**). Perhaps the best characterized example of delamination is in neural crest development^{24,25}. Importantly, evidence shows that placodes and neural crest cooperate during the formation of cranial ganglia^{26,27}. When considered broadly, placodal delamination appears to parallel neural crest cell delamination: both processes involve a physical cellular detachment from an epithelium that precedes migration and differentiation. Yet, these two processes differ in several key ways, suggesting they are in fact, distinct^{28,29}. First placodal delamination appears not to occur through a traditional epithelial mesenchymal transition (EMT), a hallmark of neural crest development^{24,25,30-33}. This is evident when comparing morphology and marker expression between neural crest and placode. Neural crest cells take on a multipolar, mesenchymal morphology and express EMT markers, while placodal neuroblasts are thought to take on a bipolar neuronal morphology and do not express EMT markers. However, placode delamination is relatively understudied, as most studies are based on samples fixed at discrete stages; it is also unclear whether the above observations can be generalized to all neurogenic placodes. Second, delamination of neural crest happens relatively quickly over the course of hours³⁵⁻³⁷, whereas placodal delamination occurs over a rather protracted period, days, as neurons are continually added²⁸. Data from the studies presented here will demonstrate that in at least one case, placodal neuroblasts do transition into mesenchymal morphology while lacking conventional EMT markers.

Figure¹⁻²



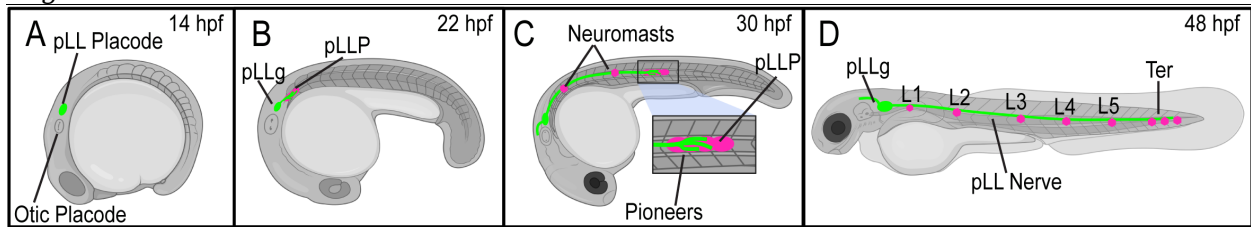
¹⁻² **Generalized schematic model of neurogenic placode delamination.** Cells from a thickened cranial placode begin to loosen contact with their neighbors and extrude from the epithelial sheet. These delaminating neuroblasts immediately take on a bipolar morphology as they migrate. They will then aggregate into a sensory ganglion. *Adapted from Breau and Schneider-Maunoury 2015²⁹.*

1.5 Posterior lateral line development

One key neurogenic placode, and the primary focus of this dissertation, is the lateral line, a mechanosensory system that enables anamniotes to detect water movement in their environment. The lateral line includes two main branches: the anterior lateral line (aLL), located anterior to the otic vesicle, and the posterior lateral line (pLL), located posterior to the otic vesicle⁶. Both branches function to convey water current information, but the aLL serves the head whereas the pLL relays information from the trunk and tail³⁸. The pLL

comprises sensory and neural components that work together to convert external stimuli into internal signals³⁹. The sensory component consists of neuromasts—specialized sensory organs arranged along the animal’s trunk. Each neuromast contains mechanoreceptive hair cells that respond to water motion and relay signals to the neurons that innervate them, forming the neural component of the pLL⁶. These afferent neurons extend axons to both the neuromasts and the CNS, creating a direct sensory pathway.

Figure 1-3



1-3 Schematic of pLL development. (A) The pLL placode, just behind the otic placode, begins to separate into two populations, a neural and a sensory population. **(B)** Delaminating neuroblasts aggregate to form the pLLg, while the sensory cells form the pLLP. **(C)** The pLLP migrates toward the tail and deposits neuromasts along the trunk of the fish. Simultaneously, pioneer axons grow outward from the pLLg and their terminals comigrate with the pLLP. **(D)** Migration and pioneer axon extension concludes at 48 hpf when both have reached the tail. Schematic created with BioRender.com.

Both the sensory cells and neurons of the pLL have distinct roles but share a common origin: the pLL placode. Compared to other cranial placodes, such as epibranchial, otic, and trigeminal, early development of the pLL is not well understood, as most investigation has been focused on processes of collective cell migration leading to neuromast innervation⁶. At 14 hours post-fertilization (hpf) in zebrafish, the pLL placode begins to separate into two populations (**Fig. 1-3A**). About 20 neuroblasts delaminate from the placode and aggregate to form a ganglion, while the ~150 remaining progenitors gather to form the sensory population of the pLL, the posterior lateral line primordium (pLLP)^{39,40}. By 22 hpf, the pLLP begins its caudal migration⁴¹⁻⁴³ (**Fig. 1-3B**). Simultaneously, several pioneer neurons from the pLL ganglion (pLLg) extend their neurites into the pLLP, embedding themselves within it while comigrating (**Fig. 1-3C**). Meanwhile, pLL follower neurons also begin to extend from the pLLg, but with a slight delay, trailing behind the primordium. Because they extend in parallel and exhibit smaller growth cones, followers are difficult to visualize during axon extension. Over the next 24 hours of migration along the trunk, the pLLP deposits small clusters of about 20 cells each. These clusters differentiate into the mechanosensory organs

which later serve as innervation targets for pLL neurons. This process of migration and extension concludes by 48 hpf, when the pLLP and pLL nerve reach the tail (**Fig. 1-3D**). The coordinated migration of the pLL primordium and the simultaneous axon extension from the pLL ganglion establish the foundation for a functional mechanosensory system—one guided by the interplay between pioneering axons and their followers.

1.6 Pioneers and followers in the pLL

Several studies have identified behavioral, morphological, and molecular differences between pLL pioneers and followers. For example, pioneers exhibit larger, more complex growth cones^{6,44–46} and larger cell bodies⁴⁵—features consistent with their role in leading axonal navigation. Additionally, within the pLLg, pioneer cell bodies occupy more dorsal positions than followers after 30 hpf^{46–48}. Notably, these dorsal-positioned pioneers display distinct targeting biases, projecting their axons to distal neuromasts, while followers project more proximally^{44,49}. Finally, electrophysiology experiments demonstrated that pLL pioneers have a lower input resistance and spontaneous firing rate and are more likely to contact multiple neuromasts, whereas followers typically exhibit higher resistance, a higher firing rate, and a single-neuromast connection⁴⁸.

The difference in targeting is closely tied to the organization and development of the pLL⁴⁸. Pioneer axons, which terminate at the tail, create a scaffold spanning the length of the nerve, guiding the extension of follower axons³⁹. As the pLL nerve develops, follower axons use the pioneered pathway to innervate sensory targets along the trunk⁴⁸. Together, these observations define key characteristics that distinguish pLL pioneers from followers.

Presumably, these differences in behavior and targeting arise from a combination of intrinsic properties and external cues. A complex interplay of signaling molecules, instructive factors, and cell adhesion mechanisms underlies pioneer pathfinding and follower fasciculation. Exploring these signaling pathways offers insight into how pLL axons navigate, establish proper connectivity, and how pioneers are specified from the outset.

1.7 Relevant signaling pathways in pLL development

The pLL placode develops just after gastrulation in a complex and dynamic signaling environment where multiple pathways coordinate morphogenesis^{50,51}. This environment is defined by a combination of guidance cues, the establishment of morphogen gradients, and the expression of molecular factors. Together, this feedback creates precise, tailored guidance to promote placode delamination, neurogenesis, and axon targeting.

A critical piece process of neurogenic placode development is the specification of neurogenic cells within the placodal epithelium. This neurogenic domain is formed by upregulation of proneural genes such as *delta*, *neurogenin1*, and *hes*^{31,52}. Notch signaling is vital for specifying neurons^{31,53-56}. This paradigm is consistent in the pLL as lateral inhibition via Delta/Notch determines placodal differentiation into Notch+ sensory progenitors or Delta+ neuroblasts⁵⁰. This same lateral inhibition network through Delta and Notch also determines cell identity later in pLL development, during sensory hair cell differentiation^{57,58}. Nevertheless, whether Notch signaling plays a role in pioneer neuron identity is an open question, which could be tested with the use of small molecule inhibitors or CRISPR knockouts targeting notch pathway members.

The fibroblast growth factor (Fgf) pathway is another central orchestrator in pLL placode development. Multiple studies have shown Fgf to be a crucial determinant in the specification of neurogenic placodes⁵⁹⁻⁶². In the pLL, however, Fgf appears to play a more nuanced role. Treatment with Fgf receptor inhibitor SU5402 expanded the pLL while simultaneously resulting in a diminished aLL⁵¹. This suggested different mechanisms for aLL vs pLL induction: Fgf activation for aLL, but Fgf inhibition for pLL formation. Further, the pLL was shown to require retinoic acid (RA) signaling for induction. Intriguingly, other studies demonstrated that Fgf signaling and RA form opposing gradients, antagonizing each other⁶³⁻⁶⁶. In the lateral line, the pLL placode appears to require RA for the inhibition of Fgf. This interplay between Fgf and RA underscores the finely tuned balance of signaling required for pLL specification.

Beyond Fgf and RA, additional signaling molecules help further refine pLL differentiation during axon extension and targeting. Previous studies have shown that larger, earlier-born pLL neurons exhibit a targeting bias toward more distal neuromasts^{44,49}, suggesting robust guidance mechanisms consistently direct these axons to their targets. One such pathway involved in pLL axon targeting is the neurotrophin signaling pathway. As the lateral line primordium migrates, it secretes glial-derived neurotrophic factor (Gdnf)⁶⁷. Gdnf's receptor, 'REarranged during Transfection' (Ret), is present on pLL neurons and plays an established role in axon pathfinding across various systems, including sympathetic⁶⁸, sensory⁶⁹, and motor axon growth⁷⁰. Our lab demonstrated that Ret is enriched in a subset of pLL neurons and is essential for complete extension of the pLL nerve. Notably, Ret is present in pioneer axon growth cones embedded within the primordium⁴⁶. Since their discovery, pioneers have largely been defined by morphology and behavior, but identifying a molecular marker like Ret presents an opportunity to explore the transcriptional differences that distinguish pioneers from followers. Chapter 2 will discuss how Ret's enrichment in pioneers facilitated our inquiry into to unique molecular factors underlying pioneer behavior.

Chapter 2: Axon targeting of transcriptionally distinct pioneer neurons is regulated by retinoic acid signaling

Benjamin M. Woodruff¹, Lauren N. Miller¹, Nicholas L. Calistri², Jacqueline R. McVay¹, Laura M. Heiser², Alex V. Nechiporuk^{1*}

¹Department of Cell, Developmental and Cancer Biology, Oregon Health & Science University, Portland, Oregon, USA

²Biomedical Engineering, Oregon Health & Science University, Portland, Oregon, USA

The revised manuscript is currently under review in Nature Communications.

2.1: Abstract

During nervous system development, pioneer neurons (pioneers) extend their axons towards distant targets, creating a scaffold for follower neurons and defining the initial structure of the nervous system. Despite years of study, whether pioneer neurons are molecularly distinct from followers is unknown. To address this question, we performed single-cell RNA sequencing (scRNA-seq) of zebrafish posterior lateral line (pLL) sensory neurons and found that pioneers and followers are transcriptionally distinct populations. Interestingly, expression profiling of differentiating pLL progenitors defines “follower” as the ground state and “pioneer” as a later developmental state, with retinoic acid (RA) signaling active in all pLL progenitors. Modulation of RA signaling within single pLL neurons showed that its downregulation is necessary for expression of a neurotrophic factor receptor *ret*, which is required for correct targeting of pioneer axons. Our study reveals molecular heterogeneity between pioneer and follower neurons and implicates RA signaling in the fidelity of pioneer neuron axonal targeting.

2.2: Introduction

The nervous system is an extensive and complex network of neural connections, many of which are established during embryonic development. Pioneer neurons (hereafter, pioneers) exhibit the remarkable ability to navigate through developing tissue and build the initial scaffold of the nervous system^{4,10}. Pioneers were discovered about 50 years ago where they were described as a class of neurons that extend their axons into a non-innervated tissue allowing the subsequent recruitment of additional, follower axons⁴. This contrasts with follower neurons which will extend later along the trail laid down by pioneers to connect to their targets. In many systems, followers exhibit difficulty navigating to appropriate targets when pioneers are ablated^{12,46,71-74}. When compared to followers in certain contexts, pioneers have larger cell bodies, more elaborate growth cones, different axon growth rates, and can undergo more complex pathfinding^{44,45,47,49,75}. This definition has endured to the present day as pioneers are still largely described by morphology and behavior^{76,77}. However, recent evidence from our work, and from others', shows at least

some molecular differences between pioneers and followers in multiple systems. For example in *C. elegans*, pioneer and follower neurons are guided by glial cells using distinct molecular cues⁷⁸. Similarly, our previous work showed that the extension of pioneers, but not followers, in the peripheral sensory system of zebrafish is directed by a specific neurotrophic factor receptor⁴⁶. Finally, manipulation of Jun kinase activity in the *Drosophila* ventral nerve cord specifically affects pioneer but not follower neurons⁷⁹. However, whether the above observations imply more profound molecular differences between pioneer and follower neurons in any system is not known.

To examine the behavior and molecular identity of pLL neurons during differentiation and axon outgrowth stages, we took advantage of the zebrafish posterior lateral line (pLL) as a model system^{46,57}. The pLL is a mechanosensory system in aquatic vertebrates that senses water movements and controls swimming behaviors like schooling, predator and prey detection, and maintenance of rheotaxis^{6,57,80,81}. The pLL consists of sensory neurons that innervate mechanosensory organs called neuromasts (NMs) located on the surface of the trunk. Both sensory and neural progenitors derive from the pLL placode, a thickening of the embryonic ectoderm, that forms shortly after the end of gastrulation (10 - 14 hours post fertilization or hpf)⁴⁰ (Fig. 2-1A). At 22 hpf, pLL neurons initiate axon extension caudally from a cranial ganglion (Fig. 2-1B). Between 3 to 6 pLL pioneer axon growth cones are embedded within the pLL primordium (pLLP), a group of sensory organ progenitors that migrates along the trunk from 22 to 48 hpf⁸² (Fig. 2-1C). As the pLLP migrates, it deposits 5 to 6 cell clusters at regular intervals as well as a terminal cluster, all of which differentiate into NMs⁸³⁻⁸⁵. By the end of primordium migration, pioneer axons reach the end of the tail and selectively innervate distal NMs. (Fig. 2-1D). Follower axons begin extension after pioneers, co-fasciculate with pioneer axons, and selectively innervate proximal NMs^{47,49,83,86}. Besides distinct targets, pLL pioneers also have larger cell bodies and more elaborate axon growth cones than followers^{44,46,49}. Components of the pLL are easily visualized by transgenic reporter lines such as TgBAC(*neurod1:EGFP*)ⁿ¹¹ (referred to as *neurod1:EGFP*) which labels neurons⁸⁷, and Tg(-8.0*cldnB:LY-EGFP*)^{zf106} (referred to as *cldnB:memgfp*)⁸⁸ which labels both pLL neurons and the pLLP. The ability to distinguish and visualize pioneer pLL neurons in a live animal makes this system uniquely suited for transcriptomic analysis

and follow up studies to define the function of genes required for pioneer axon growth and function.

Previous studies defined a developmental timeline of pLL neuron differentiation. At mid-somitogenesis (14 hpf), pLL progenitors begin to undergo neurogenesis, which can be detected by expression of proneural factors, *neurog1* and *neurod1*^{87,89}. By 18 hpf, the pLL placode separates into committed sensory and neural progenitors⁵⁰. One of the signals required for the initial formation of the pLL placode is retinoic acid (RA)⁵¹. RA is a small lipophilic molecule that acts as a morphogen to regulate gene expression and cellular differentiation⁹⁰⁻⁹⁵. Upon cellular uptake, RA is translocated to the nucleus where it binds nuclear receptors, RAR and RXR, to activate transcription⁹⁶⁻⁹⁸. Some RA signaling pathway components are also crucial mediators of RA signaling. For example, the cellular retinoic acid-binding protein 1B (*crabp1b*) binds intracellular RA to control signal intensity⁹⁹⁻¹⁰¹. RA signaling is also a well-known direct regulator of *hox* gene family members, including *hoxb5a*¹⁰²⁻¹⁰⁶. RA has been well studied in many systems, including neurodevelopment; however, whether the RA signaling network remains active through neurogenesis and differentiation in the pLL is not known.

In this study we investigated transcriptional differences between pioneer and follower neurons of the zebrafish pLL. Using a single-cell RNA-sequencing (scRNA-seq) approach, we found that pioneers have a transcriptional profile distinct from followers and with differential expression of neurotrophin receptors and members of the RA pathway. Surprisingly, analysis of pioneer and follower gene expression during early stages of pLL differentiation revealed that the default state for pLL progenitors is the follower identity, whereas pioneer is an acquired state. Live imaging of individually labeled pioneer and follower neurons revealed distinct morphology, growth, and behavior: most pioneer neurons delaminate first from the pLL placode, become bipolar, and extend their axons prior to followers. Using two-photon ablation we determine that the initial extension of pioneer axons is required for follower axon extension in the pLL. We also show that the RA pathway is initially active in all pLL progenitors; it is then selectively downregulated in pioneers. This, in turn, is required for the expression of neurotrophic factor receptor Ret, which directs

targeting of pioneer axons to distal sensory organs. We propose that a unique molecular program is accountable for the distinctive behavioral characteristics of pioneer neurons.

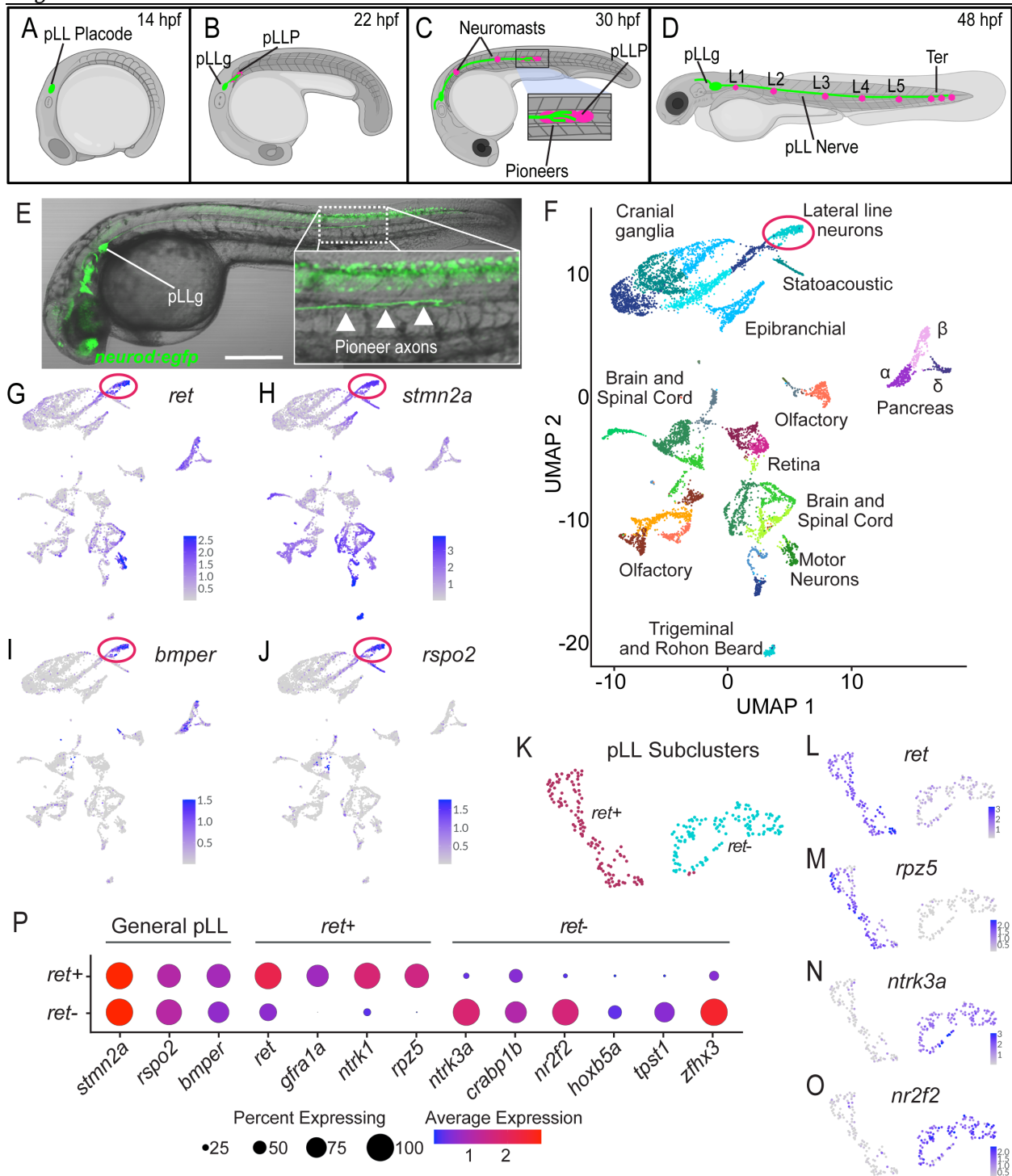
2.3: Results

2.3.1 Single cell RNA sequencing identifies two distinct populations of neurons within the pLL

We previously showed that pioneers, in addition to having distinct morphology and target innervation, are enriched with the neurotrophic factor receptor *Ret*⁴⁶. Based on these observations, we hypothesized that pLL pioneers are molecularly distinct from followers. To test this, we characterized transcriptional profiles of pLL pioneers and followers during axon extension (30 hpf) using scRNA-seq. To isolate pLL neurons, we FAC sorted cells from *neurod1:EGFP* embryos (Fig. 2-1E), as this transgene marks both CNS and PNS neurons including pLL⁸⁷. Fortuitously, the transgene is expressed at higher levels in cranial ganglia, including the pLL^{46,87}; consequently, we FAC sorted the top 2% brightest EGFP-expressing cells. This approach yielded 9242 cells, most of which were neurons, as well as some *neurod1*-expressing pancreas cells¹⁰⁷ (Fig. 2-1F and S1B) represented in 30 clusters. Using known tissue-specific markers, we identified each cell population (Fig. S2-1A). We identified the pLL by expression of known LL markers, such as *ret*⁴⁶, *stmn2a*¹⁰⁸, *bmper*¹⁰⁹, and *rspo2*¹¹⁰ (Fig. 2-1G-J), and exclusion of markers of other cranial sensory populations, such as *irx1a*¹¹¹ (otic) and *phox2bb*⁵⁹ (epibranchial) (Fig. S2-1A), as well as anterior LL marker *alcama*¹¹². We then performed unsupervised subclustering of pLL cells which yielded two distinct subpopulations (Fig. 2-1K), one of which was highly enriched for *ret*. Differential expression (DE) analysis with a minimum difference threshold set at 25% and false discovery rate of <5% yielded 101 DE genes: 60 enriched in *ret*⁺ cells, 41 in *ret*⁻ cells (Fig. S2-2). Among these 101 genes, some examples of those with the highest log₂ fold change in either the *ret*⁺ or *ret*⁻ populations are *gfra1a*, *ntkr1*, and *rpz5*, or *ntkr3a*, *nr2f2*, and *zfhx3*, respectively. (Fig. 2-1L-O and Fig. S2-2). The DE genes included several neurotrophin receptors: *ret*, *gfra1a*, and *ntkr1* were upregulated in *ret*⁺ cells, whereas *ntkr3a* was upregulated in *ret*⁻ cells (Fig. 2-1P). In addition, we found that the RA pathway member *crapb1b* and known transcriptional

targets of RA in other systems (*hoxb5a*, *nr2f2*, and *zfhx3*) were upregulated in the *ret*-population^{101,102,113-116}. In summary, scRNA-seq identified two distinct populations within the developing pLL ganglion, delineated by their relative expression of the previously defined pLL pioneer marker *ret*. Together with our previous study, these data suggested that the *ret*+ cells are pioneers, whereas the *ret*- cells are followers.

Figure 2-1



2-1 scRNA-sequencing identifies two molecularly distinct populations of pLL neurons. (A-D) Schematic of pLL development. (A) At 14 hpf the posterior lateral line placode contains both neural and sensory progenitors. (B) At 22 hpf the pLLP begins migrating and pioneer axons are embedded within the pLLP. (C) At 30 hpf, pLLP and pioneer axons reach halfway down the trunk. (D) At 48 hpf, pLLP and lateral line pioneer axons have reached the end of tail. Abbreviations: pLLg – pLL ganglion; L1 - L5 are lateral trunk NMs; Ter –

terminal cluster of NMs. **(E)** *neurod1:EGFP* transgene labels a subset of CNS and PNS neurons at 30 hpf, including the pLL. White arrowheads mark extending pioneer axons in the inset. Scale bar = 200 μ m. **(F)** UMAP of all EGFP+ sorted and sequenced cells. Major cell types are indicated. Red circle: lateral line neurons. **(G-J)** Feature plots showing expression of lateral line specific markers: *ret*, *stmn2a*, *bmper*, and *rspo2*. Red circle: lateral line neurons. **(K)** pLL subclusters: *ret+* and *ret-* populations. **(L-O)** Feature plots of subpopulations showing several differentially expressed genes in each subcluster. **(P)** Dotplot showing genes expressed in all pLL neurons as well differentially expressed genes in each subcluster. Schematic created with BioRender.com.

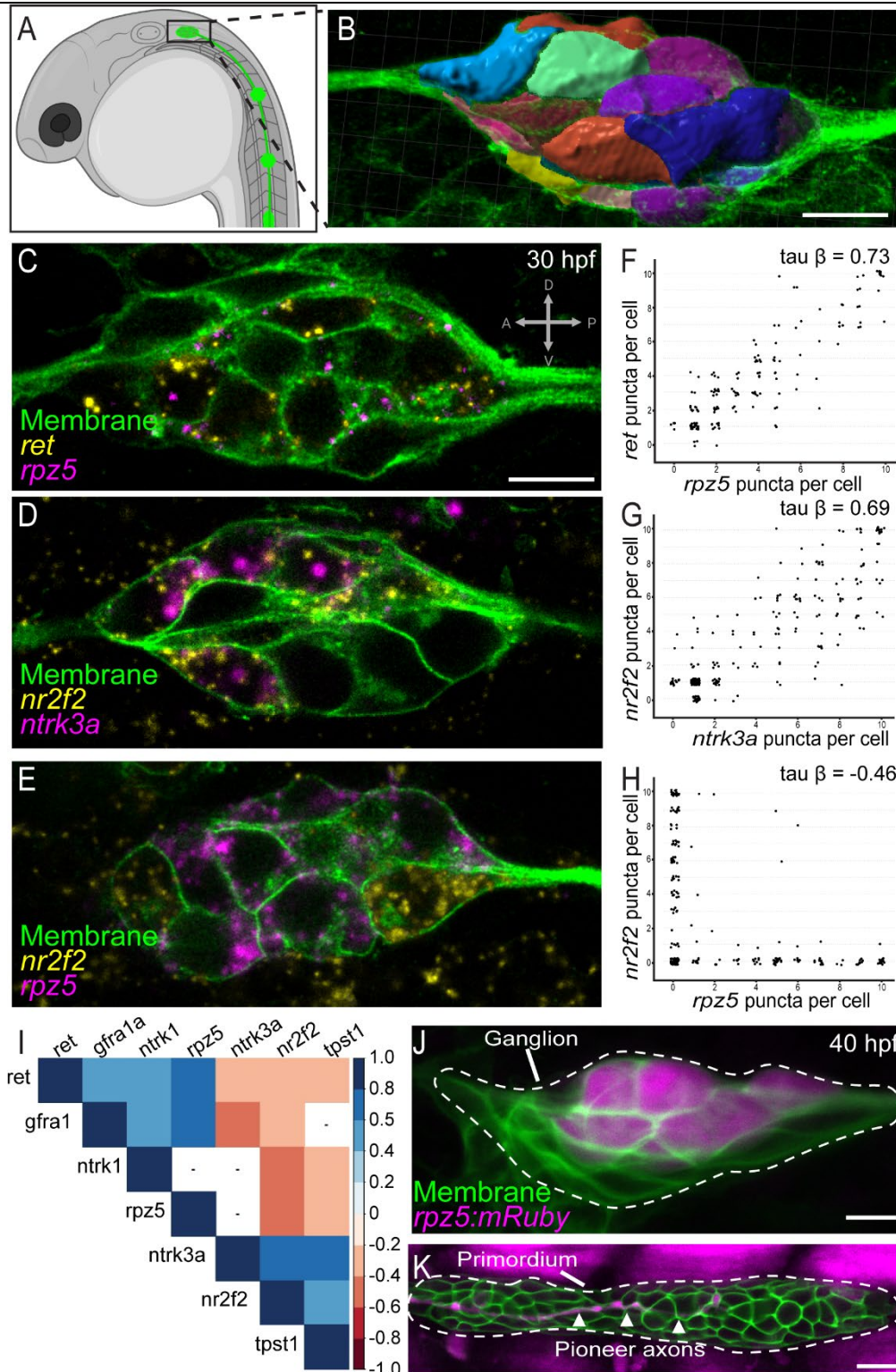
2.3.2 *ret* marks pioneer neurons

Next, we validated our sequencing data expression profiles. We performed whole-mount fluorescent *in situ* hybridization (FISH) using RNAscope^{117,118}. We used the *cldnB:memgfp* transgenic as it labels cell membranes in the pLL ganglion^{88,119} which allows identification of individual neurons for signal quantification (Fig. 2-2 A,B). We probed for genes differentially expressed in the *ret+* and *ret-* clusters in pairwise combinations (Fig. 2-2C-E). We found that genes in each cluster had high correlation coefficients amongst each other, indicating expression within the same neurons (Fig. 2-2F,G,I, S2-3A,B). By contrast, comparing gene expression between *ret+* and *ret-* clusters displayed low correlation coefficients, (Fig. 2-2H,I, S2-3C,D), indicative of mutually exclusive expression. These data validate our scRNA-seq observations that *ret+* and *ret-* cells express a distinct set of genes.

We then asked whether the *ret+* cells are in fact pioneer neurons. To address this, we knocked in a red fluorescent protein, mRuby, into the *rpz5* locus using the mBait strategy¹²⁰. We chose *rpz5* because it is the most specific and highly enriched gene within the *ret+* subpopulation (Fig. 2-1M, P). Validation of *rpz5:mRuby* expression by FISH with both *mRuby* and *rpz5* probes showed that 91% of mRuby+ cells (90/99) expressed the *rpz5* transcript (Fig. S2-4A,B), indicating that the transgene faithfully recapitulates endogenous expression of *rpz5*. As shown in Fig. 2J, mRuby marks a subset of pLL neurons during axon outgrowth (36 hpf). pLL neuron cell bodies that target distal neuromasts (i.e. pioneer neurons) gradually localize dorsally in the pLLg after 32 hpf^{46,49}; accordingly, we noted that mRuby+ cells occupied dorsal positions at 36 hpf. Importantly, mRuby always labeled distal-most pioneer axons which comigrate within the pLLP during pLL nerve extension (Fig. 2-2K). We identified between 3 and 7 mRuby+ cells within the ganglion (Fig. S2-4C). This is consistent with our previous observation demonstrating 3 to 6 pioneer neuron growth cones within the

migrating pLLP⁴⁶. In summary, our data show that pLL pioneer and follower neurons are transcriptionally distinct during axon extension.

Figure 2-2



2-2 Validation of scRNA-seq data identifies *ret*+ neurons as pioneers. **(A)** Schematic of 30 hpf embryo, a stage utilized for FISH. Membranes are labeled by *cldnB:mengfp* transgene (green). **(B)** 3D reconstruction of individual pLL neurons by Imaris using membrane-tagged *cldnB:mengfp* fluorescence. Subsequently,

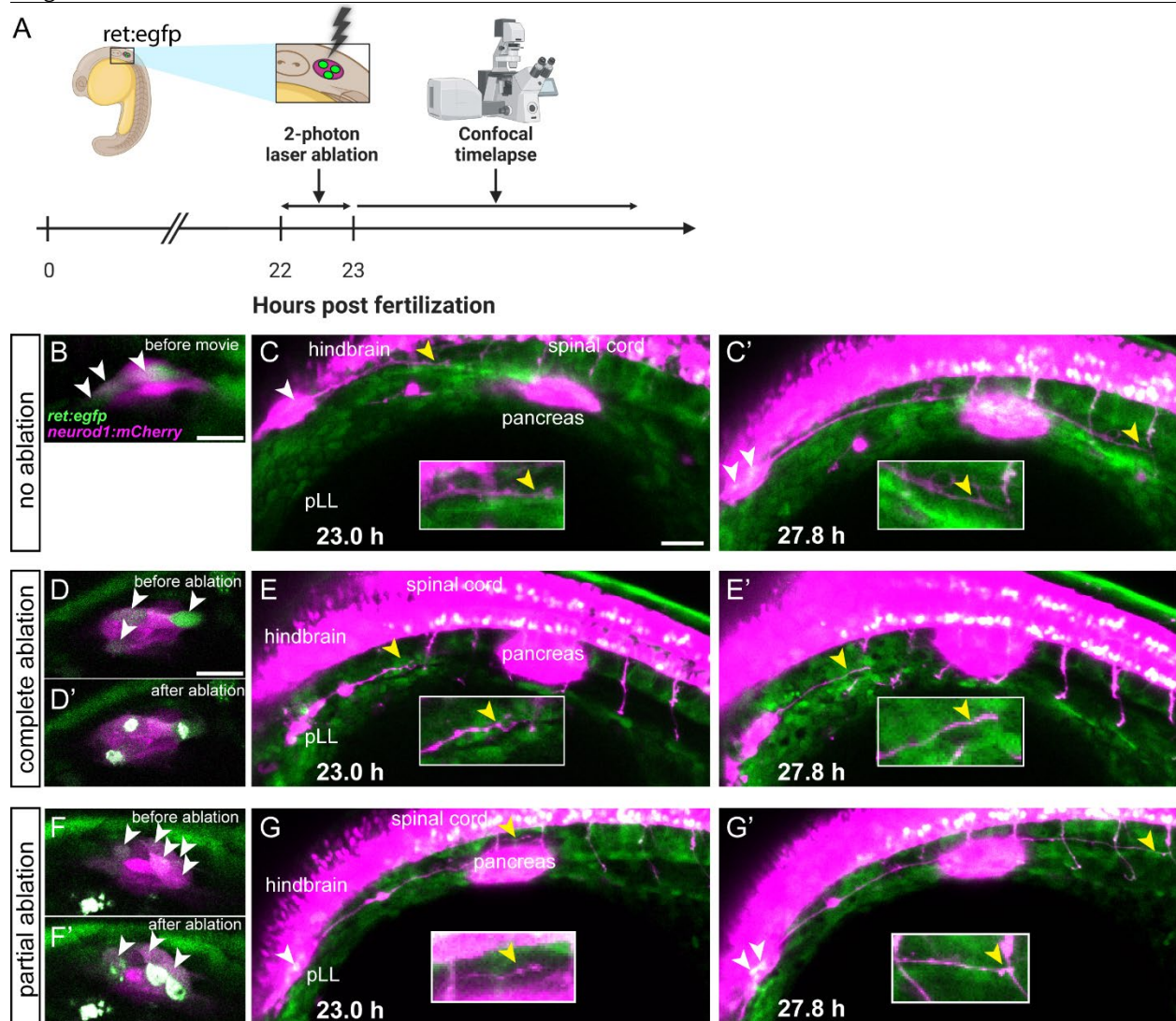
binned fluorescent puncta are counted in each individual cell. **(C-E)** Representative single Z-slice confocal images through the pLL ganglion showing pairwise FISH of two genes from *ret+* and *ret-* subclusters (*ret* and *rpz5*, *nr2f2* and *rpz5*, or *nr2f2* and *nrtrk3a*) at 30 hpf. Note that genes from the same clusters are coexpressed, whereas genes from the *ret+* and *ret-* subclusters are largely expressed in different cells. **(F-H)** Quantification of gene expression shown in 2C-E. Each dot corresponds to a single cell and the axes indicate binned gene expression levels. Each plot shows all cells across 10 embryos. Expression of genes from the same pLL subcluster strongly correlates, while expression of genes from different pLL subclusters does not correlate. Correlation coefficient Kendall tau-beta used for pairwise correlations. **(I)** Heatmap shows pairwise Kendall tau gene correlation coefficients based on examining expression of gene pairs by FISH. Empty squares are untested probe combinations. **(J)** Z-projection of *rpz5:mRuby* pLLg. Cell membranes are marked by *cldnB:memgfp* transgene. Note that only a subset of dorsal pLL neurons is mRuby-positive at 40 hpf. **(K)** Confocal image of the migrating pLL primordium from the same animal shown in **(J)**. Note the presence of mRuby-positive axons within the primordium (dashed outline) indicating that labeled pLL cells are indeed pioneer neurons. mRuby labeling dorsal to pLL primordium is muscle. All scale bars = 10 μ m. Schematic created with BioRender.com.

2.3.3 Posterior lateral line pioneer neurons are required for followers' axon extension

A typical behavioral characteristic of pioneer neurons is their ability to guide followers. To determine whether pLL pioneers are required for the followers' extension we used a two-photon cell ablation strategy to selectively remove pioneer neurons¹²¹. We utilized a transgenic line, TgBAC(*ret:EGFP*)^{b1331} (hereafter, *ret:EGFP*), to visualize *ret*-expressing pLL neurons at the onset of axon extension¹²² (Fig. 2-3A,B, S2-5A). At this stage, 2 to 5 pLL neurons begin expressing the transgene. We used this transgenic because, unfortunately, *rpz5:mRuby* fluorescence is not detectable until 24 hpf at earliest. *In situ* hybridization with the *ret* probe showed that the endogenous *ret* expression correlated well with *ret:EGFP* (65% EGFP+/*ret*+), and with brightest EGFP+ cells tend to also be the strongest expressers of *ret* (Fig. S2-5B,C). We ablated EGFP+ neurons between 22 and 24 hpf and tracked axon extension using *neurod1:mCherry* transgene for ~10 hours (Fig. 2-3A). In unablated controls, the pLL nerve migrated an average of 6.7 somites (Fig. 2-3B,C, Movie 1). In contrast, ablation of *ret:EGFP*+ neurons completely blocked pLL nerve extension. Interestingly, pLL axon terminals still displayed dynamic movements, but clearly lacked the ability to advance (Fig. 2-3D,E, Movie 2). When only a subset of *ret:EGFP*+ neurons were ablated, the pLL nerve extended comparably to controls, arguing that the ablation procedure per se does not inhibit pLL nerve extension (Fig. 2-3F,G, Movie 3, Table 1). It also showed that as few as two pioneer axons are sufficient for pLL nerve extension, a finding that has

been shown to be necessary for fasciculation in previous ablation studies¹³. These experiments, summarized in Table 1, demonstrate that pLL pioneers are required for the axon extension of followers.

Figure 2-3



2-3 pLL pioneer neurons are required for follower axon extension. (A) Schematic depicting ablation strategy. EGFP+ neurons were ablated at between 22 and 24 hpf and then imaged live using the confocal microscope. **(B)** Non-ablated pLLg at 22 hpf immediately before timelapse begins. **(C)** Stills from timelapse of the control embryo shown in **(B)** at 23 hpf **(C)** and 27.8 hpf **(C')**. **(D)** pLLg before and after **(D')** ablation of all 3 EGFP+ neurons. **(E)** Stills from timelapse recorded after complete ablation in **(D)**. **(F)** pLLg before and after ablation **(F')** of 3 out of 5 EGFP+ neurons. **(G)** Stills from timelapse recorded after partial ablation in **(F)**. White arrowhead = EGFP+ pLL neurons; yellow arrowhead = pLL nerve terminals. All scale bars = 20 μm. Schematic created with BioRender.com.

Table²⁻¹

Embryo	Condition	Axial change (23 - 28 hpf)
1	Nonablated	7
2	Nonablated	6
3	Nonablated	7
4	Nonablated	6
5	Nonablated	6
6	Nonablated	8
7	Nonablated	7
8	Complete	1
9	Complete	1
10	Complete	0
11	Complete	2
12	Complete	0
13	Partial	4
14	Partial	2

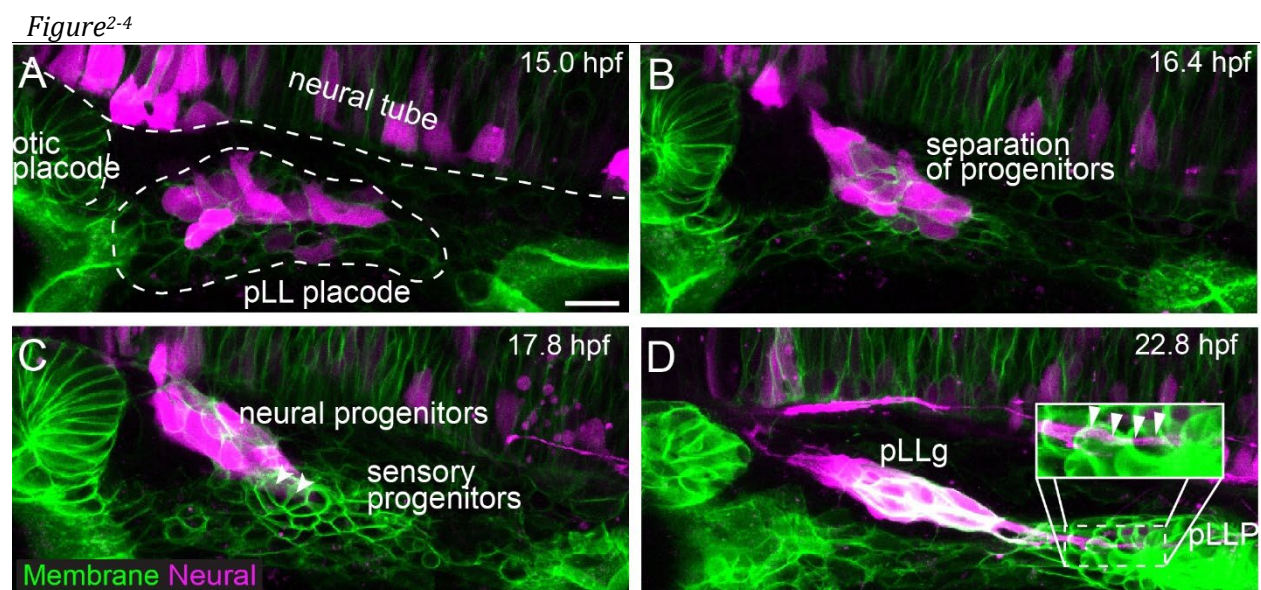
²⁻¹ **Table 1: Ret+ pioneer neurons are required for the pLL nerve extension.** Axial change = number of somites traveled along anterior-posterior axis by pLL nerve over time. Means between nonablated controls and complete ablations are statistically significant: $p = 0.0013$ (by Mann-Whitney non-parametric test).

To identify potential pLL pioneer specific signals that guide followers, we used the CellChat package to search for transmembrane cell-to-cell communications networks. We used pLLP cells as a positive control (Fig. S2-6A), as several signaling networks between extending pLL neurons and pLLP, including Ret-Gdnf and Ntrk1-Ngf, have been previously defined^{67,123}. Indeed, both receptor-ligand pairs were identified by CellChat (Fig. S2-6A,B). Ncam, Cadm3, and teneurin-latrophilin signaling had the highest communication probability of signaling between pioneers and followers (Fig. S2-6B-E). Notably, Cntn1b was the only pioneer-specific transmembrane molecule that had a follower specific partner (Fig. S2-6B-E). These findings highlight a set of candidate receptor-ligand interactions that may mediate pioneer-follower communication, with Cntn1b emerging as a uniquely pioneer-specific signal targeting followers.

2.3.4 Follower-specific markers define posterior lateral line neuron ground state

We next investigated cellular events leading to the diversification of pLL progenitors into pioneers and followers. We first visualized pLL neurogenesis via live imaging. We used the *cldnB:memgfp* transgene to label pLL placodal cells and Tg(*neurod:Zebrawow*)^{124,125} to

visualize pLL progenitors undergoing neurogenesis. Consistent with a previous report⁵⁰, neural (*neurod1+*) and sensory progenitors (*neurod1-*) were initially intermixed with the pLL placode at the onset of neurogenesis at 15 hpf (Fig. 2-4A; Movie 4). However, within a few hours *neurod+* cells delaminated from the pLL placode and migrated anterodorsally, whereas sensory progenitors moved caudally to form the pLL primordium (Fig. 2-4B, C). Concurrently, we observed extension of the first few pioneer neurites within the forming pLLP (Fig. 2-4C, D). Consistent with previous reports^{39,126}, we never observed cell divisions among *neurod+* cells, corroborating that neural pLL progenitors are post-mitotic at this stage.



2-4 Live imaging defines cellular events during pLL morphogenesis. (A-D) Stills from a timeseries (Movie 4) visualizing formation of the pLL system between 15 and 23 hpf. The pLL placode is marked by the *cldnb:memgfp* transgene and pLL progenitors undergoing neurogenesis are visualized by *Tg(neurod1:Zebrafish)*. The pLL placode, otic placode, and the neural tube are outlined by dashed lines. **(A)** At the onset of pLL neurogenesis (15 hpf), neural and sensory progenitors are intermixed within the pLL placode. **(B)** Neural and sensory progenitors are in a process of separating from the pLL ganglion and primordium, respectively. **(C)** Neural and sensory progenitors separate at 18 hpf, while neurites (arrowheads) from pLL progenitors project toward sensory progenitors. **(D)** At 22 hpf, pioneer axons (marked by arrowheads in the inset) extend with the migrating pLLP. Scale bar = 10 μ m.

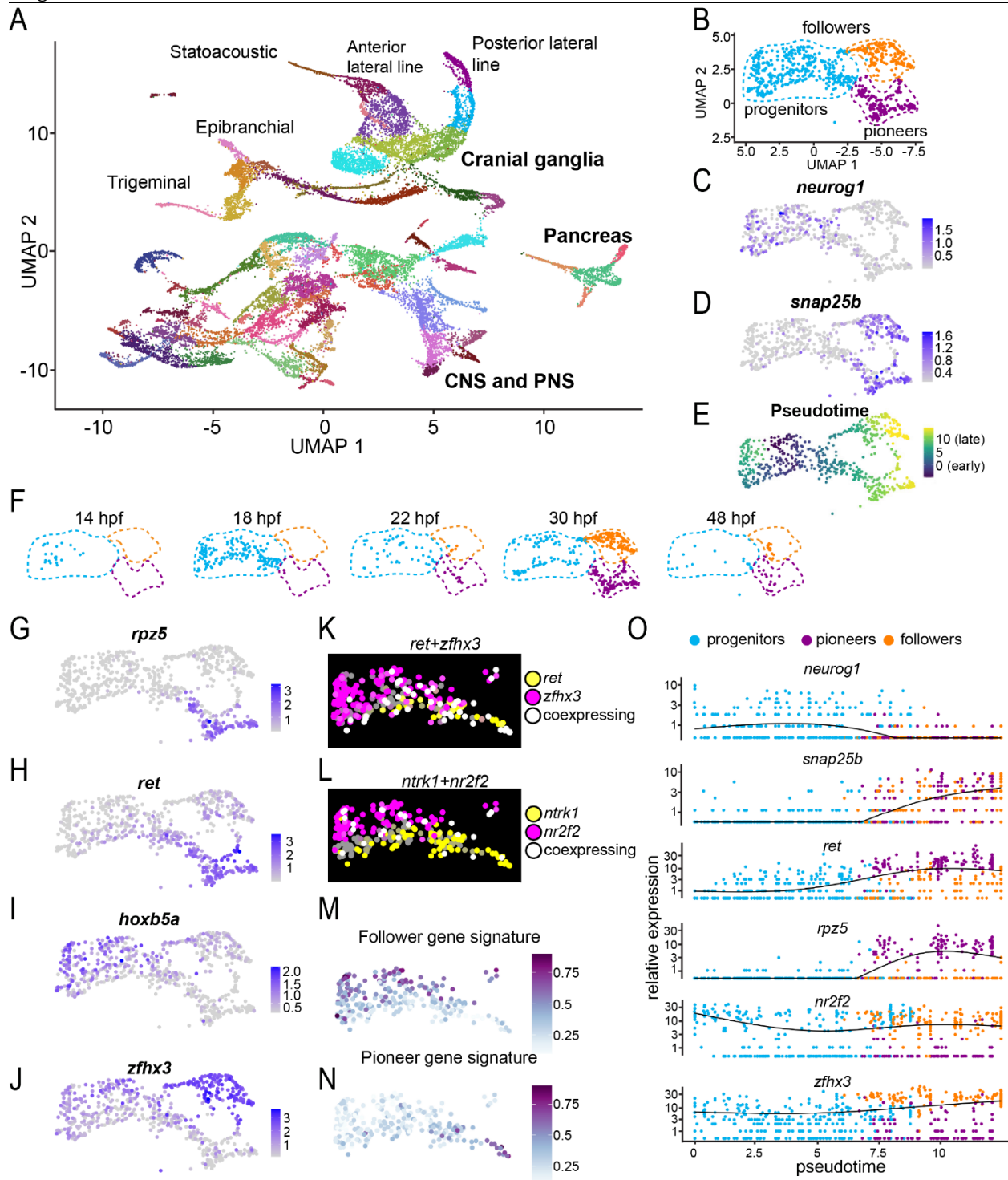
Live imaging identified several distinct steps in pioneer and follower neuron differentiation, including onset of neurogenesis (14-15 hpf), separation from sensory progenitors (18 hpf), and onset of active pioneer axon extension concurrent with the pLL primordium migration (22 hpf). Thus, we investigated pioneer and follower gene expression dynamics during these critical stages using scRNA-seq. We also included a 48 hpf timepoint

to assay whether gene expression differences between pioneers and followers persist after pioneer axon extension concludes. *neurod1:EGFP+* cells from 14, 18, and 22, and 48 hpf embryos were FAC sorted, sequenced, and combined with those from 30 hpf to identify pLL progenitors (Fig. 2-5A). Cranial ganglia, CNS and PNS, as well as pancreas were annotated using markers in Fig. S2-1. Closely clustered cells often reflect differentiation states of a particular lineage¹²⁷. Therefore, we subclustered cells that were closely associated with pLL neurons (Fig. 2-5B). Presence of *neurog1*^{47,54,89,128} (early neurogenesis marker) and absence of *snap25a*^{129,130} (differentiated neuron marker) indicates that this population represents undifferentiated neural progenitors^{128,131} (Fig. 2-5C,D). Trajectory inference applied to the scRNA-seq profile of pLL neurons supported this finding¹³² (Fig. 2-5E). Consistently, all 14 hpf cells clustered within the progenitor population, whereas differentiated clusters of pioneers and followers were dominated by cells from 30 and 48 hpf (Fig. 2-5F).

To analyze expression dynamics during pLL neurogenesis, we examined pioneer (*rpz5* and *ret*) and follower (*hoxb5a* and *zfhx3*) markers (Fig. 2-5G-J). Follower markers were expressed in most pLL progenitors at 14, 18 and 22 hpf (Fig. 2-5I,J). In contrast, pioneer markers were largely excluded from 14 hpf, and were expressed by only a small number of cells at 18 and 22 hpf (Fig. 2-5G,H). Interestingly, we noted a number of *neurog1*-positive progenitors at 30 hpf (Fig. 2-5F). These presumably represent previously described, later born neurons innervating secondary trunk NMs after 2 dpf¹²⁶. As these late progenitors do not contribute to pioneer neurons, we focused our analysis on 14, 18, and 22 hpf stages. Co-expression analysis revealed a number of cells containing both follower and pioneer markers at these three stages (Fig. 2-5K,L), potentially indicating a transitional state. To more broadly analyze expression of pioneer and follower genes at these early stages, we generated pioneer and follower marker genes signatures (top 20 upregulated genes at 30 hpf in each population) using the AddModuleScore function in Seurat. The follower gene signature was present broadly in cells from early timepoints (Fig. 2-5M), while the pioneer gene signature was present only in a few 22-hour cells at the end of the differentiation trajectory (Fig. 2-5N). Consistent with these observations, follower gene expression was maintained at similar levels over time, initially in progenitors and then in followers, whereas pioneer genes were upregulated during later stages of neurogenesis (Fig. 2-5O). Finally, we observed that

transcriptional differences between pioneers and followers persisted at 48 hpf, after the initial axon extension concluded (Fig. 2-5F). Altogether, these experiments showed that follower-specific markers are expressed in early differentiating pLL progenitors, defining the pLL ground state. They also suggested that pioneers are a later developmental state derived from follower progenitors. We also concluded that pioneers and followers maintain their distinct transcriptional profiles after pioneer axon extension is completed.

Figure 2-5



2-5 **follower is a transcriptional ground state of pLL progenitors. (A)** UMAP plot of all cells derived from 14, 18, 22, 30, and 48 hpf *neurod1:EGFP* embryos. Major cell types are indicated. **(B)** UMAP of the pLL progenitors, pioneers, and followers. **(C,D)** Feature plots showing neurogenesis marker, *neurog1*, and neural differentiation marker, *snap25b*. **(E)** Trajectory inference plot showing the predicted differentiation trajectory which is consistent with the expression of the neurogenesis and differentiation markers in **(C,D)**. **(F)** UMAP plot of pLL progenitors, pioneers, and followers grouped by timepoint. The pLL cell counts by

timepoint are as follows: 14 hpf, 23; 18 hpf, 167; 22 hpf, 67; 30 hpf, 340; 48 hpf, 50 cells. **(G,H)** Pioneer markers *rpz5* and *ret* are mainly expressed in pioneers, and not in progenitors. **(I,J)** Follower markers *hoxb5a* and *zfhx3* are expressed both in the progenitor and follower populations. **(K,L)** Feature plots showing coexpression of pioneer (*ret* or *ntrk1*) and follower (*zfhx3* or *nr2f2*) genes during differentiation (14 - 22 hpf). Note that a subset of cells coexpress a pioneer and follower markers at these stages (white cells): 25 cells co-express *ret* and *zfhx3*; 25 cells co-express *ntrk1* and *nr2f2*. Low expression cut off is set at 3 UMI per cell. **(M,N)** Gene signature plots of cells between 14 and 22 hpf. Follower gene signature is present broadly at earlier stages, while pioneer gene signature is strongest in cells from 22 hpf. **(O)** Gene expression over time as cells differentiate from progenitors to followers or pioneers. Note that follower gene expression is similar across stages, whereas pioneer genes are upregulated during later differentiation stages.

2.3.5 Pioneer precursors exhibit distinct cellular behavior

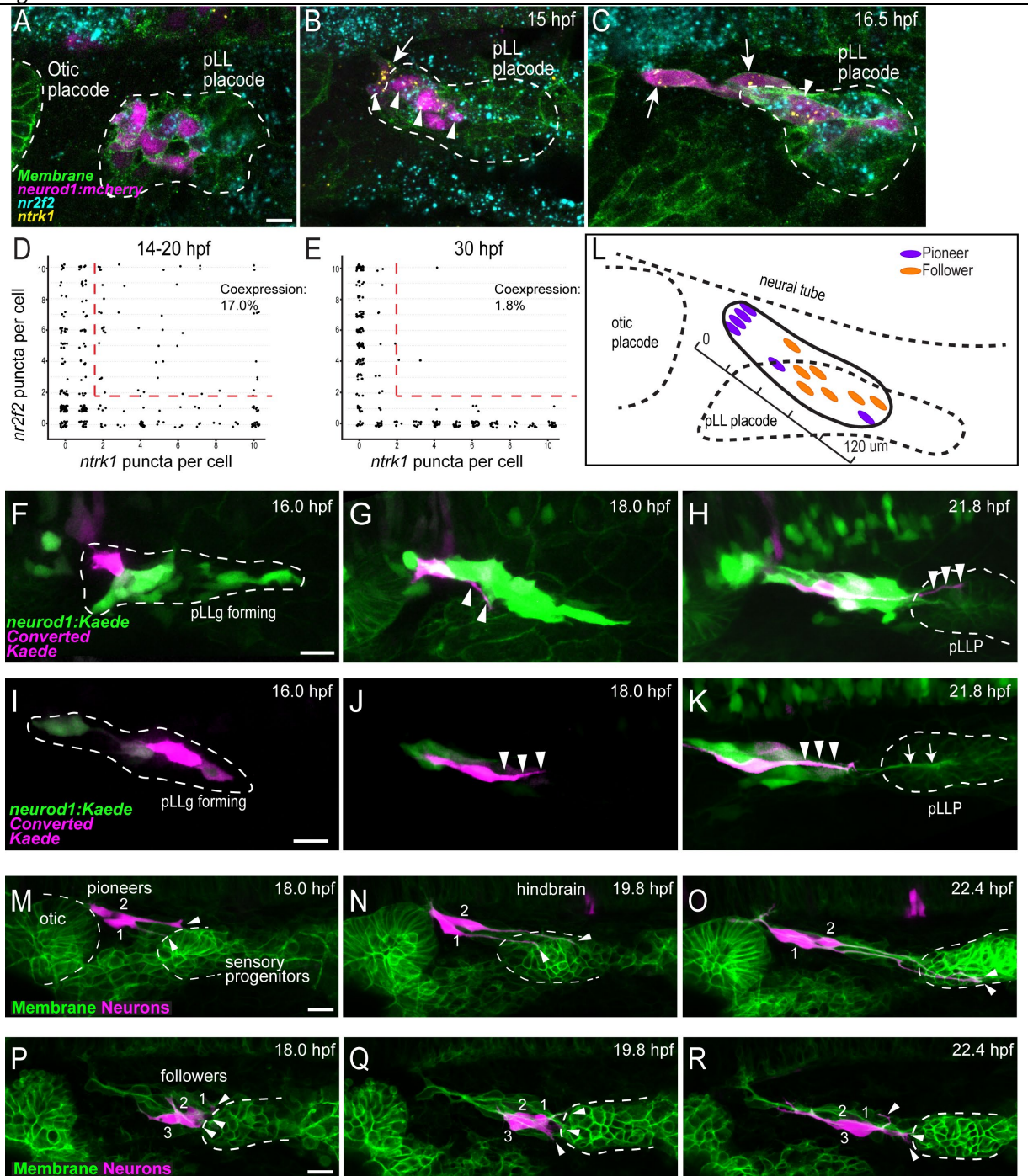
To identify pioneer precursors and to confirm the presence of a follower-to-pioneer transitional state *in vivo*, we used FISH to visualize expression of pioneer (*ntrk1*) and follower (*nr2f2*) genes at early timepoints, between 14 and 17 hpf (Fig. 2-6A-C). The *cldnB:memgfp* transgene marks pLL placode membranes and the *neurod1-5kb:mCherry* transgene marks pLL progenitors undergoing neurogenesis. Consistent with scRNA-seq, mCherry-positive neuroblasts expressed *nr2f2* but not *ntrk1* at the onset of neurogenesis (Fig. 2-6A). Within the next two hours (15-17 hpf), we observed a few *ntrk1*⁺ but *nr2f2*⁻ cells in the process of delamination from the placode (cells marked by arrows in Fig. 2-6B,C). At the same time, we also noted a several cells within the placode that coexpressed both *ntrk1* and *nr2f2* (cells marked by arrowheads in Fig. 2-6B,C). Overall, 17.0% of cells coexpressed *ntrk1* and *nr2f2* between 14 and 20 hpf (Fig. 2-6D), whereas at 30 hpf coexpression was rare, at 1.8% (Fig. 2-6E). These observations imply that pioneer neuron precursors delaminate first from the pLL placode after undergoing a transition from a follower ground state.

To observe this process in real time, we marked leading delaminating cells by photoconversion in the *Tg(neurod1:Kaede)ⁿ¹²⁹* (hereafter, *neurod1:kaede*) transgenic line and followed these cells by live imaging to visualize their axon terminals (Fig. 2-6F-H; Movie 5). Indeed, marked cells always became pioneer neurons (n = 4 of 4 cells; Fig. 2-6H). We next marked cells within the more distal region of the pLL placode. As evident by their axons lagging behind the pLLP (Fig. 2-6I-K; Movie 6), the majority of these cells became followers (n = 7 of 9 cells; Fig. 2-6L).

We also used an alternative method to visualize both differentiating pioneer and follower precursors. We injected one-cell stage *cldnB:memgfp* embryos with a

neurod:mCherry construct. Since the incorporation of plasmid during development is stochastic, we screened for embryos with *mCherry* expressed mosaically in just a few pLL cells to visualize cellular morphology and behavior. Differentiating pLL neurons exhibited two distinct behaviors. One subset of neurons rapidly changed their morphology by 17-18 hpf to spindle-like and extended a peripheral neurite that invaded the field of differentiating sensory progenitors (Fig. 2-6M-O; Movie 7). These neurites remained within the field of sensory pLL progenitors, and tracking these neurons over time identified them as pioneers (Fig. 2-6O; Movie 7). Interestingly, pioneer precursors were positioned antero-dorsally, consistent with our previous observation that these cells delaminate first. In contrast to pioneers, follower precursors exhibited a dynamic multipolar morphology until late neurogenesis (Fig. 2-6P-R; Movie 8). At ~20 hpf, they began extending their peripheral neurites; however, they never invaded the field of sensory progenitors (Fig. 2-6P; Movie 8). These cells were positioned posteroventral to pioneers and close to sensory progenitors, presumably due to delaminating later than pioneers. Overall, these data suggest that pioneer precursors first undergo a transitional state, followed by upregulation of *ntrk1* and delamination. During this process, pioneer precursors attain bipolar morphology and extend their peripheral neurites well before the same occurs in follower precursors.

Figure 2-6



2-6 Pioneer precursors exhibit distinct cellular behavior. (A-C) A single confocal Z-slice through the pLL ganglion labeled with FISH probes against *ntrk1* (yellow) and *nr2f2* (cyan) between 14 and 16.5 hpf. Cell membranes are labeled by *cldnB:memgfp*, whereas pLL neuroblasts are marked by *neurod1:mCherry*. Dashed line outlines pLL and otic placodes. Arrows mark leading tip cells upregulating pioneer marker *ntrk1*. Arrowheads mark neuroblasts co-expressing *ntrk1* and *nr2f2*. (D,E) Quantification of *ntrk1* and *nr2f2* expression between 14 and 20 hpf (D) or 30 hpf (E). Dashed red lines indicates cells that coexpress both markers. Note the significant number of co-expressing cells at 14-20 hpf (51/300 cells: 17%) compared to

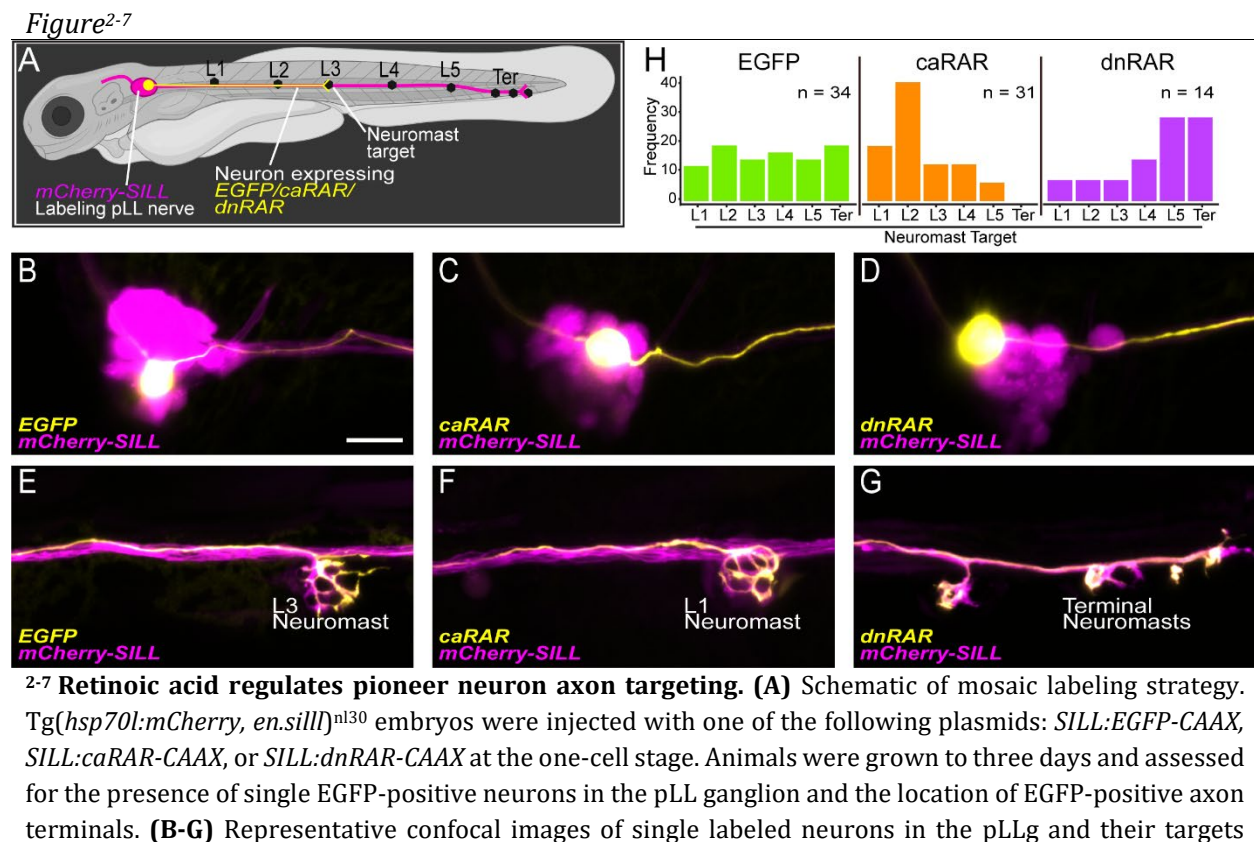
30 hpf (n = 5/285 cells: 1.8%) stages: $p < 0.001$, Chi-Square test. **(F-H)** Stills from a time series using *neurod1:kaede* photoconversion at 16 hpf. (F-H) The first delaminating tip cell was photoconverted and followed over time to visualize its peripheral axon. The converted neuron projected its axon into the pLLP, consistent with pioneer axon behavior. Arrowheads = photoconverted axons, arrows = pioneer axons. **(I-K)** A photoconversion of a proximal cell. The labeled neuron projected its axons later and did not invade the pLLP, identifying it as follower. Arrowheads = photoconverted axons, arrows = pioneer axons. **(L)** Schematic summary of photoconversions at 16 hpf. Cell location shows the region where it was photoconverted, and color indicates if it became pioneer or follower. When the delaminating tip cell was labeled by photoconversion, it became a pioneer 4 of 4 times. When distal cells were labeled, 7 of 9 became followers, and the remaining cells became pioneers. **(M-O)** Stills from a timeseries of two individually labeled neurons between 17 and 25 hpf. **(L)** The neurons, located anterodorsally, appear spindle-shaped with early neurite projections. **(N)** Their pioneer neurites localize within the pLLP. **(O)** Pioneer neurons extend their axons with the primordium as it begins migrating. Pioneer neurites marked by arrowheads. Membrane = *cldnB:memgfp* (green). **(P-R)** Stills from a timeseries of three individually labeled neurons beginning at 17 hpf. **(P)** The neurons appear more rounded when compared to pioneer precursors at this stage. **(Q)** Notably, the neurites did not extend into the pLLP. **(Q)** At 22 hpf, the follower neuron cell bodies display spindle-like morphology, but their neurites lag behind the migrating primordium. Follower neurites marked by arrowheads. Membrane = *cldnB:memgfp* (green). For experiments shown in (M-R), we imaged 7 embryos that contained 4 pioneers and 7 followers. All scale bars = 20 μ m.

2.3.6 Downregulation of retinoic acid is required for proper pioneer axon targeting

We next sought to examine molecular signals that regulate pioneer and follower neuron differentiation. Because pioneer precursors appear to undergo a transitional state where follower genes are downregulated, we searched for a pathway that was active in early pLL progenitors but absent in pioneers. We noted that RA pathway member *crabp1b*¹⁰¹ and known transcriptional targets of RA in other systems, *hoxb5a*, *nr2f2*, and *zfhx3*^{102,114-116}, were expressed in pLL progenitors between 14 and 22 hpf (Fig. 2-5I,J,O, and S2-7). Interestingly, scRNA-seq also showed that the pathway continued to be active in followers, but not pioneers, during axon extension stages (Fig. 2-5I,J,O). Thus, we asked whether *hoxb5a*, *nr2f2*, and *zfhx3* act downstream of RA signaling in the pLL neurons. To address this, we mosaically overexpressed either constitutively-active RAR (caRAR-2A-EGFPCAAX, hereafter caRAR) or dominant-negative RAR (dnRAR-2A-EGFPCAAX, hereafter dnRAR) constructs and evaluated animals with individually labeled neurons for expression of these three genes at 30 hpf (Fig. S2-8A-F). Modulation of RA signaling had no significant effect on *nr2f2* or *zfhx3* levels; in contrast activation of RA increased and inhibition of RA decreased *hoxb5a* levels,

respectively (Fig. S2-8G-J). These results show that *hoxb5a* is, and *nr2f2* and *zfhx3* are not, RA targets in the pLL neurons.

Next, we asked whether RA signaling plays a role in pioneer neuron differentiation. We used the same strategy to mosaically overexpress caRAR, dnRAR, or EGFP-CAAX control and evaluated animals with individually labeled neurons for pLL axon targeting at 72 hpf as a proxy for pioneer differentiation (Fig. 2-7A, B-G). Control neurons expressing EGFP-CAAX projected randomly between L1 and terminal cluster NMs (Fig. 2-7H). When the RA pathway was activated via caRAR expression, we observed a striking shift toward proximal neuromasts (Fig. 2-7F,H), which are known to be targets of follower neurons^{47,83,86}. Notably, none of these labeled neurons projected to the terminal cluster, targeted by pioneers. By contrast, when RA signaling was repressed using dnRAR, the axons tended to innervate distal NMs (Fig. 2-7H). This bias in axon targeting indicates that active RA signaling within pLL neurons promotes innervation of follower targets. Further, the attenuation of RA signaling biases neurons towards innervation of pioneer targets.

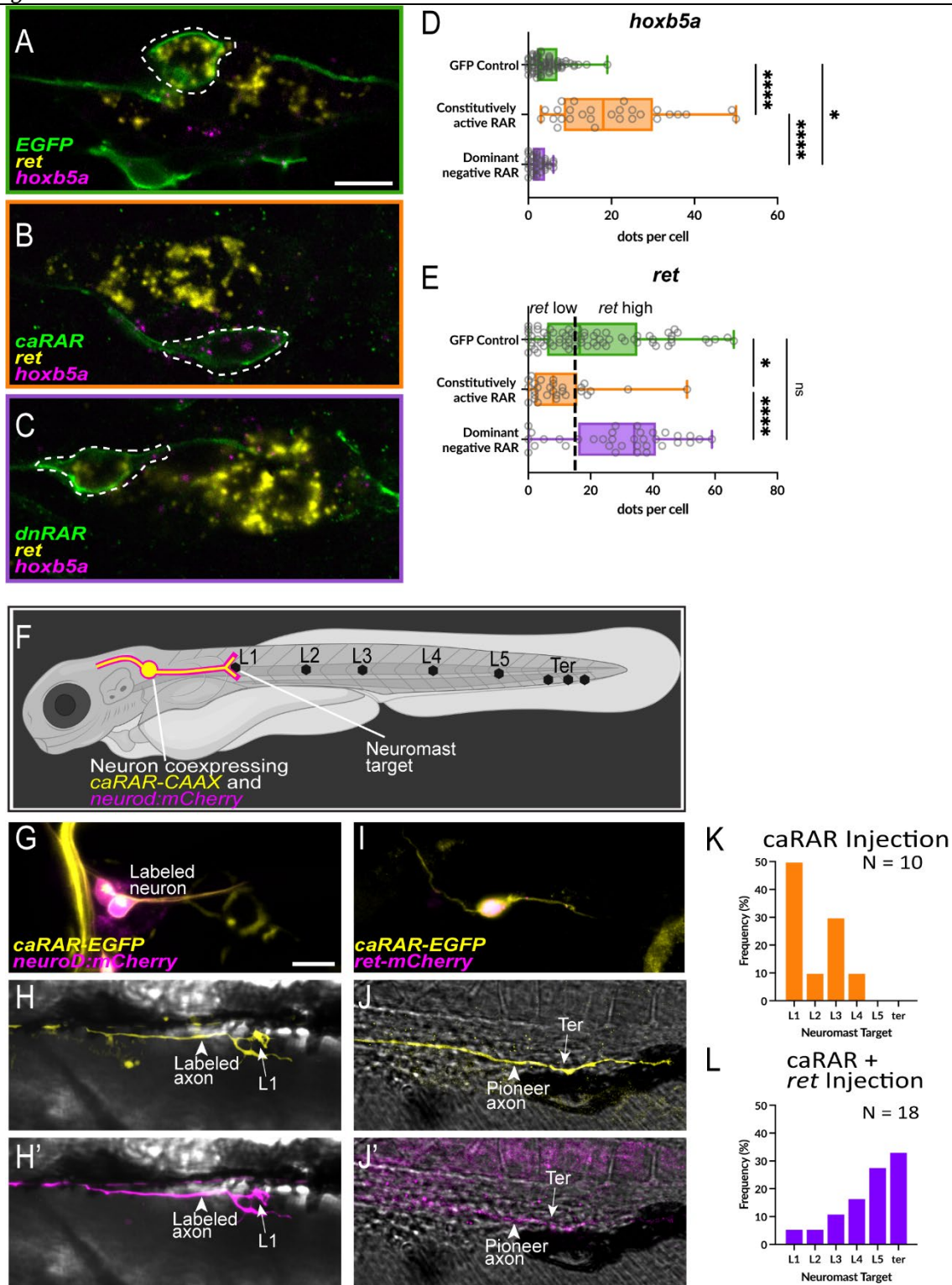


following overexpression of *EGFP* (B,E), *caRAR* (C,F), or *dnRAR* (D,G). (H) Frequency of neuromast targeting along zebrafish trunk by neurons labeled with *EGFP*, *caRAR*, or *dnRAR*. Difference in axon targeting assessed by Chi-Square: *EGFP* vs. *caRAR* $p = 0.0011$; *EGFP* vs. *dnRAR* $p = 0.0795$; *caRAR* vs *dnRAR* $p = 0.0001$. All images are lateral views with anterior to left. Scale bars=20 μm . Schematic created with BioRender.com.

2.3.7 Retinoic acid negatively regulates *ret* and is critical for correct pioneer neuron axon targeting

We next set out to identify a mechanism by which RA directs pLL axon targeting. Our previous study showed that the neurotrophin factor receptor *ret* regulates pLL axon extension. *ret* mutant embryos exhibit a nerve truncation phenotype, such that proximal NMs are innervated normally but most terminal NMs are not⁴⁶. Accordingly, we explored whether RA regulates *ret* expression in pLL neurons. Using the same strategy, we mosaically overexpressed EGFP (control), *caRAR*, or *dnRAR*. We then fixed these embryos at 30 hpf and performed FISH to measure levels of *ret* and *hoxb5a* (positive control) in EGFP-positive neurons (Fig. 2-8A-E). As expected, *hoxb5a* became almost undetectable in neurons expressing *dnRAR*. Conversely, RA activation by *caRAR* significantly increased expression of *hoxb5a* (Fig. 2-8A-D). In EGFP expressing controls, we observed two groups of *ret*-expressing cells: *ret* high and *ret* low, which are presumably pioneers and followers, respectively (Fig. 2-8E). However, neurons expressing *caRAR* had comparably lower levels of *ret* (Fig. 2-8B, E). By contrast, neurons expressing *dnRAR* had high levels of *ret* (Fig. 2-8C,E). We next asked whether RA regulates *ret* expression through Hoxb5a. To disrupt *hoxb5a*, we injected a combination of three CRISPR guides targeting the *hoxb5a* locus (Fig. S2-9A). Oxford Nanopore sequencing of the *hoxb5a* locus in the injected embryos revealed that the biallelic knockdown frequency was 99.32% (individual guide frequency were 73, 93, and 82%; Fig. S2-9A). We found that *ret* expression was significantly increased in *hoxb5a* crisprants at 30 hpf (S2-9B,C). Altogether, these results demonstrate that RA signaling, through Hoxb5a, negatively regulates *ret* levels in pLL neurons.

Figure 2-8



2-8 Retinoic acid negatively regulates *ret*. (A-C) Representative single confocal Z-slices of pLL ganglia that express EGFP (A), *caRAR* (B), or *dnRAR* (C) in single cells (dashed outlines). Expression of *ret* (yellow) and *hoxb5a* (magenta) was assessed by FISH. (D and E) Quantified expression levels of *hoxb5a* and *ret* after injection of RAR constructs. Nonparametric Kruskal-Wallis test values are shown on plots: * = $p < 0.05$; ****

= $p < 0.0001$. **(F)** Schematic of mosaic labeling using coinjection of two constructs: *caRAR-2A-EGFP* and *mCherry* (control) or *caRAR-2A-EGFP* and *ret-mCherry* driven by *neurod1* promoter. Following injection, embryos were screened at 72 hpf for the position of colabeled axon terminals. **(G,H)** Confocal image of the neuron cell body **(G)** and its axon terminal (L1) labeled by *caRAR* and *mCherry* **(H,H')**. **(I,J)** Confocal image of the neuron cell body **(I)** and its axon terminal (terminal NMs) labeled by *caRAR* and *ret-mCherry* **(J,J')**. **(K,L)** Frequency of NM targeted by labeled neurons coexpressing either *caRAR-2A-EGFP+mCherry* (N=10 embryos) or *caRAR-2A-EGFP+ret-mCherry* (N=18 embryos): $p = 0.0002$, Chi-square test. One cell was labeled in each embryo. All images are lateral views with anterior to the left. Scale bars = 20 μm . Schematic created with BioRender.com.

Previous studies have shown that RA and Fgf signaling pathways can antagonize each other during development^{51,63-66}. To determine whether this interaction occurs in the pLL during neuronal specification, we treated embryos with 50 μM SU5402, a well-characterized Fgf receptor inhibitor¹³³, between 10-18 or 10-22 hpf and assayed for *ret* and *hoxb5a* expression (Fig. S2-10A-D). While *hoxb5a* was unchanged, *ret* expression was increased at 18 hpf, but not at 22 hpf (Fig. S2-10E-H). Thus, while Fgf signaling regulates *ret* expression during early stages of the pLL development, it appears to do so independently of RA.

Based on the axon targeting bias resulting from RA modulation (Fig. 2-7H) and the corresponding change in *ret* expression, we asked whether *ret* acts downstream of RA to direct pioneer axon targeting. To test this, we again used mosaic overexpression and compared axon targeting of pLL neurons expressing *caRAR* and *mCherry* to neurons expressing *caRAR* and *ret-mCherry*⁴⁶ (Fig. 2-8F). In *caRAR;mCherry* neurons (Fig. 2-8K), similarly to Figure 7 we observed a dramatic increase in neurons projecting toward proximal targets (Fig. 2-8G,H,K) while none projected beyond NM L4. Overexpression of *ret-mCherry* with *caRAR* was able to repress this effect: these neurons exhibited a strong bias toward distal targets (Fig. 2-8I,J,L). These experiments demonstrate a mechanism by which RA regulates innervation by peripheral pLL axons: high levels of RA will direct axons towards proximal sensory organs, whereas low RA signaling directs pioneer axons to the distal sensory organs via neurotrophin factor receptor *ret*.

2.4: Discussion

2.4.1 Summary and significance of study

The term “pioneer neurones” was first coined in 1976⁴. Since then, they have been the subject of intense research investigating their unique characteristics. While their morphological and behavioral characteristics have been described in many model systems, molecular analysis has proved challenging without genetic tools that specifically label pioneers. Accordingly, whether pioneers constitute a molecularly distinct cell type from followers has not been shown. Here, we demonstrate that pioneers exhibit a unique transcriptional profile that underlies at least some of their behavioral differences, specifically, navigation through tissue towards targets distinct from followers. We also find that pioneers in the pLL are derived from a pool of neural progenitors with a follower ground state. Finally, we show that modulation of RA signaling biases axonal innervation of pLL neurons toward pioneer or follower targets. Collectively, this evidence argues that pLL pioneer and follower neurons are indeed two molecularly distinct cell types.

2.4.2 Do neurons retain molecular differences over time, once wiring is complete?

Are pLL pioneers and followers just transient neuron identities or do their differences persist beyond developmental stages? Our analyses are focused on dynamics between 14 (early neurogenesis) and 48 hpf (end of axon extension). However, previous studies have identified that there are two physiologically distinct circuits in the pLL: one innervating distal, tail neuromasts (large caliber, fast conducting pioneers), and the other of more proximal neuromasts (innervated by small caliber, slower conducting followers)^{45,47}. This is not surprising, as there are mechanical differences in hydrodynamics between the tail, where water flow is quicker, and the trunk, where flow is steadier¹³⁴. Accordingly, patch clamp recordings show a higher level of stimulation is required in distal neuromasts (L5) compared to proximal neuromasts (L2)⁴⁵. In conclusion, the molecular differences we identified, combined with the distinct physiological properties of circuits wired by pioneers

and followers, support the idea that pLL pioneers and followers maintain distinct identities even after mature circuits are established.

2.4.3 Is pioneer cell state molecularly distinct in other systems?

We were able to transcriptionally separate pioneers and followers in the pLL into distinct subpopulations. In the case where pioneer neurons set up the initial innervation pattern, is there evidence in other systems where pioneers and followers are discrete cell types? One argument in favor of this idea is the result of ablation or replacement experiments demonstrating that followers cannot compensate for pioneer function in other systems. In the pLL, *ret* mutant embryos exhibit a nerve truncation phenotype, as the nerve fails to extend to the tail and stops about 2/3 down the trunk⁴⁶. Our studies further explored this dependency on pioneer axon tracts using ablation (Fig. 2-3). Similar results have been shown in the *Drosophila* ventral nerve cord¹³, zebrafish spinal neurons^{17,18}, and mammals^{20,21}. Thus, multiple studies lend credence to the notion that pioneer neurons have a unique molecular profile that equips them with abilities absent from follower neurons.

2.4.4 A model of pioneer versus follower lineage specification

We found that the transcriptional profile of pLL progenitors is strikingly similar to followers: progenitors express a number of genes that then persist in follower neurons during later stages. The pioneer transcriptional state, on the other hand, appears to be acquired after pLL neuroblasts exit the pLL placode. Live imaging experiments showed that the cells fated to become pioneers tend to delaminate from the pLL placode first and take on a spindle-like morphology. These cells also migrated anterodorsally and were the first to exhibit detectable expression of pioneer marker *ntwk1*. The reproducible, spatiotemporal specification of pioneers suggests that instructive signaling occurs early during neurogenesis. However, it is unknown whether it is an external signal which induces pioneer fate, or an inhibitory signal produced within the placode that pioneer precursors escape while delaminating.

One potential candidate is FGF. For example, the neural tube secretes Fgf ligands that are required for the induction of the otic and epibranchial placodes at this stage^{23,59,135}. Given

the close proximity and direction of pioneer precursor migration, it is possible they are exposed to these ligands. In support of this idea, we found that Fgf signaling is required for expression of *ret*, an early pioneer marker (Fig. S2-10). Additionally, Fgf and RA form countervailing gradients to regulate neural^{63,136} and pLL induction⁵¹. Of note is how RA and Fgf work in antagonism to control the timing of neural crest cell emigration in chick embryos¹³⁶. In the pLL however, it is unknown which molecular cues drive delamination of neuroblasts. At the stages we investigated a countervailing Fgf/RA gradient does not seem to be evident, as the inhibition of the Fgf signaling does not affect *hoxb5a*, a transcriptional target of RA.

One signal that is known to specify pLL placodal progenitors into either sensory or neural cell types is Delta/Notch signaling⁵⁰. Delta is a well-established neurogenic driver⁵³⁻⁵⁵, and is required for motility of pioneer growth cones in *Drosophila*¹³⁷. Considering this, Delta/Notch, or another cell-cell signaling system, could play a similar role in specifying pioneer vs. follower states during pLL progenitor differentiation. Future studies will uncover signaling mechanisms that specify pioneers from the progenitor ground state.

2.4.5 Regulation of the pLL pioneer development by retinoic acid

During development, RA is required for the formation of the pLL placode⁵¹. Thus, it is not surprising that RA is active in all pLL progenitors. We also found that RA downregulation in maturing pLL neuroblasts is necessary for expression of at least one pioneer gene, *ret*, which in turn is required for proper innervation of pioneer targets (Fig. 2-8). Finally, we show that *Hoxb5a* regulates *ret* expression (Fig. S2-9). This raises the question of the specific mechanism leading to downregulation of RA in pioneers. RA is produced in paraxial mesoderm during somitogenesis and acts as a morphogen that controls A-P embryonic patterning, primarily through the transcriptional regulation of Hox genes^{51,93,113,114,138}. However, the population of neural pLL progenitors is relatively small (~20 cells) at the time of differentiation; thus, it seems unlikely that a substantive morphogenic gradient could be established in such a confined space. In addition, neural progenitors within the pLL placode are not uniformly distributed (Fig. 2-4A)⁵⁰, further complicating the notion of morphogen-based instruction in this system. Instead, pioneer precursors may actively downregulate

intracellular RA signaling as they exit the pLL placode. The mechanisms by which RA is differentially regulated in pLL pioneer and follower neurons will be addressed in further studies.

Downregulation of RA in pioneers is necessary for expression of *ret*, which is required for correct pLL axon targeting. Our analysis points to Ret as a crucial factor in axon targeting as overexpression of Ret is sufficient to suppress RA activation in pLL neurons. This implies that, in this particular context, Ret is an RA target. However, it remains unclear to what extent RA might more broadly command pioneer cell fate. RA typically has many transcriptional targets, so it is plausible that pioneer genes are expressed as a result of RA pathway downregulation. One interesting alternative is potential regulation of pioneer genes by Ret via retrograde signaling. It is known that in pLL axons, activated Ret is retrogradely transported to the cell body where it can regulate gene transcription⁴⁶. It is possible, then, that Ret initiates a larger signaling cascade to activate a pioneer-specific genetic program. More studies are necessary to uncover whether pioneer cell fate is regulated by modulation of RA. Alternatively, inhibition of RA may specifically regulate pioneer axon targeting, but not specification.

It appears that the function of RA signaling – to inhibit axon extension – is conserved in at least one other developmental context¹⁰⁰. The first neurons to innervate pharyngeal arches, vagal pioneer motor neurons, are regulated by a receding wave of RA such that the timing of expression of key axon outgrowth genes is initiated by RA decline¹⁰⁰. In this system, RA recession resulted in vagal neuron expression of neurotrophin receptor *met*, and this allowed the axons to respond to target-derived hepatocyte growth factor (HGF) in the pharyngeal arches. Thus, in both systems, neural precursors require the downregulation of RA to commence axon outgrowth.

2.4.6 Summary

In summary, our work reveals that pLL pioneer neurons display significant molecular differences from followers. Importantly, general features of pioneer behavior and morphology are conserved in many systems. However, whether this translates into transcriptional similarity between pioneers in different systems is yet to be determined. Our

work provides a foundation for identification of mechanisms by which pioneer neurons arise and how they are specified, which will be relevant to our understanding of pioneer neurons more broadly. Finally, identifying the main factors regulating pioneer neuron fate commitment and differentiation will create a list of novel therapeutic targets for studies involving nerve injury and regeneration.

2.5: Materials & Methods

Zebrafish husbandry

Adult zebrafish were maintained at 28.5°C. Embryos were derived from natural matings and were raised in embryo medium either at 28.5°C (standard) or at 23.5°C (to slow development). Embryo staging was conducted according to Kimmel et al. 1995⁴⁰. Strains utilized in this study were *AB, TgBac(*neurod1:EGFP*)^{nl1}, Tg(-8.0 *cldnB:LY-EGFP*)^{zf106}, TgBAC(*ret:EGFP*)^{b1331}, Tg(*rpz5:mRuby*)^{nl27}, TgBAC(*neurod1:mCherry*)^{nl28}, Tg(*prim:lyn2-mCherry*)⁸⁸, Tg(*neurod1:kaede*)^{nl29}, and Tg(*hsp70l:mCherry, en.silll*)^{nl30}.

Embryo dissociation

TgBac(*neurod1:EGFP*)+ embryos were dissociated following a modified version of the protocol from the Lawson lab¹³⁹. Briefly, 1.2 mL of protease solution (0.25% trypsin, 1 mM EDTA, pH 8.0 in PBS) was warmed in a 24-well plate at 28.5°C for 10 minutes. Embryos were then transferred to a 1.5 mL tube and embryo media was removed and replaced with 100 µL of calcium-free Ringer's solution. Embryos were deyolked by gentle pipetting 15 times with a p200, then transferred to the warmed protease solution. 27 µL of Collagenase P/HBSS (160 U/mL) was added followed by pipette mixing. Plates were incubated at 28.5°C for 15 minutes with trituration every 5 minutes by pipetting with a p1000. Digestion was halted by addition of 6x stop solution (30% calf serum, 6 mM CaCl₂, PBS), and the entire volume of each well was transferred to a microcentrifuge tube. Tubes were spun at 350xg at 4°C for 5 minutes and supernatant was removed. The cell pellet was rinsed by adding 1 mL chilled suspension solution (1% FBS, 0.8 mM CaCl₂, 50 U/mL penicillin, 0.05 mg/mL streptomycin, DMEM) and then spun down again at 350 x g at 4°C for 5 minutes; the by supernatant was removed. The cell pellet was resuspended in 700 µL suspension solution and passed through a 40 µm cell strainer into a FACs tube on ice.

FACS

Dissociated cells were sorted based on EGFP fluorescence and gated such that only the top 2% brightest EGFP+ cells were collected for analysis for 30 and 48 hpf. Cells were sorted into 50 µL 1xPBS/2% BSA in siliconized microcentrifuge tubes. Cell suspension was spun down at 350xg at 4°C for 5 minutes and the top 50 µL was removed to enrich for viable cells.

Single Cell RNA Sequencing

EGFP+ cells from, on average, 50-100 dissociated embryos were used to create scRNA-seq libraries with Single Cell 3' v3 (10X Genomics) gene expression kits following manufacturer protocol. Samples were sequenced targeting approximately 50,000 reads per cell. Reads were aligned to GRCz11 using Cell Ranger version 3.1.0 (10X Genomics). Primary analysis was performed using Seurat v4¹⁴⁰. Cell containing droplets were filtered to retain cells with: 1,000-75,000 UMI counts, 1,900-9,000 unique genes expressed and less than 5% mitochondrial RNA. After quality control filtering we retained: 1759 for 14 hpf; 10136 for 18 hpf dataset; 1378 for 22 hpf dataset; 9242 for two 30 hpf datasets; and 2107 for 48 hpf data set¹⁴¹. All data sets, except one 30 hpf data set¹⁴², were generated for this study. The pLL cluster was identified by expression of known lateral line markers but lack of marker expression of other cranial sensory neurons (*irx1a* and *phox2bb*) as well as anterior lateral line neurons (*alcama*). This cluster was then subjected to unsupervised subclustering, which yielded two distinct subpopulations, one of which was enriched for *ret*. Trajectory inference of pLL neurons from 14, 18, 22, 30, and 48 hpf was performed using Monocle3 with default parameters, with trajectory inference rooted (originating) at the pLL cell with the highest normalized *neurog1* expression.

Differential Expression and Gene Signature Analysis

To identify genes enriched in pioneer or follower pLL neuron subpopulations, we performed a differential expression (DE) analysis with a minimum difference threshold set at 25% and FDR < 5% using the 'FindMarkers' function of Seurat. This analysis yielded 101 genes: 60 expressed in pioneers, 41 in followers. Genes with an average log₂ fold change >0.7 and p value below 1x10⁻⁵ were considered enriched (20 enriched pioneer genes, and 7 enriched follower genes).

We used the Seurat function AddModuleScore to create gene signatures for pioneers and followers. Each signature consisted of top 20 DE gene at 30 hpf (sorted by log₂ fold change). The range of expression of each signature was normalized from 0 to 1 in order to visualize both signatures on the same scale (Fig. 2-5M,N).

Fluorescent in situ hybridization (RNAscope®)

Embryos were fixed in BT-fix (4% paraformaldehyde, 0.15 mM CaCl₂, 4% sucrose, 0.1 M PO₄ buffer, pH=7.3) overnight at 4°C. Fixative was removed by 3x5 min washes in 1x PBS/0.01% Tween, followed by dehydration in a methanol series. Samples were then stored at -20°C until processing. We used the RNAscope® Multiplex Fluorescent Detection Kit v2 following the Gross-Thebing et al. 2014 protocol with several modifications. Methanol was removed and samples were rehydrated with 1x PBS - 0.01% Tween. The protease step was omitted for samples younger than 48 hpf. Samples were then incubated overnight at 40°C in 1:50 diluted probes. Probes were recovered and samples were washed in 0.2X SSCT (0.2X SSC and 0.01% Tween). Samples were then incubated at 40°C according to the protocol in Amp1-3

using 2 drops of solution. After amplification, 2 drops of HRP matching the probe channel were added and samples were again incubated at 40°C. Opal dyes 405, 570, and 650 were used at 1:1000. Washes between Amp solutions, HRP solutions, and Opal dyes were conducted using 1 quick rinse and 2x 15-minute 0.2x SSCT rinses. HRP blocker was used between channels prior to conjugating new HRPs but omitted before antibody incubation.

Immunofluorescence

Fluorescent *in situ* hybridization was followed by immunostaining to enhance transgene fluorescence. Samples underwent postfixation in 4% PFA for 10 minutes at RT. Fixative was then removed and embryos were washed in PBST (1x PBS/0.1% Triton) 3x 20 minutes and blocked with 2% goat serum for 1 hour at room temperature. Primary antibody (anti-EGFP 1:1000, anti-mCherry 1:1000) antibody was added and samples were incubated overnight at 4°C with agitation. The primary antibody was removed with 3x 15-minute washes with PBST and secondary antibody (goat anti-chick 1:1000) was added and incubated for 4 hours at 4°C with agitation. Secondary antibody was washed out the same way, and DAPI (1:10000) was added to the final wash for samples requiring DNA labeling.

Confocal Microscopy

For live imaging, embryos were mounted in 1.5% low melting point agarose in embryo medium on a glass cover slip and submersed in embryo media containing 0.02% tricaine. To observe neurogenesis and axon extension, embryos were imaged beginning at 14 hpf at 5-8 min intervals. All live imaging was performed on an upright Fluoview3000 confocal microscope (Olympus) using a 40x NA=1.25 silicon oil immersion lens. Images through the pLLg or axon terminals were acquired with sufficient depth to capture the entire structure and all labeled cells/growth cones present. For fixed imaging, embryos were mounted in 50% glycerol/1x PBS and imaged on an upright Fluoview3000 confocal microscope (Olympus) using a 60x NA=1.4 oil immersion lens.

Two-photon Ablation

We followed the published two-photon axotomy protocol¹²¹ with adaptations for whole cell ablations. Embryos were mounted at ~ 22 hpf, at the onset of pLL axon extension. on the multiphoton Zeiss LSM 980 NLO microscope. Small, circular ROIs were drawn within each EGFP+ neuron and ablation was conducted using 80% laser intensity for 1 microsecond at 910 nm. A brief 10 frame timelapse was taken, spanning the ablation, to ensure cells were ablated. After ablation, embryos were placed on the FV3000 confocal microscope and recorded for timelapse imaging over a period of ~10 hours.

Plasmid Construction

The following plasmids were generated for this study: 5kb-*neurod1:ret51-mcherry*⁴⁶, 5kb-*neurod1:EGFP-CAAX*, 5kb-*neurod1:caRAR-EGFP-CAAX*, 5kb-*neurod1:dnRAR-EGFP-CAAX*, *hsp70l:EGFP-CAAX;en.sill*, *hsp70l:caRAR-EGFP-CAAX;en.sill*, and *hsp70l:dnRAR-EGFP-*

CAAX;en.sill using the Tol2kit¹⁴³. Plasmids containing middle entry dnRAR and caRAR were generously provided by the Waxman and Moens labs^{100,144}. Final constructs contained a 5' 5kb-*neurod1* promoter¹⁴⁵ or a 3' *sill* enhancer¹⁴⁶. Plasmids were purified using Qiagen column purification. Five to ten picograms of DNA constructs were injected into embryo cytoplasm at the 1- or 2-cell stage.

Creation of transgenic zebrafish lines

Tg(rpz5:mRuby)^{nl27} was created by knocking-in *mRuby* into the *rpz5* locus using a previously described mBait knock-in strategy¹⁴⁷. Briefly, dualTRE *mBait-hsp70:mRuby* plasmid was injected into fertilized embryos together with the gRNA/Cas9 RNPs. gRNA targeted the start site at the *rpz5* locus: AGCGGTGTTTATGACTTCCG. The mBait-mRuby3 construct was a gift from the Raible lab which modified the original Shin-Ichi Higashijima's mBait-GFP construct. They generated the mBait-mRuby3 construct via Gibson assembly (Gibson et al., 2009), replacing the GFP protein sequence for the coding sequence of mRuby3. Following injections, fish were raised to adulthood and screened for transgene integration via fluorescence. Positive F1 progeny were validated via FISH using probes against mRuby and the endogenous *rpz5* message (Fig. S2-4A).

TgBAC(neurod1:mCherry)^{nl28}, *Tg(neurod1:kaede)*^{nl29} and *Tg(hsp70l:mCherry, en.sill)*^{nl30} were created by injecting 5 pg of each plasmid into fertilized embryos together with 35 pg of codon-optimized transposase¹⁴³. Following injections, F0 fish were raised to adulthood and their progeny were screened for transgene integration via fluorescence. Positive F1 adults were outcrossed one additional time before performing experiments to minimize use of animals with multiple integrations.

Kaede photoconversion

Photoconversions were performed using 40x NA=1.25 silicon oil lens. Once the target cell was identified, a 20x zoom was used to magnify a region within the cell. An approximately 1 μm circular ROI was created and the region was scanned 20x with the 405 nm laser at 10% laser power. N = 7 embryos imaged, 11 neurons analyzed (4 pioneers, 7 followers).

Pioneer and Follower mosaic analysis

Mosaic embryos were generated by injection of 5 pg of *neurod1:mcherry* at the one-cell stage. Embryos were sorted for 1-3 pLL neurons labeled.

Quantification of axon targeting

To mosaically label neurons, embryos were injected with 10 pg of plasmid. They were then screened at 48 hpf to identify embryos with 1-2 fluorescent cells. To track axon targeting, embryos were imaged between 48 and 72 hpf. Axons were followed from cell body and neuromast target was recorded. Only embryos containing 1 to 2 neurons were used for the

analysis, as additional labeled neurons impose greater difficulty in resolving single axon targets.

Quantification of fluorescent in situ hybridization

Confocal stacks of the pLLg were exported to Imaris (Bitplane) and analyzed using the Cells function. Neuron cell borders were constructed using the green channel from *cldnB:memgfp*. Accuracy of total cell numbers was achieved by counterstaining with DAPI such that every cell contained exactly one nucleus. The amplification from RNAscope results in detectable individual mRNA transcripts, so fluorescent puncta were totaled in each cell. mRNA counts were separated into distinct bins from 0 to 10, with 10 as the maximum and 0 as the minimum observed in each embryo, for standardization across embryos.

CRISPR-Cas9-mediated knockout

Three guides targeting exon 1 of *hoxb5a* were designed and injected as described previously¹⁴⁸. 5 pg of this triplex was injected into *cldnB:memgfp* embryos at the one-cell stage. At 30 hpf EGFP+ embryos were screened and either fixed for RNAscope or dissociated for *hoxb5a* sequencing to assess indel frequency. All guides were efficient in producing indels: guide 1, 73%; guide 2, 93%; guide 3, 82% (Fig. S2-9A).

SU5402 drug treatment

Embryos were incubated in 50 μ M SU5402 in 1% DMSO between 10-18 or 10-22 hpf. Followed incubation embryos were fixed in 4% PFA in 1x PBS and processed for in situ hybridization as described above.

Statistical Analysis

Statistics were performed in either GraphPad or in RStudio. Kendall Tau beta correlation coefficient was used to compare pairwise expression of candidate genes by FISH. When comparing expression of *ret* and *hoxb5a* after overexpression of RAR constructs, Kruskal-Wallis test with Dunn's multiple comparisons was used as the data were nonparametric. When performing a single comparison between two groups for nonparametric data, such as *ret* expression after *hoxb5a* CRISPR knockout, and *ret/hoxb5a* expression after SU5402 treatment, Mann-Whitney test was used.

2.6: Acknowledgements

Thank you to the members of the OHSU Advanced Light Microscopy Core for training, troubleshooting on Imaris, and for help developing the ablation assay. Thank you to the Moens lab for the RAR constructs, and the Ganz lab for the *ret:EGFP* line.

2.7: Supplemental Information

2.7.1 Movie Legends

Movie 1: pLL nerve extension in control embryos. *neurod1:mCherry; ret:EGFP* embryo was mounted at 23 hpf for timelapse imaging. The pLL nerve reaches axial level 8 by 28 hpf. EGFP+ neurons are marked by yellow arrowheads, whereas pLL axon terminals are marked by white arrowhead. Z-stacks were collected every 5 min.

Movie 2: Complete pioneer neurons ablation blocks pLL nerve extension. *neurod1:mCherry; ret:EGFP* embryo was mounted at 23 hpf for timelapse imaging after all *ret:EGFP*-positive neurons were ablated. Note that the pLL nerve does not enter the trunk over 10 hours of imaging, although axon terminals remain dynamic. Axon terminals are marked by white arrowhead. Z-stacks were collected every 5 min.

Movie 3: pLL nerve extension is comparable to controls when pioneers are partially ablated. *neurod1:mCherry; ret:EGFP* embryo was mounted at 23 hpf for timelapse imaging after 3 out 5 EGFP+ neurons were ablated. Note the pLL axon terminals extended to axial level 7 by 28 hpf, comparable to the control. EGFP+ neurons are marked by yellow arrowheads, whereas pLL axon terminals are marked by white arrowhead. Z-stacks were collected every 5 min.

Movie 4: Separation of neural and sensory progenitors during formation of the pLL system. Time lapse confocal movie from the embryo carrying *cldnB:memgfp* and *Tg(neurod:Zebrawow)* transgenes between 15 and 28 hpf (6.6 min intervals). The pLL and otic placodes as well neural tube are outlined. Note that *Tg(neurod:Zebrawow)*-positive cells begin delaminating from the placode at ~16 hpf. Sensory and neural progenitors fully separate by 18 hpf. Scale bar = 20 μ m.

Movie 5: Cell that delaminates first from the pLL placode differentiates into pioneer neurons. Time lapse confocal movie from the embryo carrying *neurod1:kaede* and *cldnB:memgfp* transgenes between 15 and 25 hpf at 6 min intervals. Kaede was photoconverted just before the beginning of timelapse in the leading, delaminating cell. Note

that the labeled neurite comigrates with the pLLP (marked by *cldnB:memgfp*) identifying it as the pioneer axon.

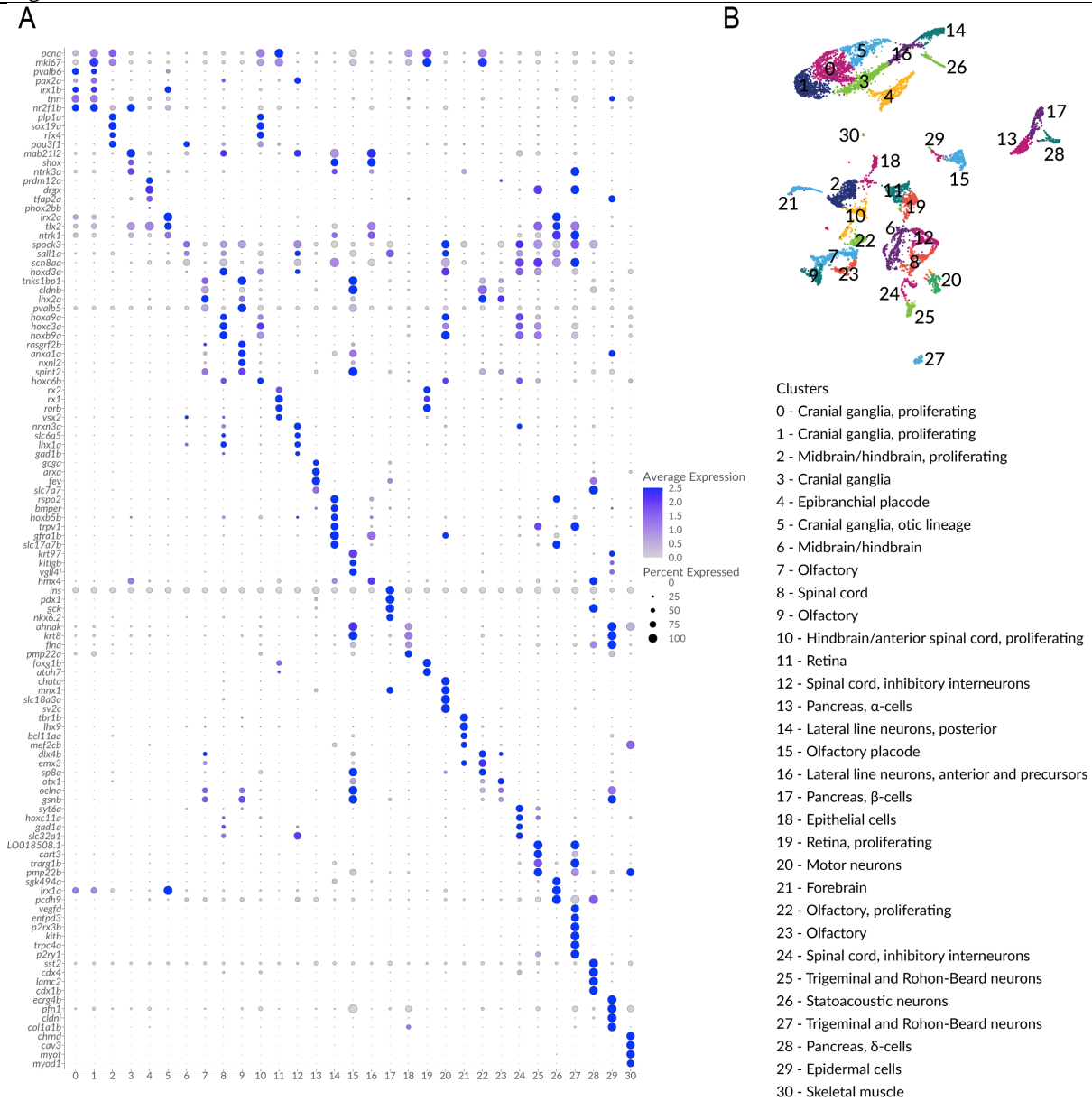
Movie 6: Late delaminating cells differentiate into follower neurons. Time lapse confocal projections of *neurod1:kaede;cldnB:memGFP* expressing cells in a wild-type embryo. Embryo was imaged between 15 and 25 hpf at 6 min intervals. Kaede was photoconverted in the cell located a few cell diameters proximal to leading cells, just before the beginning of timelapse. Note that the labeled neurite lags behind the pLLP, identifying it as the follower axon.

Movie 7: Pioneer neuron precursors exhibit distinct morphology and behavior. Pioneer neurons were transiently labeled using *neurod5kb:mCherry* plasmid injections into *cldnB:memgfp* embryos and imaged between 17 and 27 hpf at 6.6 min intervals. Note that two mCherry positive pioneer neurons precursors have a spindle-like shape at the movie onset (17 hpf) and their peripheral neurites (arrows) contact the pLL sensory cells.

Movie 8: Follower neuron precursor morphology is distinct from pioneer morphology. Follower neurons were transiently labeled using *neurod5kb:mCherry* plasmid injections into *cldnB:memgfp* embryos and imaged between 17 and 27 hpf at 6 min intervals. Note that in contrast to pioneers, follower precursors initially have multipolar morphology. Their neurites (arrows) do not invade the sensory domain.

2.7.2 Supplemental Figures

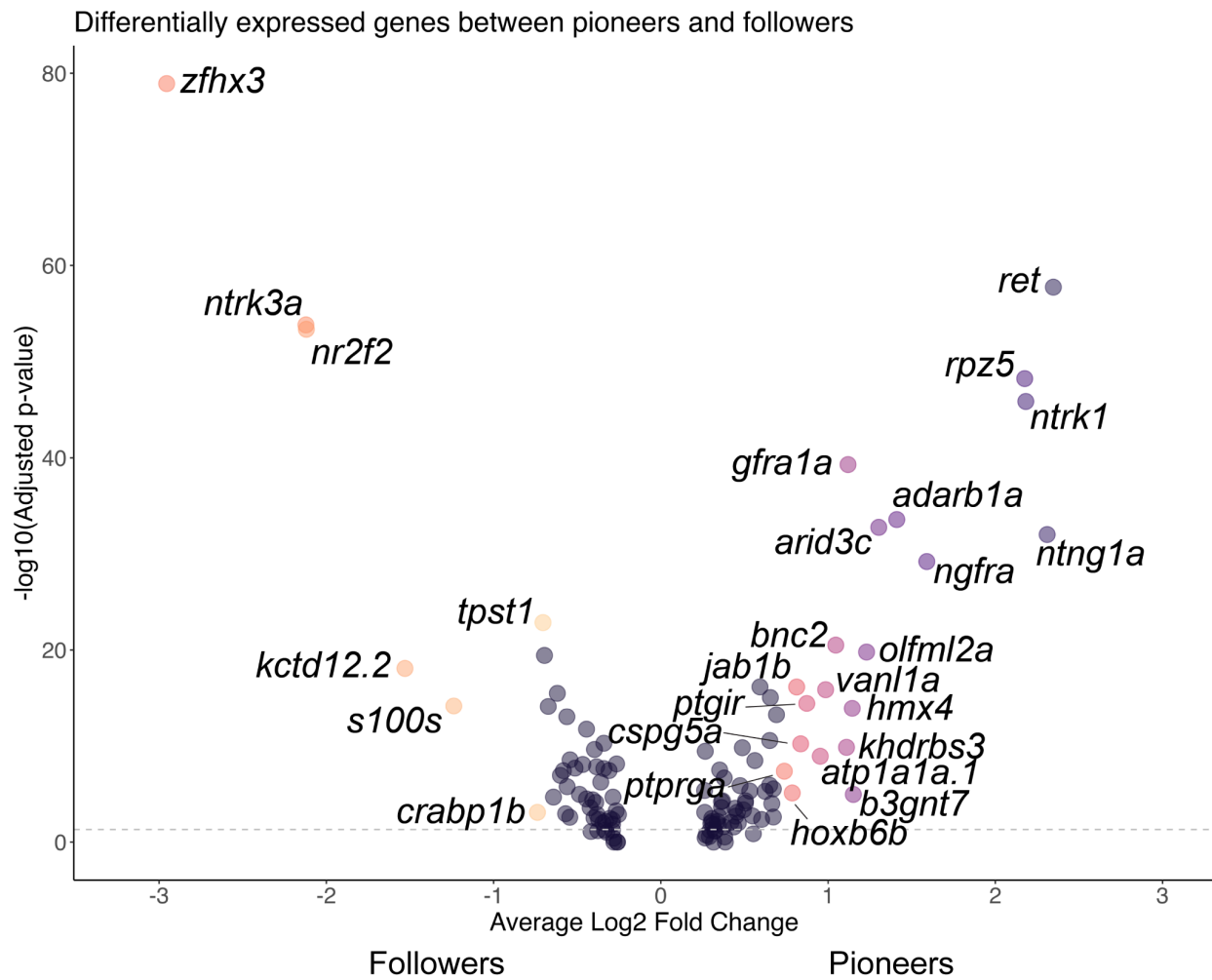
Figure S2-1



S2-1 scRNA-seq identifies many neural populations. (A) Expression of genes used to identify individual clusters from 30 hpf UMAP plot shown in (B).

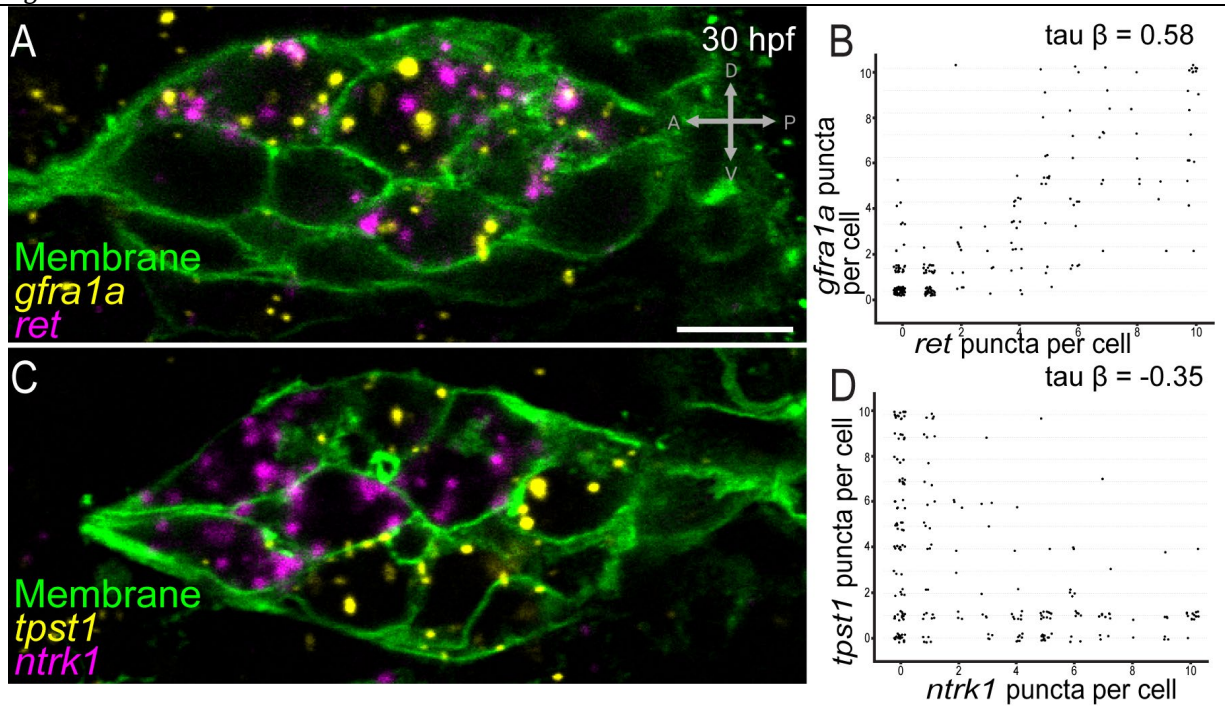
Figure S2-2

A



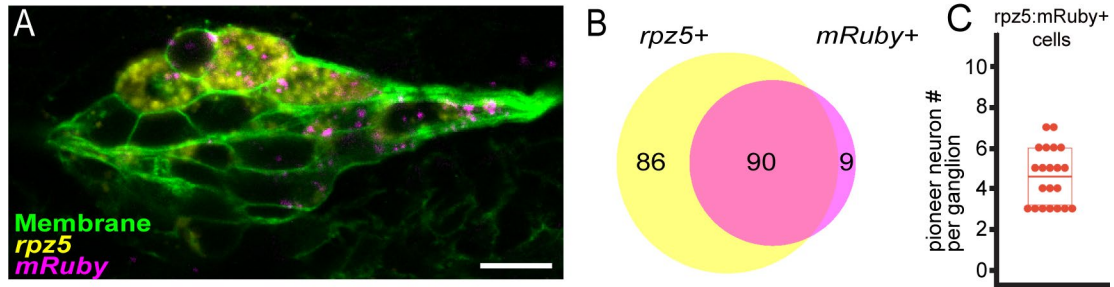
S2-2 Volcano plot of differentially expressed genes in *ret*⁺ and *ret*⁻ neurons. (A) Differentially expressed genes in *ret*⁺ and *ret*⁻ neurons. Dotted line set at $p = 0.05$. Average log₂ fold change set at 0.07.

Figure S2-3



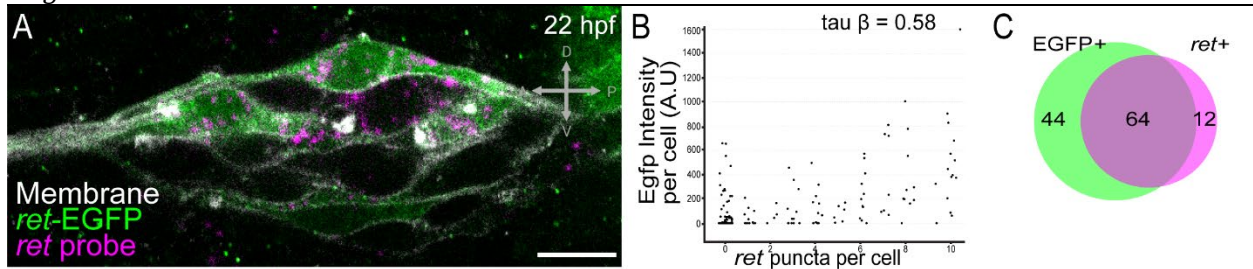
S2-3 **Validation of additional markers from heatmap.** (A, B) Representative single Z-slice confocal images through the pLL ganglion showing pairwise FISH of *gfra1a* and *ret* (A) or *tpst1* and *ntrk1* (B). Scale bar = 10 μm . (C, D) Quantification of images represented by A and B.

Figure^{S2-4}



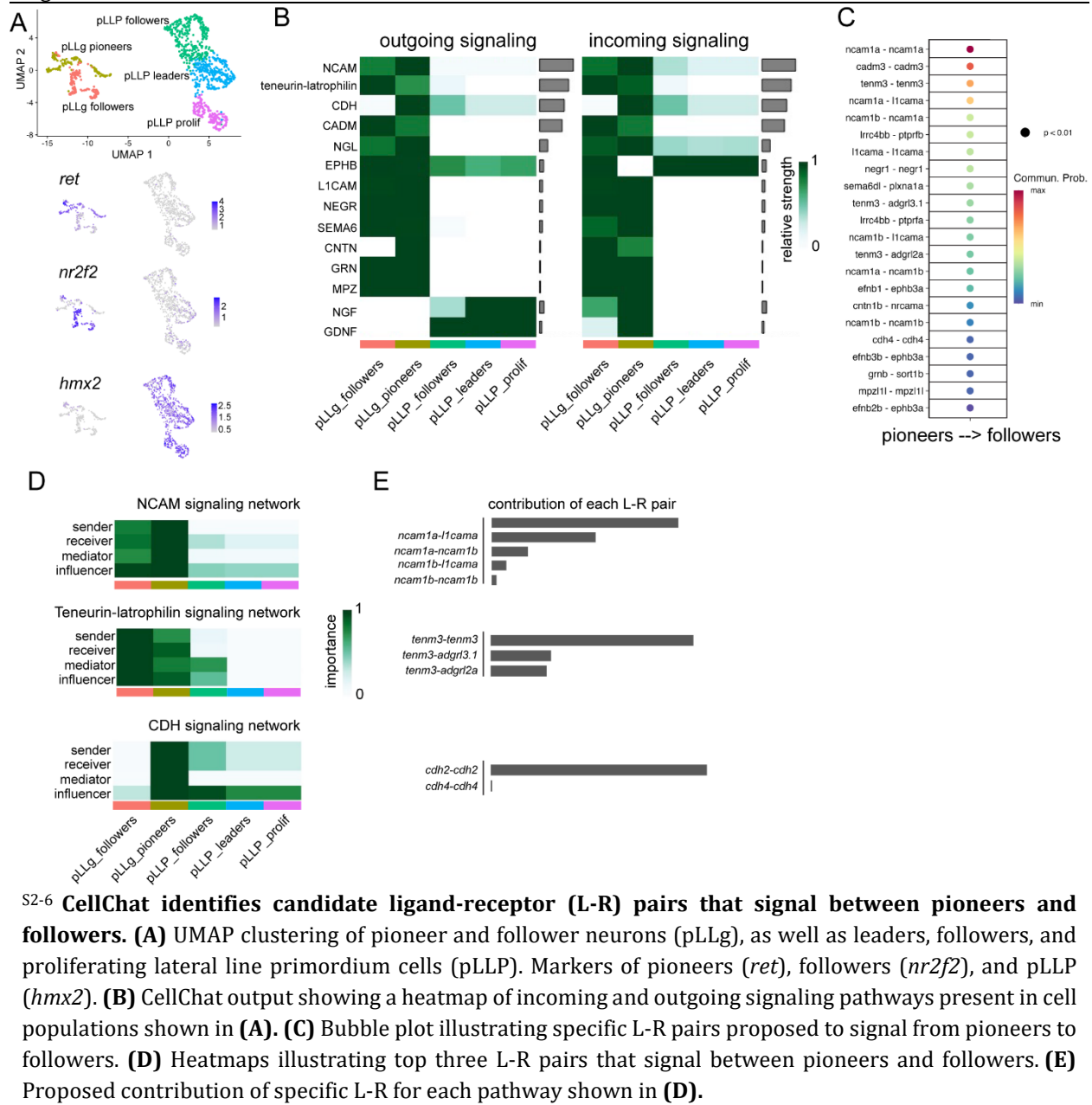
^{S2-4} ***rpz5:mRuby* transgene expression largely recapitulates endogenous *rpz5*.** (A) Representative single confocal Z-slice of the pLL ganglion from the *Tg(rpz5:mRuby)^{nl27}; cldn:memgfp* transgenic animal at 36 hpf was assessed for expression of *rpz5* (yellow) and *mRuby* (magenta). Scale bar = 10 μ m. (B) Venn diagram demonstrating a majority (91%) of *mRuby*-positive cells also express the endogenous transcript. (C) Quantification of number of *mRuby*+ pioneer cell bodies per ganglion.

Figure^{S2-5}



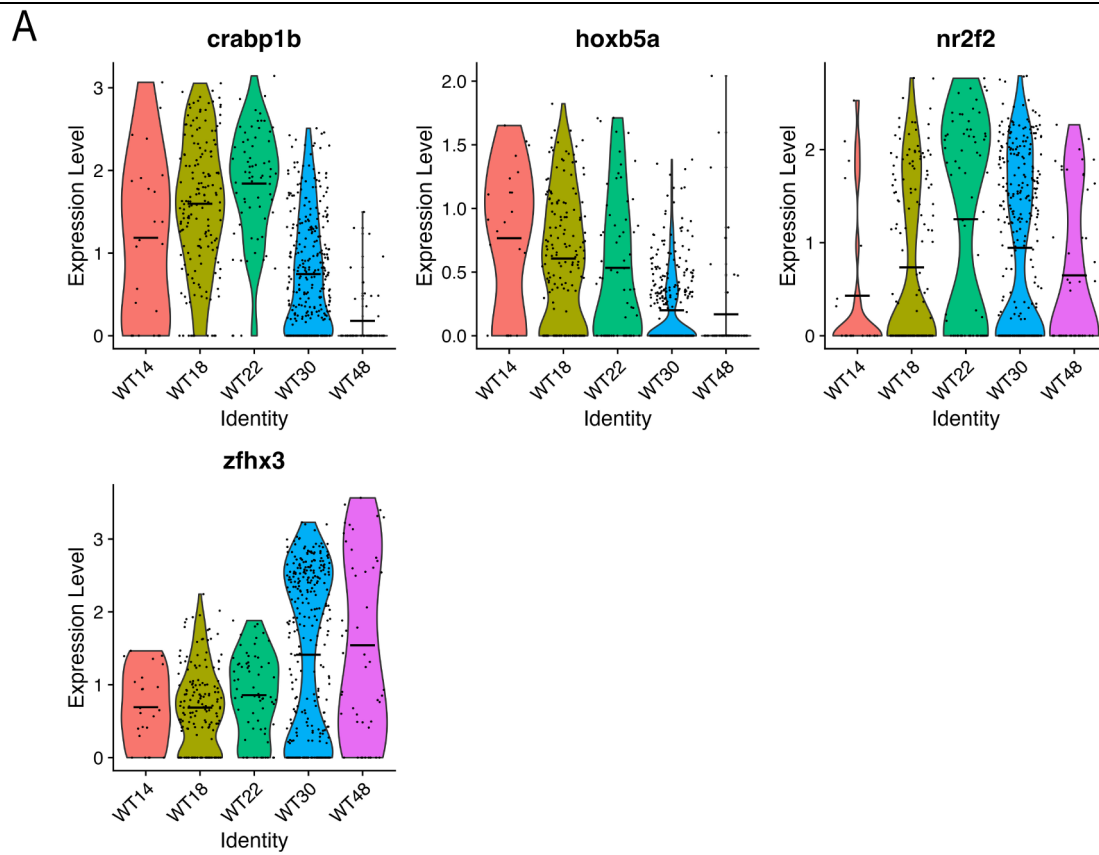
^{S2-5} **Validation of *ret:EGFP* line.** (A) Representative single confocal Z-slice of the pLL ganglion from *ret:EGFP*¹²²; *sox10:mcherry*^{88,149} transgenic animal was assessed at 22 hpf for expression of *ret* (magenta) and presence of EGFP (green). Scale bar = 10 μ m. (B) Dotplot showing EGFP intensity against binned *ret* puncta counts per cell. (C) Venn diagram showing the proportion of overlap between EGFP+ cells and *ret* expressing cells.

FigureS2-6



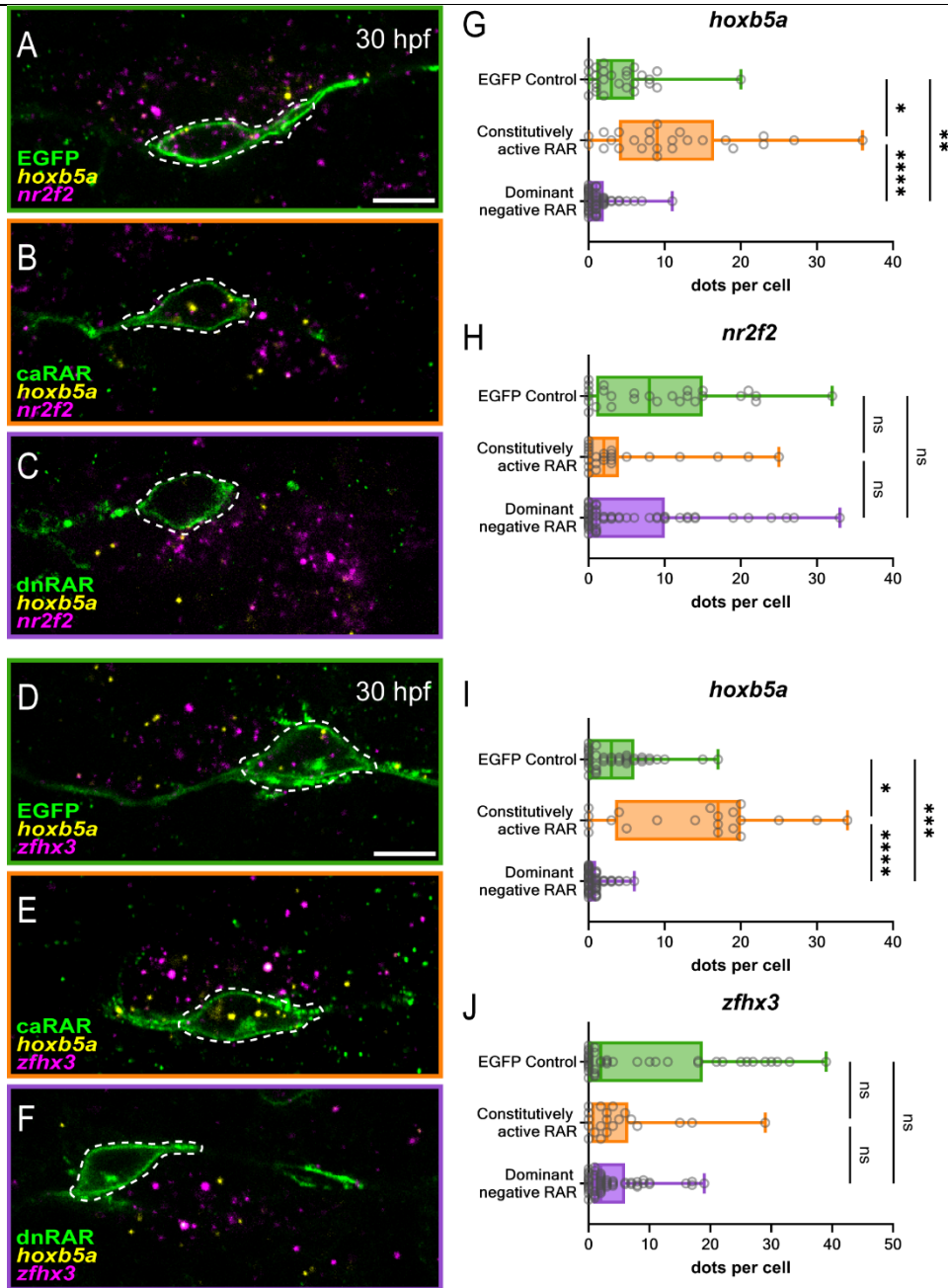
S2-6 **CellChat identifies candidate ligand-receptor (L-R) pairs that signal between pioneers and followers.** (A) UMAP clustering of pioneer and follower neurons (pLLg), as well as leaders, followers, and proliferating lateral line primordium cells (pLLP). Markers of pioneers (*ret*), followers (*nr2f2*), and pLLP (*hmx2*). (B) CellChat output showing a heatmap of incoming and outgoing signaling pathways present in cell populations shown in (A). (C) Bubble plot illustrating specific L-R pairs proposed to signal from pioneers to followers. (D) Heatmaps illustrating top three L-R pairs that signal between pioneers and followers. (E) Proposed contribution of specific L-R for each pathway shown in (D).

Figure^{S2-7}



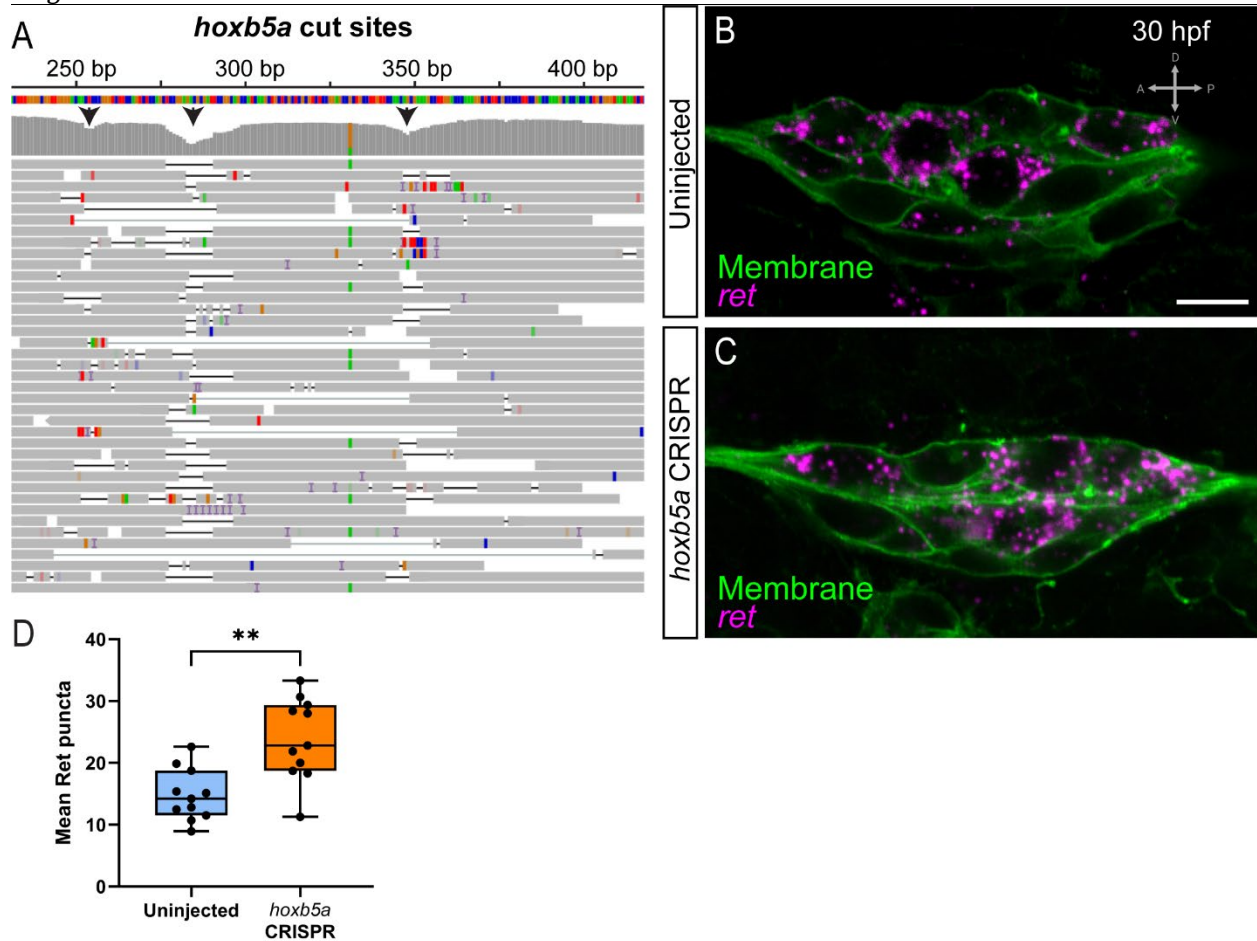
S2-7 pLL progenitors and neurons express RA pathway target genes. (A) Violin plot showing expression of RA pathway member *crabp1b* as well as known transcriptional targets of RA *hoxb5a*, *nr2f2*, and *zfhx3* at 14, 18, 22, 30, and 48 hpf in pLL progenitors as well pLL neurons.

Figure S2-8



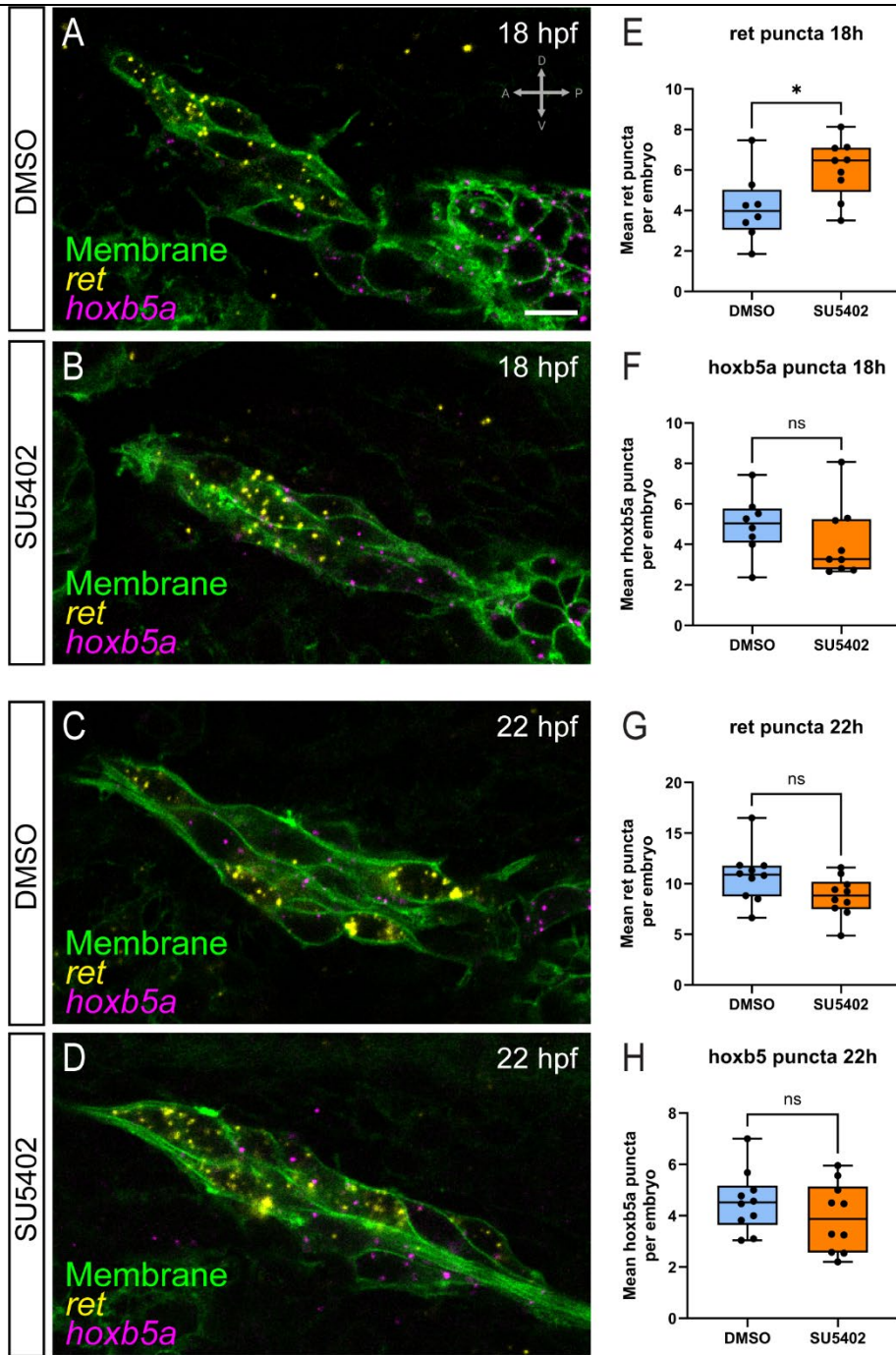
S2-8 *hoxb5*, but not *nr2f2* and *zfhx3*, are RA target genes in pLL neurons. (A-F) Representative images of EGFP, caRAR, or dnRAR-expressing neurons in the pLLg. Fluorescent *in situ* hybridization of *hoxb5*, *nr2f2*, and *zfhx3*. Dotted outline = labeled neuron. Scale bar = 10 μ m. (G-J) Quantified expression levels of *hoxb5a*, *nr2f2*, and *zfhx3* after injection of RAR constructs. Nonparametric Kruskal-Wallis test values are shown on plots: * = $p < 0.05$; ** = $p < 0.001$; *** = $p < 0.0005$; **** = $p < 0.0001$.

Figure^{S2-9}



^{S2-9} ***hoXB5a* CRISPR knockdown shows upregulation of *ret* in the early pLL.** (A) Sequencing results showing the region of exon1 in *hoXB5a* targeted by three guides. >99% of sequences have one or more indels in exon 1. Black arrowheads = cut sites. (B, C) Representative single Z-slice confocal images through the pLL ganglion in *clDNB:memGFP* (green) embryos showing *ret* expression in uninjected control embryos (A) and *hoXB5a* crisprants (B). (D) Quantification of *ret* expression from B and C (n = 11 embryos each).

FigureS2-10



S2-10 **SU5402 treatment indicates regulation of *ret* by Fgf at early stages. (A-D)** Representative single z-slices from *cldnB:memgfp* (green) embryos processed for FISH with *ret* (yellow) and *hoxb5a* (magenta) FISH probes after treatment with DMSO or SU5402 between 14 and 18 hpf (**A,B**) or 22 (**C,D**). **(E-H)** Quantification of *ret* and *hoxb5a* expression in all cells across 8-10 embryos per treatment condition.

2.7.3 Key Resources Table

REAGENT or RESOURCE	SOURCE	IDENTIFIER
Antibodies		
Chicken anti-GFP 1:1000	Aves Labs Inc.	Cat# GFP-1020
Rat anti-mCherry 1:1000	Thermo Fisher Scientific	Cat# M11217
Alexa Fluor 488 Goat anti-chicken	Invitrogen	Cat# A-11039
Alexa Fluor 568 Goat anti-rat IgG (H+L)	Invitrogen	Cat# A-11077
Bacterial and virus strains		
Commercial TOP10 Cells	Thermo Fisher Scientific	Cat# C404003
Chemicals, peptides, and recombinant proteins		
DAPI	ThermoFisher	Cat# D1306
N-phenylthiourea	Sigma	Cat# P7629
Low Melt Agarose	GenePure	Cat# E-3216-125
Tricaine	Pentair Aquatic Eco Systems	Cat# TRS1
Opal dye 405	Biotium	Cat# 96057
Opal dye 570	Akoya Biosciences	Cat# FP1488001KT
Opal dye 650	Akoya Biosciences	Cat# FP1496001KT
SU5402	Selleck Chemicals	Cat# S7667
Critical commercial assays		
QIAprep Spin Miniprep Kit	Qiagen	Cat# 27104
RNAscope Multiplex Fluorescent V2 Assay	Advanced Cell Diagnostics	Cat# 323100
Deposited data		
Single cell RNA-sequencing data	This paper	GSE266312, GSE264323
Single cell RNA-sequencing data	142	GSE240721
Experimental models: Organisms/strains		
<i>TgBAC(neurod1:EGFP)^{nl1};</i> <i>neurod1:EGFP</i>	87	
<i>Tg(-8.0 cldnB:LY-EGFP)^{zf106} ;</i> <i>cldnB:memgfp</i>	88	ZDB-TGCONSTRUCT- 070117-15
<i>Tg(rpz5:mRuby)^{nl27}</i>	This paper	N/A
<i>TgBAC(ret:EGFP)^{b1331};</i> <i>ret-gfp</i>	122	ZDB-TGCONSTRUCT- 240415-3

<i>TgBAC(neurod1:mCherry)^{nl28};</i> <i>neurod1:mCherry</i>	This paper	N/A
<i>Tg(prim:lyn2-mCherry);</i> <i>sox10:mcherry</i>	88	ZDB-TGCONSTRCT-190412-1
<i>Tg(neurod:Zebrawow)^{a131}</i>	124,125	ZDB-TGCONSTRCT-130816-1
<i>Tg(5kbneurod1:kaede)^{nl29};</i> <i>neurod1:kaede</i>	This paper	N/A
<i>Tg(hsp70l:mCherry, en.sill)^{nl30}</i>	This paper	N/A
Oligonucleotides		
<i>ret</i> Probe	Advanced Cell Diagnostics	Cat# 579531
<i>gfra1a</i> Probe	Advanced Cell Diagnostics	Cat# 1053251
<i>ntrk1</i> Probe	Advanced Cell Diagnostics	Cat# 1036971
<i>ntrk3a</i> Probe	Advanced Cell Diagnostics	Cat# 873841
<i>ngfra</i> Probe	Advanced Cell Diagnostics	Cat# 1036991
<i>hoxb5a</i> Probe	Advanced Cell Diagnostics	Cat# 1036951
<i>zhx3</i> Probe	Advanced Cell Diagnostics	Cat# 1036961
<i>nr2f2</i> Probe	Advanced Cell Diagnostics	Cat# 881151
<i>rpz5</i> Probe	Advanced Cell Diagnostics	Cat# 1053231
<i>tpst1</i> Probe	Advanced Cell Diagnostics	Cat# 1053291
Recombinant DNA		
Plasmid: 5kb- <i>neurod1:ret51-mCherry</i>	46	N/A
Plasmid: 10XUAS:EGFP-CAAX-pA	100,144	N/A
Plasmid: 10XUAS:DN-hRAR α -2A-EGFP-CAAX-pA	100,144	N/A
Plasmid: 10XUAS: CA-RAR α -2A-EGFP-CAAX-pA	100,144	N/A
Plasmid: <i>neurod1:EGFP-CAAX</i>	This paper	N/A
Plasmid: <i>neurod1:mcherry</i>	This paper	N/A
Plasmid: <i>neurod:caRAR-2A-EGFP-CAAX</i>	This paper	N/A
Plasmid: <i>neurod:dnRAR-2A-EGFP-CAAX</i>	This paper	N/A
Plasmid: <i>SILL-EGFP-CAAX</i>	This paper	N/A
Plasmid: <i>SILL-caRAR-2A-EGFP-CAAX</i>	This paper	N/A
Plasmid: <i>SILL-dnRAR-2A-EGFP-CAAX</i>	This paper	N/A
Software and algorithms		

BioRender		http://www.biorender.com
Custom R Code	This Paper	https://github.com/anechipor/Nechiporuk-lab-Woodruff_et_al_2024
GraphPad Prism	GraphPad	http://www.graphpad.com
Imaris	Bitplane	http://imaris.oxinst.com
ImageJ	150	N/A
Illustrator	Adobe	http://adobe.com
RStudio/R	Posit	https://posit.co/

Chapter 3: Conclusions and Future Directions

Section 3.1: Summary

This body of work presents several key findings that deepen our understanding of pioneer neurons. First, computational analysis via scRNA-seq in Chapter 2 provides strong evidence that pioneers and followers in the pLL are transcriptionally distinct populations—a conclusion rigorously supported through in situ hybridization and the generation of the *rpz5:mRuby* knock-in line. Additionally, two-photon ablations confirm that pLL follower neurons rely on pioneers for proper axon extension. We also discovered that delamination timing controls pioneer cell fate: using timelapse microscopy, we observed that the first neurons to delaminate become pioneers. By probing our early scRNA-seq datasets, we found that progenitor default is a follower state, suggesting that pioneer identity is an acquired state dependent on RA downregulation. Furthermore, we demonstrated that RA signaling regulates both pioneer axon extension and at least one key pioneer marker, *ret*. Lastly, we show that the pLL pioneer gene signature is shared by other neuronal populations across the nervous system, indicating that pioneer neurons may be similarly distinct in other systems beyond the pLL. These findings open several avenues for future research, particularly in uncovering the broader functional significance of pioneer neurons and the mechanisms that regulate their identity across different contexts.

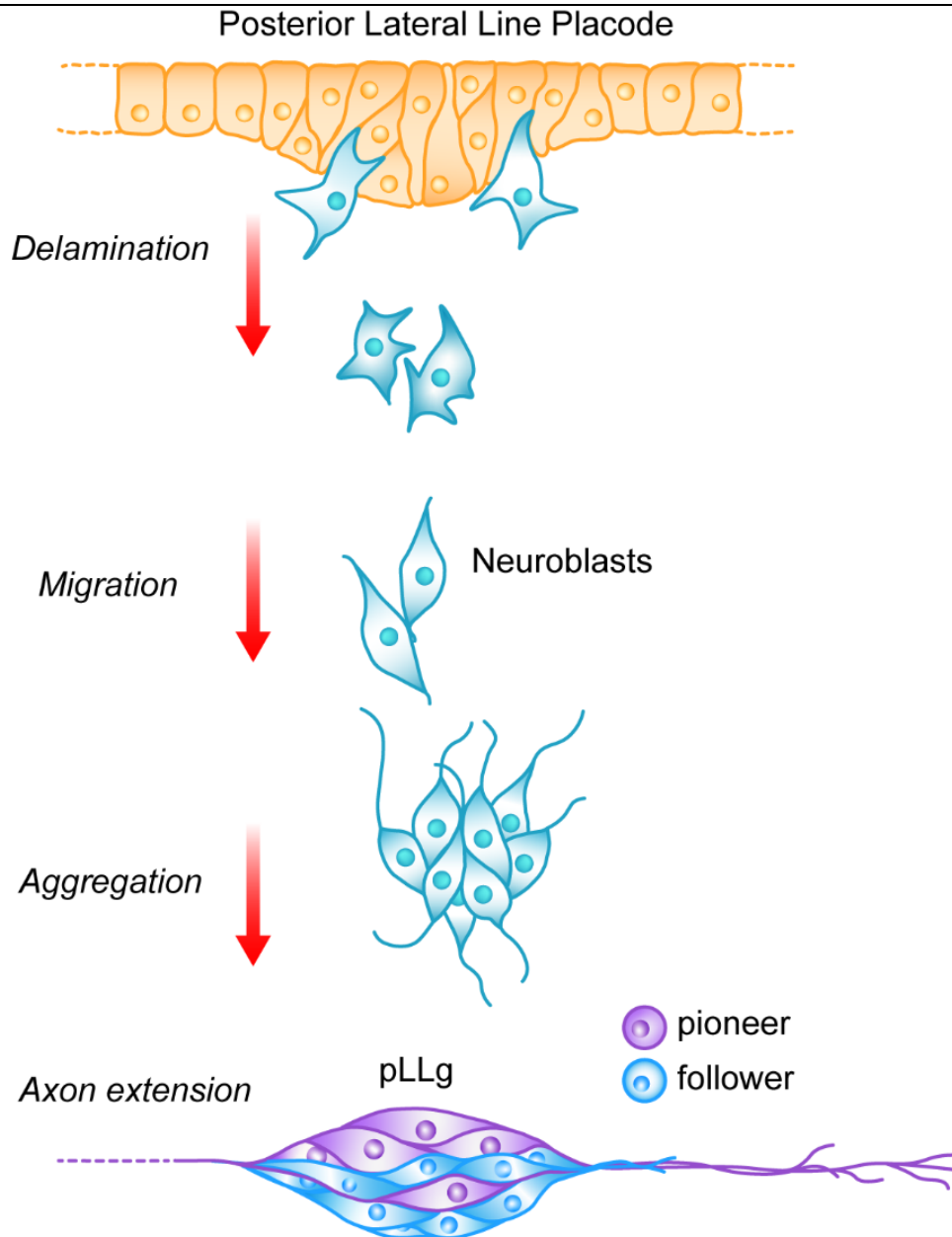
Section 3.2: Future Directions

The findings presented in **Chapter 2** are both illuminating and compelling, yet, as with many scientific inquiries, they provoke novel ideas and unveil intriguing unanswered questions. These discoveries lay the groundwork for future studies aimed at further dissecting the molecular mechanisms that distinguish pioneers from followers. Further, addressing these open questions will not only improve our understanding of neural development, but may also have broader implications for regeneration and repair in the nervous system.

Subsection 3.2.1: An updated view of pLL delamination

Chapter 1 discussed a commonly held hypothesis regarding placodal delamination in relation to neural crest delamination: that while there are parallels between the two, there are also key distinctions²⁹. It is certainly tempting to compare neural crest delamination to placodal delamination, but our studies necessitate a more nuanced model. For example, in **Chapter 2**, we provide evidence that supports a hypothesized distinction between the neural crest and placodal delamination. During pLL placodal delamination, neuroblasts adopted a multipolar morphology just before migration, similar to neural crest cells, followed by a transition to a bipolar neuron morphology (**Fig. 3-1**). This contrasts with studies in mouse and chick, which report that delaminating placodal neuroblasts immediately take on a bipolar morphology after delamination^{28,34}. Our studies also revealed a key similarity—one that challenges the prevailing view. In the pLL, this dynamic shift in cell shape was not accompanied by expression of canonical EMT markers such as Snail, Twist, or RhoB^{24,32,33}, a finding that is consistent with previous reports. Considering that these EMT markers are known to drive expression of enzymes that degrade the basement membrane³², this suggests that delaminating pLL neuroblasts do not actively break down ECM. Instead, they may migrate opportunistically, after the ECM is broken down separately. If that is the case, what facilitates the breach in the ECM that allows neuroblasts to escape from the placode? One possibility is that a local stream of neural crest cells plays this role ahead of delaminating cells in a coordinated manner. There is evidence that the postotic stream of cranial neural crest migrates adjacent to the pLL placode^{25,151,152}. Additionally, there is a significant interaction and cooperation between the aLL and cranial neural crest, such that aLL neuromasts are disrupted in the absence of neural crest¹⁵³. Still, the extent of the pLL interaction with local neural crest stream, including the cellular and molecular bases of this cross talk is not known. Investigating these potential interactions could provide insight into how the local environment influences pLL delamination and migration.

Figure³⁻¹



³⁻¹**Schematic of early pLL development.** Cells from the thickened pLL placodal epithelium delaminate and transition to multipolar forms. They take on bipolar morphology as they migrate together and form a ganglion (pLLg). Pioneers extend their axons outward first, while follower axons extend later, trailing behind. Adapted from Breau and Schneider-Maunoury 2015²⁹.

Subsection 3.2.2: Notch signaling in neuron specification

Our results show that each pLLg contains an average of five pioneers among 20–30 pLL progenitors. How is this subset of progenitors selected to become pioneers? During this stage of pLL development, robust mechanisms must be in place to specify pioneers within

the larger pool of progenitors. As discussed in **Chapter 2**, the pLL employs Notch signaling early on to direct placodal progenitors toward either a neural or sensory fate⁵⁰. Could this same system be repurposed to further partition neurons into pioneers vs followers? The Notch/Jagged signaling pathway is known to mediate lateral inhibition, patterning a relatively uniform population into distinct cell types arranged in a mosaic pattern¹⁵⁴. Among our findings, one particular result supports this hypothesis in the pLL: in **Chapter 2**, Figure S2, we show that *jag1b* is enriched in pioneers. Temporal trajectory analysis revealed that this gene is upregulated in pLL progenitors, maintained in pioneers, and downregulated in followers—one of very few genes to follow this expression pattern. This trend will need to be validated *in vivo* by fluorescent *in situ* hybridization. To further study this pathway, *notch* depletion and *notch* gain-of-function experiments could be used to interrogate the effects on specification. For example, using a heat shock inducible transgenic that drives notch intracellular domain would allow temporal control over Notch overexpression⁵⁰. CRISPRs targeting specific *notch* receptors or *jag1b* could be used for gene depletion studies. These experiments will test whether the lateral inhibition through *notch* and *jag1b* specify pioneers and followers.

Subsection 3.2.3: Retinoic acid downregulation in pioneers

Another unresolved question from **Chapter 2** concerns the mechanism of RA downregulation in pLL neuroblasts. Our findings show that RA levels decrease in neuroblasts slated for differentiation into pioneers, a process necessary for *ret* expression and distal axon targeting. However, the exact mechanism of RA attenuation remains unknown. One possibility is that an external factor, such as Fgf, antagonizes RA signaling in the pLL, as has been demonstrated during earlier stages of pLL placode induction⁵¹. Another possibility is internal deregulation via metabolic enzymes like CYP26^{99,155}. However, scRNA-seq data did not reveal particularly high or differential expression of *cyp26*. Interestingly, **Chapter 2** results indicate that a known RA shuttle, the cellular retinoic acid binding protein, *crabp1b*^{101,156}, is expressed in followers. This protein is thought to transport intracellular RA for degradation^{98,157,158}, but whether this activity actively drives differentiation into pioneers or simply modulates RA signal intensity remains unclear. Finally, the spatial transition of neuroblasts as they migrate from the pLL placode to anterodorsal positions may expose

them to a new signaling environment, separate from the placodal epithelium. This movement could remove neuroblasts from a region of active RA signaling, potentially subjecting them to different regulatory cues. Determining how these spatial and molecular cues converge to regulate RA downregulation in pioneers will be crucial for uncovering their specification.

Subsection 3.2.4: Interactions between pioneers and followers

As discussed, pioneers play a crucial role in establishing initial pathways of the nervous system, but the function of these pathways is dependent on interactions with followers that reinforce and extend along these routes. Ablation experiments from **Chapter 2** demonstrated followers' dependency on pioneer axons, so what regulates interaction between the two? Pioneers and followers of the pLL must coordinate ganglion aggregation, axon extension timing, and differential target innervation, so how do they communicate to one another? We probed our scRNA-seq dataset for clues directing us toward potential pioneer-follower signaling networks using CellChat (**Fig. S2-6**). L1 and NCAM signaling were highly expressed by both pioneers and followers; these factors are known to regulate neuronal migration, axon guidance, and axon fasciculation in the pLL^{159,160}. These findings suggest that cell adhesion molecules play a role in these processes in the pLL. It could indicate that pioneers and followers express these molecules to form axon bundles and maintain fasciculation. Alternatively, if they are also expressed during delamination, they could be used to guide neuroblast migration after delamination. We also observed strong expression of additional cell-cell contact molecules, including N-cadherins. Given the close association between pioneers and followers, and their axons, cadherins may primarily mediate cell-cell contact or axon fasciculation. However, previous studies suggest a more profound role for N-cadherins, such as those involved in epithelial detachment and neuroblast differentiation¹⁶¹⁻¹⁶⁴. The precise role of these molecules in coordinating pLL development remains unclear, but their presence suggests a strong dependence on cell-cell communication.

Subsection 3.2.5: Tool development for early stages of pioneer and follow development

Chapter 2 utilized two key genetic zebrafish models that allowed specific labeling of pioneers, *rpz5:mRuby* and *ret:EGFP*. As discussed, specific genetic markers of pioneers were the first step that enabled us to study them in depth. However, the contribution of follower neurons to the nervous system should not be understated. Hence, tools to reliably label followers specifically would further benefit studying neurodevelopment. Similarly to *rpz5:mRuby*, knock in remains a viable strategy to generate a follower-specific label. The fact that pioneers stem from a follower-like progenitor state does complicate this endeavor, however, as fluorescent proteins often have long half-lives^{165,166}. One possible approach is to use shorter-lived, destabilized fluorescent variants, which are better suited for molecular labeling in cells, such as pLL progenitors, that experience dynamic gene expression^{167,168}. Another promising alternative is the use of genetically encoded affinity reagents (GEARs), a modular tagging system that bypasses the need for proper protein folding¹⁶⁹. This approach enables fluorescent detection based on *in vivo* binding of small variable chain fragments to their protein targets. Because these fragments are expressed ubiquitously, rather than by a gene of interest's promotor, fluorescence is detectable almost instantly once the tagged protein is present. Applying GEARs to the pLL could provide a reliable method both for early labeling of pioneers and for specifically labeling followers while avoiding labeling nascent pioneers. It would allow us to visualize proteins associated with pioneer and follower identity as soon as they are translated. We would likely utilize an early pioneer marker, such as *nrk1*, to label pioneers at early timepoints. The benefits of creating these tools extends beyond helping to differentiate pioneers from followers—it would also provide deeper insight into the molecular transitions that shape neuronal identity. With more precise labeling strategies, future studies could dig deeper into what sets these populations apart and how they contribute to neural development and regeneration.

Subsection 3.2.6: Pioneers in the context of regeneration

Perhaps the most clinically relevant reason to study pioneer neurons is their potential to inform strategies for axon regeneration after injury. In organisms and tissues with

regenerative capacity, the mechanisms driving regeneration frequently mirror those of development^{170,171}. Likewise, the question of why mammals exhibit such a stark deficit in regenerative ability has fueled extensive research¹⁷²⁻¹⁷⁴. These efforts have uncovered fascinating regenerative mechanisms in a variety of models, including flatworms, amphibians, zebrafish, and neonatal mice. In mammals, it is generally accepted that CNS axons lack the ability to regenerate after injury¹⁷⁵⁻¹⁷⁷, and albeit to a lesser extent, PNS axons as well. However, nervous system repair is a complex, multi-faceted challenge, with outcomes depending heavily on the nature of the injury. Injured neurons face a range of obstacles, including re-epithelialization, glial scarring, immune responses, and—most relevant to pioneer neurons—axon regrowth^{173,174,177-179}. For successful regeneration, damaged neural tissue requires two key elements: an injury environment conducive to repair and neurons capable of axon regrowth. Both are defining features of the developmental context in which pioneer axons extend. By studying the molecular regulation of pioneer neurons, we can begin to pinpoint which signals or capacities are missing in mature, adult neurons, bringing us closer to unlocking their regenerative potential.

Together, these proposed directions will expand our knowledge of how pioneer neurons emerge and function. Addressing the unanswered questions regarding molecular specification, environmental interactions, and regenerative potential will provide further insight into fundamental mechanisms within neurodevelopment and their clinical relevance.

Section 3.3: Acknowledgements

I am deeply grateful to my advisor, Alex, for five years of exceptional mentorship and unwavering support. Your door was always open, and you never made me feel like an inconvenience. You offered guidance when I needed direction and gave me the freedom to explore when I felt confident.

I also want to thank Lauren Miller, for both friendship and mentorship at every step during graduate school.

Bibliography

1. Von Gerlach, J. & University College, L. L. S. *Handbuch Der Lehre von Den Geweben Des Menschen Und Der Thiere [Electronic Resource]*. (Leipzig : Engelmann, 1871).
2. López-Muñoz, F., Boya, J. & Alamo, C. Neuron theory, the cornerstone of neuroscience, on the centenary of the Nobel Prize award to Santiago Ramón y Cajal. *Brain Research Bulletin* **70**, 391–405 (2006).
3. Ramón y Cajal, S. *Histology of the Nervous System of Man and Vertebrates*. (New York : Oxford University Press, 1911).
4. Bate, C. M. Pioneer neurones in an insect embryo. *Nature* **260**, 54–56 (1976).
5. Raper, J. & Mason, C. Cellular Strategies of Axonal Pathfinding. *Cold Spring Harb Perspect Biol* **2**, a001933 (2010).
6. Ghysen, A. & Dambly-Chaudière, C. Development of the zebrafish lateral line. *Current Opinion in Neurobiology* **14**, 67–73 (2004).
7. Montgomery, J., Carton, G., Voigt, R., Baker, C. & Diebel, C. Sensory processing of water currents by fishes. *Phil. Trans. R. Soc. Lond. B* **355**, 1325–1327 (2000).
8. Keshishian, H. The origin and morphogenesis of pioneer neurons in the grasshopper metathoracic leg. *Developmental Biology* **80**, 388–397 (1980).
9. Keshishian, H. & Bentley, D. Embryogenesis of peripheral nerve pathways in grasshopper legs: III. Development without pioneer neurons. *Developmental Biology* **96**, 116–124 (1983).
10. Ho, R. K. & Goodman, C. S. Peripheral pathways are pioneered by an array of central and peripheral neurones in grasshopper embryos. *Nature* **297**, 404–406 (1982).

11. Klose, M. & Bentley, D. Transient Pioneer Neurons Are Essential for Formation of an Embryonic Peripheral Nerve. *Science* **245**, 982–984 (1989).
12. Lin, D. M., Auld, V. J. & Goodman, C. S. Targeted neuronal cell ablation in the drosophila embryo: Pathfinding by follower growth cones in the absence of pioneers. *Neuron* **14**, 707–715 (1995).
13. Hidalgo, A. & Brand, A. H. Targeted neuronal ablation: the role of pioneer neurons in guidance and fasciculation in the CNS of Drosophila. *Development* **124**, 3253–3262 (1997).
14. Sulston, J. E., Schierenberg, E., White, J. G. & Thomson, J. N. The embryonic cell lineage of the nematode *Caenorhabditis elegans*. *Developmental Biology* **100**, 64–119 (1983).
15. Hedgecock, E. M., Culotti, J. G., Hall, D. H. & Stern, B. D. Genetics of cell and axon migrations in *Caenorhabditis elegans*. *Development* **100**, 365–382 (1987).
16. Durbin, R. Studies on the development and organisation of the nervous system of *Caenorhabditis elegans*. (University of Cambridge, 1987).
17. Kuwada, J. Y. Cell recognition by neuronal growth cones in a simple vertebrate embryo. *Science* **233**, 740–746 (1986).
18. Eisen, J. S., Myers, P. Z. & Westerfield, M. Pathway selection by growth cones of identified motoneurons in live zebra fish embryos. *Nature* **320**, 269–271 (1986).
19. Nordlander, R. H. Axonal growth cones in the developing amphibian spinal cord. *Journal of Comparative Neurology* **263**, 485–496 (1987).
20. McConnell, S. K., Ghosh, A. & Shatz, C. J. Subplate Neurons Pioneer the First Axon Pathway from the Cerebral Cortex. *Science* **245**, 978–982 (1989).

21. Ghosh, A., Antonini, A., McConnell, S. K. & Shatz, C. J. Requirement for subplate neurons in the formation of thalamocortical connections. *Nature* **347**, 179–181 (1990).
22. Godement, P., Salaün, J. & Mason, C. A. Retinal axon pathfinding in the optic chiasm: Divergence of crossed and uncrossed fibers. *Neuron* **5**, 173–186 (1990).
23. Schlosser, G. Induction and specification of cranial placodes. *Developmental Biology* **294**, 303–351 (2006).
24. Theveneau, E. & Mayor, R. Neural crest delamination and migration: From epithelium-to-mesenchyme transition to collective cell migration. *Developmental Biology* **366**, 34–54 (2012).
25. Rocha, M., Singh, N., Ahsan, K., Beiriger, A. & Prince, V. E. Neural crest development: Insights from the zebrafish. *Dev Dyn* **249**, 88–111 (2020).
26. Theveneau, E. *et al.* Chase-and-run between adjacent cell populations promotes directional collective migration. *Nat Cell Biol* **15**, 763–772 (2013).
27. Freter, S., Fleenor, S. J., Freter, R., Liu, K. J. & Begbie, J. Cranial neural crest cells form corridors prefiguring sensory neuroblast migration. *Development* **140**, 3595–3600 (2013).
28. Graham, A., Blentic, A., Duque, S. & Begbie, J. Delamination of cells from neurogenic placodes does not involve an epithelial-to-mesenchymal transition. *Development* **134**, 4141–4145 (2007).
29. Breau, M. A. & Schneider-Maunoury, S. Cranial placodes: Models for exploring the multi-facets of cell adhesion in epithelial rearrangement, collective migration and neuronal movements. *Developmental Biology* **401**, 25–36 (2015).

30. Jimenez, L. *et al.* Phenotypic chemical screening using a zebrafish neural crest EMT reporter identifies retinoic acid as an inhibitor of epithelial morphogenesis. *Dis Model Mech* **9**, 389–400 (2016).
31. Lassiter, R. N. T., Ball, M. K., Adams, J. S., Wright, B. T. & Stark, M. R. Sensory Neuron Differentiation is Regulated by Notch Signaling in the Trigeminal Placode. *Dev Biol* **344**, 836–848 (2010).
32. Thiery, J. P., Acloque, H., Huang, R. Y. J. & Nieto, M. A. Epithelial-Mesenchymal Transitions in Development and Disease. *Cell* **139**, 871–890 (2009).
33. Duband, J.-L. Diversity in the molecular and cellular strategies of epithelium-to-mesenchyme transitions: Insights from the neural crest. *Cell Adhesion & Migration* **4**, 458–482 (2010).
34. Shiao, C. E., Das, R. M. & Storey, K. G. An effective assay for high cellular resolution time-lapse imaging of sensory placode formation and morphogenesis. *BMC Neurosci* **12**, 37 (2011).
35. Lumsden, A., Sprawson, N. & Graham, A. Segmental origin and migration of neural crest cells in the hindbrain region of the chick embryo. *Development* **113**, 1281–1291 (1991).
36. Berndt, J. D., Clay, M. R., Langenberg, T. & Halloran, M. C. Rho-kinase and myosin II affect dynamic neural crest cell behaviors during epithelial to mesenchymal transition in vivo. *Dev Biol* **324**, 236–244 (2008).
37. Schilling, T. F. & Kimmel, C. B. Segment and cell type lineage restrictions during pharyngeal arch development in the zebrafish embryo. *Development* **120**, 483–494 (1994).

38. Raible, D. W. & Kruse, G. J. Organization of the lateral line system in embryonic zebrafish. *Journal of Comparative Neurology* **421**, 189–198 (2000).
39. Metcalfe, W. K. Organization and Development of the Zebrafish Posterior Lateral Line. in *The Mechanosensory Lateral Line* (eds. Coombs, S., Görner, P. & Münz, H.) 147–159 (Springer, New York, NY, 1989). doi:10.1007/978-1-4612-3560-6_7.
40. Kimmel, C. B., Ballard, W. W., Kimmel, S. R., Ullmann, B. & Schilling, T. F. Stages of embryonic development of the zebrafish. *Developmental Dynamics* **203**, 253–310 (1995).
41. Harrison, R. G. Experimentelle Untersuchungen Über die Entwicklung der Sinnesorgane der Seitenlinie bei den Ampkibien. *Archiv f. mikrosk. Anat.* **63**, 35–149 (1903).
42. Baker, C. V. H. & Bronner-Fraser, M. Vertebrate Cranial Placodes I. Embryonic Induction. *Developmental Biology* **232**, 1–61 (2001).
43. Schlosser, G. Development and evolution of lateral line placodes in amphibians I. Development. *Zoology* **105**, 119–146 (2002).
44. Gompel, N., Dambly-Chaudière, C. & Ghysen, A. Neuronal differences prefigure somatotopy in the zebrafish lateral line. *Development* **128**, 387–393 (2001).
45. Liao, J. C. & Haehnel, M. Physiology of afferent neurons in larval zebrafish provides a functional framework for lateral line somatotopy. *J Neurophysiol* **107**, 2615–2623 (2012).
46. Tuttle, A., Drerup, C. M., Marra, M., McGraw, H. & Nechiporuk, A. V. Retrograde Ret signaling controls sensory pioneer axon outgrowth. *eLife* **8**, e46092 (2019).
47. Pujol-Martí, J., Baudoin, J.-P., Faucherre, A., Kawakami, K. & López-Schier, H. Progressive neurogenesis defines lateralis somatotopy. *Developmental Dynamics* **239**, 1919–1930 (2010).

48. Liao, J. C. Organization and physiology of posterior lateral line afferent neurons in larval zebrafish. *Biol Lett* **6**, 402–405 (2010).
49. Sato, A., Koshida, S. & Takeda, H. Single-cell analysis of somatotopic map formation in the zebrafish lateral line system. *Developmental Dynamics* **239**, 2058–2065 (2010).
50. Mizoguchi, T., Togawa, S., Kawakami, K. & Itoh, M. Neuron and Sensory Epithelial Cell Fate Is Sequentially Determined by Notch Signaling in Zebrafish Lateral Line Development. *J. Neurosci.* **31**, 15522–15530 (2011).
51. Nikaido, M., Navajas Acedo, J., Hatta, K. & Piotrowski, T. Retinoic acid is required and Fgf, Wnt, and Bmp signaling inhibit posterior lateral line placode induction in zebrafish. *Developmental Biology* **431**, 215–225 (2017).
52. Schlosser, G. Chapter Four - Making Senses: Development of Vertebrate Cranial Placodes. in *International Review of Cell and Molecular Biology* (ed. Jeon, K.) vol. 283 129–234 (Academic Press, 2010).
53. Guo, M., Jan, L. Y. & Jan, Y. N. Control of Daughter Cell Fates during Asymmetric Division: Interaction of Numb and Notch. *Neuron* **17**, 27–41 (1996).
54. Bertrand, N., Castro, D. S. & Guillemot, F. Proneural genes and the specification of neural cell types. *Nat Rev Neurosci* **3**, 517–530 (2002).
55. Blader, P., Fischer, N., Gradwohl, G., Guillemot, F. & Strähle, U. The activity of Neurogenin1 is controlled by local cues in the zebrafish embryo. *Development* **124**, 4557–4569 (1997).
56. Ma, Q., Kintner, C. & Anderson, D. J. Identification of *neurogenin*, a Vertebrate Neuronal Determination Gene. *Cell* **87**, 43–52 (1996).
57. Chitnis, A. B., Dalle Nogare, D. & Matsuda, M. Building the posterior lateral line system in zebrafish. *Developmental Neurobiology* **72**, 234–255 (2012).

58. Matsuda, M. & Chitnis, A. B. Atoh1a expression must be restricted by Notch signaling for effective morphogenesis of the posterior lateral line primordium in zebrafish. *Development* **137**, 3477–3487 (2010).
59. Nechiporuk, A., Linbo, T. & Raible, D. W. Endoderm-derived Fgf3 is necessary and sufficient for inducing neurogenesis in the epibranchial placodes in zebrafish. *Development* **132**, 3717–3730 (2005).
60. Bailey, A. P., Bhattacharyya, S., Bronner-Fraser, M. & Streit, A. Lens Specification Is the Ground State of All Sensory Placodes, from which FGF Promotes Olfactory Identity. *Developmental Cell* **11**, 505–517 (2006).
61. Canning, C. A., Lee, L., Luo, S. X., Graham, A. & Jones, C. M. Neural tube derived Wnt signals cooperate with FGF signaling in the formation and differentiation of the trigeminal placodes. *Neural Dev* **3**, 35 (2008).
62. Kawauchi, S. *et al.* Fgf8 expression defines a morphogenetic center required for olfactory neurogenesis and nasal cavity development in the mouse. *Development* **132**, 5211–5223 (2005).
63. del Corral, R. D. *et al.* Opposing FGF and Retinoid Pathways Control Ventral Neural Pattern, Neuronal Differentiation, and Segmentation during Body Axis Extension. *Neuron* **40**, 65–79 (2003).
64. Martínez-Morales, P. L. *et al.* FGF and retinoic acid activity gradients control the timing of neural crest cell emigration in the trunk. *Journal of Cell Biology* **194**, 489–503 (2011).
65. Cunningham, T. J. & Duyster, G. Mechanisms of retinoic acid signalling and its roles in organ and limb development. *Nat Rev Mol Cell Biol* **16**, 110–123 (2015).

66. Deschamps, J. & van Nes, J. Developmental regulation of the Hox genes during axial morphogenesis in the mouse. *Development* **132**, 2931–2942 (2005).
67. Schuster, K., Dambly-Chaudière, C. & Ghysen, A. Glial cell line-derived neurotrophic factor defines the path of developing and regenerating axons in the lateral line system of zebrafish. *Proc Natl Acad Sci U S A* **107**, 19531–19536 (2010).
68. Enomoto, H. *et al.* RET signaling is essential for migration, axonal growth and axon guidance of developing sympathetic neurons. *Development* **128**, 3963–3974 (2001).
69. Honma, Y., Kawano, M., Kohsaka, S. & Ogawa, M. Axonal projections of mechanoreceptive dorsal root ganglion neurons depend on Ret. *Development* **137**, 2319–2328 (2010).
70. Bonanomi, D. *et al.* Ret is a multifunctional co-receptor that integrates diffusible- and contact-axon guidance signals. *Cell* **148**, 568–582 (2012).
71. Sánchez-Soriano, N. & Prokop, A. The Influence of Pioneer Neurons on a Growing Motor Nerve in *Drosophila* Requires the Neural Cell Adhesion Molecule Homolog FasciclinII. *J. Neurosci.* **25**, 78–87 (2005).
72. Patel, C. K., Rodriguez, L. C. & Kuwada, J. Y. Axonal outgrowth within the abnormal scaffold of brain tracts in a zebrafish mutant. *Journal of Neurobiology* **25**, 345–360 (1994).
73. Chitnis, A. B. & Kuwada, J. Y. Elimination of a brain tract increases errors in pathfinding by follower growth cones in the zebrafish embryo. *Neuron* **7**, 277–285 (1991).
74. Pike, S. H., Melancon, E. F. & Eisen, J. S. Pathfinding by zebrafish motoneurons in the absence of normal pioneer axons. *Development* **114**, 825–831 (1992).

75. Kulkarni, R. P., Bak-Maier, M. & Fraser, S. E. Differences in protein mobility between pioneer versus follower growth cones. *Proceedings of the National Academy of Sciences* **104**, 1207–1212 (2007).
76. Nichols, E. L. & Smith, C. J. Pioneer axons employ Cajal's battering ram to enter the spinal cord. *Nat Commun* **10**, 562 (2019).
77. Rapti, G. Regulation of axon pathfinding by astroglia across genetic model organisms. *Front. Cell. Neurosci.* **17**, (2023).
78. Rapti, G., Li, C., Shan, A., Lu, Y. & Shaham, S. Glia initiate brain assembly through noncanonical Chimaerin–Furin axon guidance in *C. elegans*. *Nat Neurosci* **20**, 1350–1360 (2017).
79. Karkali, K., Vernon, S. W., Baines, R. A., Panayotou, G. & Martín-Blanco, E. Puckered and JNK signaling in pioneer neurons coordinates the motor activity of the *Drosophila* embryo. *Nat Commun* **14**, 8186 (2023).
80. Piotrowski, T. & Baker, C. V. H. The development of lateral line placodes: Taking a broader view. *Developmental Biology* **389**, 68–81 (2014).
81. McGraw, H. F., Drerup, C. M., Nicolson, T. & Nechiporuk, A. V. The Molecular and Cellular Mechanisms of Zebrafish Lateral Line Development. in *Auditory Development and Plasticity: In Honor of Edwin W Rubel* (eds. Cramer, K. S., Coffin, A. B., Fay, R. R. & Popper, A. N.) 49–73 (Springer International Publishing, Cham, 2017). doi:10.1007/978-3-319-21530-3_3.
82. Gilmour, D., Knaut, H., Maischein, H.-M. & Nüsslein-Volhard, C. Towing of sensory axons by their migrating target cells in vivo. *Nat Neurosci* **7**, 491–492 (2004).

83. Faucherre, A., Pujol-Martí, J., Kawakami, K. & López-Schier, H. Afferent Neurons of the Zebrafish Lateral Line Are Strict Selectors of Hair-Cell Orientation. *PLOS ONE* **4**, e4477 (2009).
84. Nagiel, A., Andor-Ardó, D. & Hudspeth, A. J. Specificity of Afferent Synapses onto Plane-Polarized Hair Cells in the Posterior Lateral Line of the Zebrafish. *J. Neurosci.* **28**, 8442–8453 (2008).
85. Gompel, N. *et al.* Pattern formation in the lateral line of zebrafish. *Mechanisms of Development* **105**, 69–77 (2001).
86. Alexandre, D. & Ghysen, A. Somatotopy of the lateral line projection in larval zebrafish. *PNAS* **96**, 7558–7562 (1999).
87. Obholzer, N. *et al.* Vesicular Glutamate Transporter 3 Is Required for Synaptic Transmission in Zebrafish Hair Cells. *J Neurosci* **28**, 2110–2118 (2008).
88. Haas, P. & Gilmour, D. Chemokine Signaling Mediates Self-Organizing Tissue Migration in the Zebrafish Lateral Line. *Developmental Cell* **10**, 673–680 (2006).
89. Andermann, P., Ungos, J. & Raible, D. W. Neurogenin1 Defines Zebrafish Cranial Sensory Ganglia Precursors. *Developmental Biology* **251**, 45–58 (2002).
90. Albalat, R. & Cañestro, C. Identification of Aldh1a, Cyp26 and RAR orthologs in protostomes pushes back the retinoic acid genetic machinery in evolutionary time to the bilaterian ancestor. *Chemico-Biological Interactions* **178**, 188–196 (2009).
91. Li, H. *et al.* Genetic contribution of retinoid-related genes to neural tube defects. *Human Mutation* **39**, 550–562 (2018).
92. Thaller, C. & Eichele, G. Identification and spatial distribution of retinoids in the developing chick limb bud. *Nature* **327**, 625–628 (1987).

93. Durston, A. J. *et al.* Retinoic acid causes an anteroposterior transformation in the developing central nervous system. *Nature* **340**, 140–144 (1989).
94. Horton, C. & Maden, M. Endogenous distribution of retinoids during normal development and teratogenesis in the mouse embryo. *Developmental Dynamics* **202**, 312–323 (1995).
95. Costaridis, P., Horton, C., Zeitlinger, J., Holder, N. & Maden, M. Endogenous retinoids in the zebrafish embryo and adult. *Developmental Dynamics* **205**, 41–51 (1996).
96. Ghyselinck, N. B. *et al.* Role of the retinoic acid receptor beta (RARbeta) during mouse development. *Int J Dev Biol* **41**, 425–447 (1997).
97. Lohnes, D. *et al.* Function of the retinoic acid receptors (RARs) during development (I). Craniofacial and skeletal abnormalities in RAR double mutants. *Development* **120**, 2723–2748 (1994).
98. Rhinn, M. & Dollé, P. Retinoic acid signalling during development. *Development* **139**, 843–858 (2012).
99. Pennimpede, T. *et al.* The role of CYP26 enzymes in defining appropriate retinoic acid exposure during embryogenesis. *Birth Defects Research Part A: Clinical and Molecular Teratology* **88**, 883–894 (2010).
100. Isabella, A. J., Barsh, G. R., Stonick, J. A., Dubrulle, J. & Moens, C. B. Retinoic Acid Organizes the Zebrafish Vagus Motor Topographic Map via Spatiotemporal Coordination of Hgf/Met Signaling. *Developmental Cell* **53**, 344–357.e5 (2020).
101. Liu, R.-Z. *et al.* Retention of the duplicated cellular retinoic acid-binding protein 1 genes (crabp1a and crabp1b) in the zebrafish genome by subfunctionalization of tissue-specific expression. *The FEBS Journal* **272**, 3561–3571 (2005).

102. Oosterveen, T. *et al.* Retinoids regulate the anterior expression boundaries of 5' Hoxb genes in posterior hindbrain. *EMBO J* **22**, 262–269 (2003).
103. Mahony, S. *et al.* Ligand-dependent dynamics of retinoic acid receptor binding during early neurogenesis. *Genome Biol* **12**, R2 (2011).
104. Kessel, M. Respecification of vertebral identities by retinoic acid. *Development* **115**, 487–501 (1992).
105. Kessel, M. & Gruss, P. Homeotic transformations of murine vertebrae and concomitant alteration of *Hox* codes induced by retinoic acid. *Cell* **67**, 89–104 (1991).
106. Waxman, J. S., Keegan, B. R., Roberts, R. W., Poss, K. D. & Yelon, D. Hoxb5b Acts Downstream of Retinoic Acid Signaling in the Forelimb Field to Restrict Heart Field Potential in Zebrafish. *Developmental Cell* **15**, 923–934 (2008).
107. Matsuda, H. & Kubota, Y. Zebrafish pancreatic β cell clusters undergo stepwise regeneration using Neurod1-expressing cells from different cell lineages. *Cell Tissue Res* **394**, 131–144 (2023).
108. Burzynski, G. M., Delalande, J.-M. & Shepherd, I. Characterization of spatial and temporal expression pattern of SCG10 during zebrafish development. *Gene Expression Patterns* **9**, 231–237 (2009).
109. Rentzsch, F., Zhang, J., Kramer, C., Sebald, W. & Hammerschmidt, M. Crossveinless 2 is an essential positive feedback regulator of Bmp signaling during zebrafish gastrulation. *Development* **133**, 801–811 (2006).
110. Wada, H., Dambly-Chaudière, C., Kawakami, K. & Ghysen, A. Innervation is required for sense organ development in the lateral line system of adult zebrafish. *Proceedings of the National Academy of Sciences* **110**, 5659–5664 (2013).

111. Cheng, C. W. *et al.* Zebrafish homologue *irx1a* is required for the differentiation of serotonergic neurons. *Developmental Dynamics* **236**, 2661–2667 (2007).
112. Wilson, A. L. *et al.* Cadherin-4 Plays a Role in the Development of Zebrafish Cranial Ganglia and Lateral line System. *Dev Dyn* **236**, 893–902 (2007).
113. Dupé, V. *et al.* In vivo functional analysis of the *Hoxa-1* 3' retinoic acid response element (3'RARE). *Development* **124**, 399–410 (1997).
114. Serpente, P. *et al.* Direct crossregulation between retinoic acid receptor β and *Hox* genes during hindbrain segmentation. *Development* **132**, 503–513 (2005).
115. Kruse, S. W. *et al.* Identification of COUP-TFII Orphan Nuclear Receptor as a Retinoic Acid-Activated Receptor. *PLoS Biol* **6**, (2008).
116. Kim, T.-S. *et al.* The ZFH3 (ATBF1) transcription factor induces PDGFRB, which activates ATM in the cytoplasm to protect cerebellar neurons from oxidative stress. *Disease Models & Mechanisms* **3**, 752–762 (2010).
117. Wang, F. *et al.* RNAscope: A Novel in Situ RNA Analysis Platform for Formalin-Fixed, Paraffin-Embedded Tissues. *The Journal of Molecular Diagnostics* **14**, 22–29 (2012).
118. Gross-Thebing, T., Paksa, A. & Raz, E. Simultaneous high-resolution detection of multiple transcripts combined with localization of proteins in whole-mount embryos. *BMC Biol* **12**, 55 (2014).
119. Olson, H. M. *et al.* RhoA GEF *Mcf2lb* regulates rosette integrity during collective cell migration. *Development* **151**, dev201898 (2024).
120. Ota, S. *et al.* Functional visualization and disruption of targeted genes using CRISPR/Cas9-mediated eGFP reporter integration in zebrafish. *Sci Rep* **6**, 34991 (2016).

121. O'Brien, G. S. *et al.* Two-photon axotomy and time-lapse confocal imaging in live zebrafish embryos. *Journal of Visualized Experiments (JoVE)* e1129 (2009) doi:10.3791/1129.
122. Bandla, A. *et al.* A New Transgenic Tool to Study the Ret Signaling Pathway in the Enteric Nervous System. *Int J Mol Sci* **23**, 15667 (2022).
123. Nittoli, V. *et al.* A comprehensive analysis of neurotrophins and neurotrophin tyrosine kinase receptors expression during development of zebrafish. *Journal of Comparative Neurology* **526**, 1057–1072 (2018).
124. Pan, Y. A. *et al.* Zebrabow: multispectral cell labeling for cell tracing and lineage analysis in zebrafish. *Development* **140**, 2835–2846 (2013).
125. Cook, Z. T. *et al.* Combining near-infrared fluorescence with Brainbow to visualize expression of specific genes within a multicolor context. *MBoC* **30**, 491–505 (2019).
126. Sarrazin, A. F. *et al.* Origin and Early Development of the Posterior Lateral Line System of Zebrafish. *J Neurosci* **30**, 8234–8244 (2010).
127. Becht, E. *et al.* Dimensionality reduction for visualizing single-cell data using UMAP. *Nat Biotechnol* **37**, 38–44 (2019).
128. Madelaine, R., Garric, L. & Blader, P. Partially redundant proneural function reveals the importance of timing during zebrafish olfactory neurogenesis. *Development* **138**, 4753–4762 (2011).
129. Washbourne, P. *et al.* Genetic ablation of the t-SNARE SNAP-25 distinguishes mechanisms of neuroexocytosis. *Nat Neurosci* **5**, 19–26 (2002).
130. Tafoya, L. C. R. *et al.* Expression and Function of SNAP-25 as a Universal SNARE Component in GABAergic Neurons. *J Neurosci* **26**, 7826–7838 (2006).

131. Ahmed, M., Xu, J. & Xu, P.-X. EYA1 and SIX1 drive the neuronal developmental program in cooperation with the SWI/SNF chromatin-remodeling complex and SOX2 in the mammalian inner ear. *Development* **139**, 1965–1977 (2012).
132. Trapnell, C. *et al.* The dynamics and regulators of cell fate decisions are revealed by pseudotemporal ordering of single cells. *Nat Biotechnol* **32**, 381–386 (2014).
133. Mohammadi, M. *et al.* Structures of the Tyrosine Kinase Domain of Fibroblast Growth Factor Receptor in Complex with Inhibitors. *Science* **276**, 955–960 (1997).
134. Bleckmann, H. *Flow Sensing in Air and Water: Behavioral, Neural and Engineering Principles of Operation*. (Springer, Berlin, Heidelberg, 2014). doi:10.1007/978-3-642-41446-6.
135. Maroon, H. *et al.* Fgf3 and Fgf8 are required together for formation of the otic placode and vesicle. *Development* **129**, 2099–2108 (2002).
136. Martínez-Morales, P. L. *et al.* FGF and retinoic acid activity gradients control the timing of neural crest cell emigration in the trunk. *J Cell Biol* **194**, 489–503 (2011).
137. Kuzina, I., Song, J. K. & Giniger, E. How Notch establishes longitudinal axon connections between successive segments of the *Drosophila* CNS. *Development* **138**, 1839–1849 (2011).
138. Begemann, G. & Meyer, A. Hindbrain patterning revisited: timing and effects of retinoic acid signalling. *BioEssays* **23**, 981–986 (2001).
139. Covassin, L. *et al.* Global analysis of hematopoietic and vascular endothelial gene expression by tissue specific microarray profiling in zebrafish. *Developmental Biology* **299**, 551–562 (2006).

140. Hao, Y. *et al.* Integrated analysis of multimodal single-cell data. *Cell* **184**, 3573-3587.e29 (2021).
141. Satija, R., Farrell, J. A., Gennert, D., Schier, A. F. & Regev, A. Spatial reconstruction of single-cell gene expression. *Nat Biotechnol* **33**, 495–502 (2015).
142. Tuttle, A. M. *et al.* Single-Cell Analysis of Rohon–Beard Neurons Implicates Fgf Signaling in Axon Maintenance and Cell Survival. *J. Neurosci.* **44**, (2024).
143. Kwan, K. M. *et al.* The Tol2kit: A multisite gateway-based construction kit for Tol2 transposon transgenesis constructs. *Developmental Dynamics* **236**, 3088–3099 (2007).
144. Waxman, J. S. & Yelon, D. Zebrafish retinoic acid receptors function as context-dependent transcriptional activators. *Developmental biology* **352**, 128 (2011).
145. Mo, W. & Nicolson, T. Both Pre- and Postsynaptic Activity of Nsf Prevents Degeneration of Hair-Cell Synapses. *PLOS ONE* **6**, e27146 (2011).
146. Pujol-Martí, J. *et al.* Neuronal Birth Order Identifies a Dimorphic Sensorineural Map. *J Neurosci* **32**, 2976–2987 (2012).
147. Kimura, Y., Hisano, Y., Kawahara, A. & Higashijima, S. Efficient generation of knock-in transgenic zebrafish carrying reporter/driver genes by CRISPR/Cas9-mediated genome engineering. *Sci Rep* **4**, 6545 (2014).
148. Shah, A. N., Davey, C. F., Whitebirch, A. C., Miller, A. C. & Moens, C. B. Rapid reverse genetic screening using CRISPR in zebrafish. *Nat Methods* **12**, 535–540 (2015).
149. Wang, J. *et al.* Anosmin1 Shuttles Fgf to Facilitate Its Diffusion, Increase Its Local Concentration, and Induce Sensory Organs. *Developmental Cell* **46**, 751-766.e12 (2018).
150. Schneider, C. A., Rasband, W. S. & Eliceiri, K. W. NIH Image to ImageJ: 25 years of image analysis. *Nat Methods* **9**, 671–675 (2012).

151. Bronner-Fraser, M. Neural crest cell formation and migration in the developing embryo. *The FASEB Journal* **8**, 699–706 (1994).
152. Nieto, M. A., Sechrist, J., Wilkinson, D. G. & Bronner-Fraser, M. Relationship between spatially restricted Krox-20 gene expression in branchial neural crest and segmentation in the chick embryo hindbrain. *The EMBO Journal* **14**, 1697–1710 (1995).
153. Venkataraman, V. *et al.* Development of the zebrafish anterior lateral line system is influenced by underlying cranial neural crest. 2025.02.11.637483 Preprint at <https://doi.org/10.1101/2025.02.11.637483> (2025).
154. Fortini, M. E. Notch Signaling: The Core Pathway and Its Posttranslational Regulation. *Developmental Cell* **16**, 633–647 (2009).
155. White, R. J., Nie, Q., Lander, A. D. & Schilling, T. F. Complex Regulation of *cyp26a1* Creates a Robust Retinoic Acid Gradient in the Zebrafish Embryo. *PLoS Biology* **5**, e304 (2007).
156. Nhieu, J., Lin, Y.-L. & Wei, L.-N. CRABP1 in Non-Canonical Activities of Retinoic Acid in Health and Diseases. *Nutrients* **14**, 1528 (2022).
157. Cai, A. Q. *et al.* Cellular retinoic acid-binding proteins are essential for hindbrain patterning and signal robustness in zebrafish. *Development* **139**, 2150–2155 (2012).
158. Schilling, T. F., Nie, Q. & Lander, A. D. Dynamics and precision in retinoic acid morphogen gradients. *Curr Opin Genet Dev* **22**, 562–569 (2012).
159. Barry, J., Gu, Y. & Gu, C. Polarized Targeting of L1-CAM Regulates Axonal and Dendritic Bundling in vitro. *Eur J Neurosci* **32**, 1618–1631 (2010).

160. Schmid, R. S. & Maness, P. F. L1 and NCAM ADHESION MOLECULES AS SIGNALING CO-RECEPTORS IN NEURONAL MIGRATION AND PROCESS OUTGROWTH. *Curr Opin Neurobiol* **18**, 245–250 (2008).
161. Rousso, D. L. *et al.* Foxp-Mediated Suppression of N-Cadherin Regulates Neuroepithelial Character and Progenitor Maintenance in the CNS. *Neuron* **74**, 314–330 (2012).
162. Das, R. M. & Storey, K. G. Apical abscission alters cell polarity and dismantles the primary cilium during neurogenesis. *Science* **343**, 200–204 (2014).
163. Wong, G. K. W., Baudet, M.-L., Norden, C., Leung, L. & Harris, W. A. Slit1b-Robo3 signaling and N-cadherin regulate apical process retraction in developing retinal ganglion cells. *J Neurosci* **32**, 223–228 (2012).
164. Kurusu, M., Katsuki, T., Zinn, K. & Suzuki, E. Developmental changes in expression, subcellular distribution, and function of Drosophila N-cadherin, guided by a cell-intrinsic program during neuronal differentiation. *Dev Biol* **366**, 204–217 (2012).
165. Corish, P. & Tyler-Smith, C. Attenuation of green fluorescent protein half-life in mammalian cells. *Protein Engineering, Design and Selection* **12**, 1035–1040 (1999).
166. Heng, Y. C. & Foo, J. L. Development of destabilized mCherry fluorescent proteins for applications in the model yeast *Saccharomyces cerevisiae*. *Biotechnology Notes* **3**, 108–112 (2022).
167. Deichsel, H. *et al.* Green fluorescent proteins with short half-lives as reporters in *Dictyostelium discoideum*. *Dev Genes Evol* **209**, 63–68 (1999).

168. Kitsera, N., Khobta, A. & Epe, B. Destabilized green fluorescent protein detects rapid removal of transcription blocks after genotoxic exposure. *BioTechniques* **43**, 222–227 (2007).
169. Boswell, C. W. *et al.* Genetically encoded affinity reagents (GEARs): A toolkit for visualizing and manipulating endogenous protein function in vivo. 2023.11.15.567075 Preprint at <https://doi.org/10.1101/2023.11.15.567075> (2023).
170. Iismaa, S. E. *et al.* Comparative regenerative mechanisms across different mammalian tissues. *npj Regen Med* **3**, 1–20 (2018).
171. Aztekin, C. Mechanisms of regeneration: to what extent do they recapitulate development? *Development* **151**, dev202541 (2024).
172. Storer, M. A. & Miller, F. D. Cellular and molecular mechanisms that regulate mammalian digit tip regeneration. *Open Biology* **10**, 200194 (2020).
173. Verjans, R., van Bilsen, M. & Schroen, B. Reviewing the Limitations of Adult Mammalian Cardiac Regeneration: Noncoding RNAs as Regulators of Cardiomyogenesis. *Biomolecules* **10**, 262 (2020).
174. Gawriluk, T. R. *et al.* Complex Tissue Regeneration in Mammals Is Associated With Reduced Inflammatory Cytokines and an Influx of T Cells. *Front. Immunol.* **11**, (2020).
175. Canty, A. J. *et al.* In-vivo single neuron axotomy triggers axon regeneration to restore synaptic density in specific cortical circuits. *Nat Commun* **4**, 2038 (2013).
176. Akassoglou, K. *et al.* In Vivo Imaging of CNS Injury and Disease. *J. Neurosci.* **37**, 10808–10816 (2017).

177. Huebner, E. A. & Strittmatter, S. M. Axon Regeneration in the Peripheral and Central Nervous Systems. in *Cell Biology of the Axon* (ed. Koenig, E.) 305–360 (Springer, Berlin, Heidelberg, 2009). doi:10.1007/400_2009_19.
178. Poss, K. D. & Tanaka, E. M. Hallmarks of regeneration. *Cell Stem Cell* **31**, 1244–1261 (2024).
179. Guerin, D. J., Kha, C. X. & Tseng, K. A.-S. From Cell Death to Regeneration: Rebuilding After Injury. *Front. Cell Dev. Biol.* **9**, (2021).